

Kh Rahat Usman

# Safe Rivers – Identification of critical locations along steep watercourses during flood events

Master Thesis

Trondheim, June 2019

Supervisor: Oddbjørn Bruland, IBM

Co-Supervisors: Knut Alfredsen, IBM  
Katherine Aurand, SWECO



Kh Rahat Usman

# Safe Rivers – Identification of critical locations along steep watercourses during flood events

Master's thesis in Hydropower Development  
Supervisor: Oddbjørn Bruland  
June 2019

Norwegian University of Science and Technology  
Faculty of Engineering  
Department of Civil and Environmental Engineering

 **NTNU**  
Norwegian University of  
Science and Technology





Kh Rahat Usman

# Safe Rivers – Identification of critical locations along steep watercourses during flood events

Master Thesis

Trondheim, June 2019

Supervisor: Oddbjørn Bruland  
Co-Supervisors: Knut Alfredsen  
Katherine Aurand

Norwegian University of Science and Technology  
Faculty of Engineering  
Department of Civil and Environmental Engineering



Norwegian University of  
Science and Technology



## **Abstract**

Floods are the most common of the natural disasters seen by human race over the past couple of decades and their frequency is forecasted to increase owing to climate change and increased human activity. Flood analysis and modeling has remained popular among engineers and scientists to reduce flood impacts and provide a safe environment to the society. Steep river, however, provide a special challenge due to their complex hydraulics resulting from a number of factors such as, high gradients, complex river morphology and limitations in bed roughness estimation. This work is focused on identifying the relationships that exist between steep river hydraulics and its topography through hydrodynamic modeling of idealized steep rivers carrying idealized discharges. Different hydraulic and topographic parameters were analyzed to assess their interdependencies. Discharge was found to be the most influential parameters. Moreover, the influence of river geometry (both longitudinal and cross-sectional) is also quite significant. River bends and cross-sectional contractions also influence the river's hydrodynamics and present a challenge to river bank stability during floods.



## **Acknowledgements**

This section belongs to all those wonderful people without whom this work would not have been possible.

I hold my highest regards and gratitude to all these people who inspired me, encouraged me, enriched me, believed in me and guided me when I could not determine the sense. First in the list is my main supervisor Oddbjørn Bruland for his continued support and guidance throughout the process, ensuring I have all the tools and resources available to carryout this work.

I would like to extend special thanks to Knut Alfredsen whose dedication and commitment inspired me and for all those 5 minutes meetings which ended after two hours.

Katherine Aurand has been an important part of this work and I am very thankful to her for her support and guidance despite her busy schedule at SWECO.

My debt to Adina Moraru is the highest. I cannot thank her enough for her support, encouragment, guidance and mentoring throughout this work.

I would also like to thank Michal Pavlíček for his guidance and assistance in this work and for carrying out simulations in TELEMAT 2-D.

At the end I would like to thank my parents and rest of my family and friends who have prayed for me, supported me, tolerated me and encouraged me throughout this work.



# Table of Contents

<b>Abstract .....</b>	<b>i</b>
<b>List of Figures .....</b>	<b>ix</b>
<b>List of Tables.....</b>	<b>xiii</b>
<b>Abbreviations.....</b>	<b>xiv</b>
<b>1 Introduction .....</b>	<b>1</b>
1.1 River Classification .....	3
1.2 Steep Channel Characteristics: .....	4
1.3 Steep Channel Hydraulics: .....	4
<b>2 Flood Modeling.....</b>	<b>7</b>
2.1 Empirical Approaches .....	7
2.2 Hydrodynamic Approach.....	8
2.2.1 1-D Hydrodynamic Models.....	8
2.2.2 2-D Hydrodynamic Models.....	10
2.2.3 3-D Hydrodynamic Models.....	12
2.3 Terrain based Flood Modeling Approaches .....	13
2.3.1 Rapid Flood Spreading Model (RFSM) .....	13
2.3.2 Teng Vaze and Dutta Inundation Model .....	14
2.3.3 Height Above Nearest Drainage Model (HAND).....	15
2.4 Recent Developments in Flood Modeling .....	16
2.5 1-D versus 2-D Hydrodynamic Models.....	19
<b>3 Methodology.....</b>	<b>21</b>
3.1 Hydrodynamic Modeling.....	21
3.1.1 Modeling package .....	21
3.1.2 HEC-RAS .....	22
3.2 Idealized Rivers .....	23
3.2.1 River Selection .....	23
3.2.2 Digital Elevation Model .....	25
3.2.3 Terrain Manipulation.....	26
3.3 Parameters for the Study.....	29

3.3.1	Bed Slope ( $s$ ) .....	30
3.3.2	Channel Width ( $w$ ) .....	30
3.3.3	Relative Section Width ( $W_{xs}$ ).....	31
3.3.4	Lateral Confinement Index ( $W_r$ ) .....	31
3.3.5	Channel Bend ( $B$ ).....	32
3.3.6	Discharge ( $Q$ ) .....	32
3.3.7	Flow Depth ( $D$ ) .....	32
3.3.8	Flow Velocity ( $V$ ) .....	33
3.3.9	Shear Stress ( $S$ ) .....	33
3.3.10	Stream Power ( $SP$ ) .....	33
3.4	Scenario Idealization .....	34
3.4.1	Slope Idealization .....	34
3.4.2	Discharge Idealization.....	34
3.5	Statistical Methods.....	35
3.5.1	Box Plots .....	35
3.5.2	Frequency Analysis .....	36
3.5.3	Correlation Test.....	36
<b>4</b>	<b>Simulations.....</b>	<b>37</b>
4.1	Model Set-up .....	37
4.1.1	Terrain Creation .....	37
4.1.2	Geometry .....	38
4.1.3	Roughness Coefficients.....	39
4.1.4	Boundary Conditions.....	42
4.2	Computation Parameters.....	45
4.2.1	Equation Set .....	46
4.2.2	Computation Time Step.....	46
4.3	Simulation of Scenarios.....	48
4.4	Comparison of Simulations .....	49
4.5	Result Extraction .....	50
<b>5</b>	<b>Results.....</b>	<b>53</b>
5.1	Longitudinal Variation of Hydraulic Parameters .....	53



5.1.1	Water Depth Variation .....	53
5.1.2	Velocity Variation .....	55
5.1.3	Shear Stress Variation .....	57
5.1.4	Stream Power Variation .....	59
5.2	Variation of Hydraulic Parameters with Varying Slope.....	61
5.2.1	Depth .....	62
5.2.2	Velocity .....	64
5.2.3	Shear Stress .....	67
5.2.4	Stream Power .....	70
5.3	Variation of Hydraulic Parameters at Varying Discharge .....	73
5.3.1	Depth .....	73
5.3.2	Velocity .....	76
5.3.3	Shear Stress .....	79
5.3.4	Stream Power .....	82
5.4	Correlation Identification.....	85
5.4.1	Box Plots .....	86
5.4.2	Frequency Analysis .....	89
5.4.3	Correlation Test.....	92
5.5	Influence of Bends .....	95
5.5.1	Influence on Bends on Water Surface Elevation.....	98
5.5.2	Influence of Bends on Velocity.....	100
5.5.3	Influence of Bends on Shear Stress.....	101
5.5.4	Influence of Bends on Stream Power .....	102
5.6	Class Summary .....	103
5.7	Comparison Results from TELEMAC 2-D .....	104
<b>6</b>	<b>Discussion .....</b>	<b>107</b>
6.1	Slope .....	108
6.2	Discharge .....	109
6.3	Correlation Between Hydraulic and Topographical Parameters ...	110
6.4	Bends in Rivers.....	112
6.5	Critical Areas in Steep Rivers.....	112

<b>7</b>	<b>Recommendation and Future Work.....</b>	<b>115</b>
<b>8</b>	<b>References .....</b>	<b>117</b>
<b>A.</b>	<b>APPENDIX A – Byrteåi Lavvannskart.....</b>	<b>125</b>

## List of Figures

Figure 3-1 Byrteåi River catchment, Tokke, Telemark.....	24
Figure 3-2 Time Series of Byrteåi river. Average annual discharge 2.59 m <sup>3</sup> /s. .....	25
Figure 3-3 Digital Elevation Model of Byrteåi River Catchment .....	26
Figure 3-4 Original River Section considered for Terrain Manipulation.....	27
Figure 3-5 River section after Terrain Modification at a slope of 4.5% .....	28
Figure 3-6 Original (Left) and Modified River (Right). The modified river has 4.5% slope .....	28
Figure 3-7 Original and Modified Cross-Section.....	29
Figure 3-8 Bend angle measurement methodology in the study .....	32
Figure 4-1 Byrteåi River Catchment Terrain imported in RAS Mapper.....	37
Figure 4-2 2-D Flow Area Defined for Simulation .....	39
Figure 4-3 Byrteåi Catchment Land use Map .....	40
Figure 4-4 Flow Hydrograph showing Initial flow Conditions in the River..	44
Figure 4-5 Flow condition at inflow and outflow boundaries.....	45
Figure 4-6 Input Flood Hydrographs for different slope Scenarios .....	45
Figure 4-7 Comparison between Diffusion Wave and Full Momentum Equation Sets.....	46
Figure 4-8 WSE for Simulated Scenario (s=4.5%, Q <sub>50</sub> ). Values go from 465 m (green tones) to 595 m (pink tones).....	48
Figure 4-9 Reach Selected for Comparison with TELEMAC 2-D (Water Depth layer turned in HEC-RAS). Scenario s= 5.5%, Q= Q <sub>200</sub> .....	49
Figure 4-10 Data Extraction scheme for results .....	51
Figure 5-1 Water Depth Variation along River Right Bank .....	53
Figure 5-2 Water Depth Variation along River Center .....	54
Figure 5-3 Depth Variation along River Left Bank .....	54
Figure 5-4 Velocity Variation along the River Right Bank .....	56
Figure 5-5 Velocity Variation along the River Center .....	56
Figure 5-6 Velocity Variation along the River Left Bank.....	57

Figure 5-7 Shear Stress Variation along the River Right Bank .....	58
Figure 5-8 Shear Stress Variation along the River Center .....	58
Figure 5-9 Shear Stress Variation along the River Left Bank.....	59
Figure 5-10 Stream Power Variation along the River Right Bank.....	60
Figure 5-11 Stream Power Variation along River Center .....	60
Figure 5-12 Stream Power Variation along River Left Bank.....	61
Figure 5-13 Average Percentage Variation of Depth with Slope at Constant Discharge at River Right Bank.....	62
Figure 5-14 Average Percentage Variation of Depth with Slope at Constant Discharge at River Center .....	63
Figure 5-15 Average Percentage Variation of Depth with Slope at Constant Discharge at River Left Bank .....	63
Figure 5-16 Relationship Between Slope Change and Depth Change .....	64
Figure 5-17 Average Percentage Variation of Velocity with Slope at Constant Discharge at River Right Bank.....	65
Figure 5-18 Average Percentage Variation of Velocity with Slope at Constant Discharge at River Center .....	65
Figure 5-19 Average Percentage Variation of Velocity with Slope at Constant Discharge at River Left Bank .....	66
Figure 5-20 Relationship Between Slope Change and Velocity Change .....	67
Figure 5-21 Average Percentage Variation of Shear Stress with Slope at Constant Discharge at River Right Bank .....	68
Figure 5-22 Average Percentage Variation of Shear Stress with Slope at Constant Discharge at River Center .....	68
Figure 5-23 Average Percentage Variation of Shear Stress with Slope at Constant Discharge at River Left Bank.....	69
Figure 5-24 Relationship Between Slope Change and Shear Stress Change .	70
Figure 5-25 Average Percentage Variation of Stream Power with Slope at Constant Discharge at River Right Bank .....	71
Figure 5-26 Average Percentage Variation of Stream Power with Slope at Constant Discharge at River Center .....	71
Figure 5-27 Average Percentage Variation of Stream Power with Slope at Constant Discharge at River Left Bank.....	72

Figure 5-28 Relationship Between Slope Change and Stream Power Change .....	73
Figure 5-29 Average Percentage Variation of Depth with Discharge at Constant Slope at River Right Bank.....	74
Figure 5-30 Average Percentage Variation of Depth with Discharge at Constant Slope at River Center .....	74
Figure 5-31 Average Percentage Variation of Depth with Discharge at Constant Slope at River Left Bank.....	75
Figure 5-32 Relationship Between Discharge Change and Depth Change....	76
Figure 5-33 Average Percentage Variation of Velocity with Discharge at Constant Slope at River Right Bank.....	77
Figure 5-34 Average Percentage Variation of Velocity with Discharge at Constant Slope at River Center .....	77
Figure 5-35 Average Percentage Variation of Velocity with Discharge at Constant Slope at River Left Bank.....	78
Figure 5-36 Relationship Between Discharge Change and Velocity Change	79
Figure 5-37 Average Percentage Variation of Shear Stress with Discharge at Constant Slope at River Right Bank.....	80
Figure 5-38 Average Percentage Variation of Shear Stress with Discharge at Constant Slope at River Center .....	80
Figure 5-39 Average Percentage Variation of Shear Stress with Discharge at Constant Slope at River Left Bank.....	81
Figure 5-40 Relationship Between Discharge Change and Shear Stress Change .....	82
Figure 5-41 Average Percentage Variation of Stream Power with Discharge at Constant Slope at River Right Bank.....	83
Figure 5-42 Average Percentage Variation of Stream Power with Discharge at Constant Slope at River Center .....	83
Figure 5-43 Average Percentage Variation of Stream Power with Discharge at Constant Slope at River Left Bank.....	84
Figure 5-44 Relationship Between Discharge Change and Stream Power Change.....	85
Figure 5-45 Box Plot for Depth (DR= Depth at Right Bank, DC= Depth at Center, DL= Depth at Left Bank).....	86
Figure 5-46 Box Plot for Velocity (VR= Velocity at Right Bank, VC= Velocity at Center, VL= Velocity at Left Bank).....	87

Figure 5-47 Box Plot for Shear Stress (SR= Shear Stress at Right Bank, SC= Shear Stress at Center, SL= Shear Stress at Left Bank).....	88
Figure 5-48 Box Plot for Stream Power (SP R= Stream Power at Right Bank, SP C= Stream Power at Center, SP L= Stream Power at Left Bank).....	89
Figure 5-49 Lateral confinement ( $W_r$ ) Histogram.....	90
Figure 5-50 Relative Section Width Histogram .....	90
Figure 5-51 Depth Histogram.....	91
Figure 5-52 Velocity Histogram.....	91
Figure 5-53 Shear Stress Histogram.....	92
Figure 5-54 Stream Power Histogram.....	92
Figure 5-55 Scatter Matrix Plot for Parameters .....	95
Figure 5-56 Bend Measurement in the Modelled River Reach.....	96
Figure 5-57 Shear Stress comparison at bends.....	98
Figure 5-58 Location of Bends under consideration within the modelled reach .....	99
Figure 5-59 Water Surface Elevation at Bend 8.....	99
Figure 5-60 Water Surface Elevation at Bend 9.....	100
Figure 5-61 Influence of Bends on Velocity .....	101
Figure 5-62 Influence of Bends on Shear Stress .....	102
Figure 5-63 Influence of Bends on Stream Power .....	103
Figure 5-64 Computed Water Surface Elevation Comparison between HEC-RAS and TELEMAC 2-D .....	105
Figure 6-1 Non-Linear Curve fitting to Stream Power Data.....	111

## List of Tables

Table 3-1 Summary of different software packages available for 2-D modeling .....	22
Table 3-2 List of Parameters for the Study .....	29
Table 3-3 Discharge scenarios considered for simulation.....	35
Table 4-1 Manning's n Values adopted for different land use features.....	40
Table 4-2 Hydrograph Data showing initial flow conditions in the river .....	43
Table 5-1 Average Change in Water Depth with Slope Variation.....	64
Table 5-2 Average Change in Velocity with Slope Variation.....	66
Table 5-3 Average Change in Shear Stress with Slope Variation.....	69
Table 5-4 Average Change in Stream Power with Slope Variation.....	72
Table 5-5 Average Change in Depth with Discharge Variation .....	75
Table 5-6 Average Change in Velocity with Discharge Variation .....	78
Table 5-7 Average Change in Shear Stress with Discharge Variation.....	81
Table 5-8 Average Change in Stream Power with Discharge Variation.....	84
Table 5-9 Correlation Matrix for Different Parameters .....	93
Table 5-10 Details of Bends in the Modelled River Reach.....	96
Table 5-11 Classes for Stream Power based on Data from Stream Center..	103
Table 6-1 Non-Linear Curve fitting Model Statistics for Stream Power .....	111
Table 6-2 Critical Locations in the Modeled Steep Rivers .....	113







## Abbreviations

DEM	=	Digital Elevation Model
IZ	=	Impact Zone
LiDAR	=	Light Detection and Ranging
NVE	=	Norwegian Water and Energy Directorate
SAR	=	Synthetic Aperture Radar
SWEs	=	Shallow Water Equations
TVD	=	Total Variation Diminishing
WSE	=	Water Surface Elevation
1-D	=	One-dimensional
2-D	=	Two-dimensional
3-D	=	Three-dimensional

## 1 Introduction

Of the various natural disasters encountered today, floods are the most common. In the past two decades around 3,148 flooding events were reported across the globe, which contributes to a hefty 43.4% of the total reported natural disasters, leading to an economic loss of 656 Billion USD (Wallemacq & House, 2018). These events consumed over a hundred thousand lives and affected 2 billion people (Wallemacq & House, 2018). Flood frequency is likely to increase as a result of rapidly growing population leading to rapid and significant land use changes as well as due to global climate change (Kvočka, Ahmadian, & Falconer, 2017). Warmer climate will lead to higher snow melt, and evaporation; changes in precipitation patterns and its spatiotemporal distribution, as well as reduced precipitation in the form of snow (Schumann, Bates, Apel, & Aronica, 2018).

Steep rivers are characterized by high gradients – typically in the range of 0.04 to 0.1 m/m; low width to depth ratio (*i.e.*  $W/D < 12$ ) and cascading bed features (Rosgen, 1994). Steep rivers are usually located in mountainous regions such as valleys or steep coastlines, where they go on to either drain in another river or sea or may continue to flow in lower lands with moderate ( $0.01 \text{ m/m} < s < 0.04 \text{ m/m}$ ) to low gradients ( $s < 0.01 \text{ m/m}$ ). Due to increasing urbanization and touristic opportunities in such regions, socio-economic activity has grown in these areas. However, these endeavors are often shaken by flash floods that cause a major disruption and pose threat to human activity and even human life (Petrucci, M, & Pasqua, 2010). Thus, it is essential to study such rivers and to identify the areas within these reaches that are susceptible in a flooding event.

For long, floods have remained an area of great scientific endeavors for understanding, assessing and predicting events and their impacts. These efforts have led to the development of various flood inundation models which are used

for flood risk mapping (Ward et al., 2015), flood damage assessment (Mattia Amadio, Mysiak, Carrera, & Koks, 2016), real-time flood forecasting (Cox et al., 2002; Ma & Fu, 2012) and water resources planning (J. Teng et al., 2017). The application of these models is dependent on the predictive output of interest, for instance determination of flood inundation extents; assessment of flood damage level or flood risk assessment due to land use changes etc., input data and its spatiotemporal scales, required accuracy levels and computational efficiency demands. It is important to note that in the development of these models two main approaches have attained most attention from researchers: one is the Empirical approach based on survey, remote sensing and subsequent statistical models; the other is the hydrodynamic approach (1D, 2D and 3D modeling) based on the application of physical laws to fluids in motion (Prakash, Rothauge, & Cleary, 2014; Stelling & Verwey, 2006).

Irrespective of the approach followed in flood modeling, topographical data is a necessary input for both procedures. The Geographic Information Systems (or simply GIS) is a very handy tool that provides a platform to establish a spatially referenced database to store; update; analyze and visualize. Furthermore, GIS facilitates the integration of data from various sources (such as web based or field measurements) to model flood plains and visualize hazard extents. GIS has been successfully applied to develop GIS-based Flood Information Systems (GFIS) (Yang & Tsai, 2000), flood zoning maps (Dano, Balogun, Abubakar, & Aina), flood hazard maps (Gigović, Pamučar, Bajić, & Drobnjak, 2017) and flood crisis management applications (Abdeyazdan & Jodaki, 2015). Thus, it has proved its utility in flood risk assessment and management.

This work's methodology is committed to make use of existing hydrodynamic modeling techniques, *i.e.* 2D modeling in HEC-RAS to identify relevant set of parameters primarily based on topographical parameters of the channel and

channel hydraulics. The study will focus on identifying the relationship between topographic and hydraulic parameter sets through a hydrodynamic modeling approach. The aim is to use these relationships in order to determine a criterion that can be used to develop a specialized methodology in a GIS based environment to identify critical areas in steep rivers.

The thesis is structured to provide a logical flow of information with Chapter 1 covering the introduction to the problem and discussion on steep rivers. Chapter 2 incorporates the discussion on flood modeling approaches and state of the art techniques in this domain. Chapter 3 describes the methodology followed to carryout this work. Chapter 4 covers the simulation program and model set-up details. Chapter 5 contains the results from the simulations. Chapter 6 is the discussion of the results and findings. Chapter 7 contains the recommendations of the author.

## **1.1 River Classification**

River system classification is essential to this work as to set the extents of investigations. Classification system proposed by Rosgen (1994) is used for the study, hence, furtherly described in the current and next sections. The advantage of this classification system is that it incorporates detailed stream geometry and stream morphology, which are key parameters considered within the scope of this study.

This classification system focuses on a broad geomorphic characterization and morphological description of rivers. The geomorphological characterization classifies rivers based on landform, lithology, channel slope, cross-section morphology, valley morphology, climate, and general river pattern. The morphological description furtherly distinguishes streams based on channel characteristics, such as width to depth ratio (W/D), entrenchment ratio (*i.e.* vertical containment, calculated as the ratio between flood prone area width,

*i.e.* width at twice bankfull depth, to channel's bankfull surface width), sinuosity, channel pattern (meandering, braided etc.).

Rosgen's classification is an alphanumeric system where initially the streams are classified broadly in alphabets ranging from A to G and, then, further broken down into categories based on decreasing dominant bed material particle size (*i.e.* from 1 to 6, with bedrock being 1 and silt/clay being 6).

The scope of this research is limited to steep rivers hence, the classification system developed by Rosgen helps define these rivers by outlining their geomorphic characteristics.

## **1.2 Steep Channel Characteristics:**

Following Rosgen's classification system, steep channels are defined as "A" type streams, ranging from A1 to A6. According to this system, steep streams are characterized by "*Steep, cascading, step/pool bed features*". Steep rivers are entrenched (entrenchment ratio  $< 1.4$ ), the stream shape is mainly straight (*i.e.* low sinuosity, sinuosity  $< 1.2$ ), high bed slopes (*i.e.* ranging from 0.04 to 0.1m/m), channel geometry is usually V-shaped (*i.e.*  $W/D < 12$ ), however, it can be different depending upon the bed and bank material. Steep streams with competent and/or very coarse bed material such as bedrock or boulders have low erosion potential and consequently low bed material supply whereas those with finer bed materials such as gravel, sand, silt/clay have high erosion potential and, resultantly, high bed material supply (Rosgen, 1994).

The hydraulic characteristics of this type of rivers are described in the following **section 1.3**.

## **1.3 Steep Channel Hydraulics:**

Steep channels have extremely complex hydraulics owing to the combined effect of topography, hydrology, channel morphology, high reach gradient, low discharge (under normal hydrological conditions) and sediment transport

(Francesco Comiti & Mao, 2012). Comiti & Mao (2012) pointed out the low relative submergence (*i.e.*  $h/D$ , where  $h$  is the depth of flow and  $D$  is the characteristic grain size) as another characteristic of steep channels which influences sediment transport mode.

The morphology of steep channels is characterized by step-pools and cascades. Gravel jams and/or bedrock outcrop lead to formation of steps while pools are formed by scouring action (F. Comiti, Cadol, & Wohl, 2009), (Harada, Ikari, Shimizu, Khayyer, & Gotoh, 2018). Stream bed roughness at these pools is difficult to estimate due to the presence of wide range of particle sizes (*i.e.* bedrock outcrop, debris, coarse bed material) (Galia & Skarpich, 2015), (Harada *et al.*, 2018). These steps have sizes on a scale comparable to the water depth in the stream, thus, causing changes in flow regime (*i.e.* subcritical to supercritical and vice-versa) (Harada *et al.*, 2018). The flow regime in steep channels was named as “tumbling flow” by Peterson and Mohanty (1960) due to these rapid alternations at steps and pools.

The steps act as accelerators, causing the flow to go beyond the critical flow regime ( $Fr=1$ ) while the pools have a deceleration effect, bringing the flow back to sub-critical flow regime ( $Fr<1$ ). A hydraulic jump is formed in these pools; dissipating the energy gained at the steps (Francesco Comiti & Mao, 2012). Most of the energy dissipated in the process is potential energy rather than kinetic energy, indicating less reduction in velocities (Andrew C Wilcox, Wohl, Comiti, & Mao, 2011). A common misconception regarding flow in steep channels is that the flow regime is governed by super-critical flow ( $Fr >1$ ). This idea is supported by the wrong application of flow resistance formulas developed for streams featuring gravel beds to steep channels, whose geomorphology is rather dominated by boulders and rock outcrops forming steps (Francesco Comiti & Mao, 2012).

Resistance to flow is an interesting aspect of fluvial geomorphology, as it determines the conveyance capacity of the stream, water velocity and flow depth (Bathurst, 1993). Much work has been done to understand flow resistance in steep streams as it differs significantly from lowland streams (*i.e.* streams with low gradients; slope < 0.01 m/m) (Lee, 2000), (Francesco Comiti & Mao, 2012). Flow resistance in the former is a combination of steps (*e.g.* due to protruding boulders), hydraulic jumps, relative flow depth, and the presence of debris in the channel (*e.g.* large pieces of suspended wood). These studies, however, show that the contribution of the grain size to flow resistance is only 10~15% and that flow resistance is usually dominated by bed form, debris and discharge (Francesco Comiti & Mao, 2012). Laboratory flume investigations carried out by Andrew C. Wilcox, Nelson, and Wohl (2006) and F. Comiti *et al.* (2009) showed that discharge plays a significant role in the interaction of the aforementioned resistance components which make up the overall resistance of the channel.



## **2 Flood Modeling**

Rossi (1994) describes two main objectives for flood modeling: (i) being of practical value, aimed at obtaining design parameters for hydraulic structures, or developing non-structural flood control systems such as flood forecasting and flood warning systems, and (ii) being purely theoretical, aimed at understanding the phenomenon behind floods (considering hydrology, topography, catchment response, etc.).

Flood modeling is dependent on the predictive output of interest, input data and its spatiotemporal scales, required accuracy levels and computational efficiency demands (J. Teng et al., 2017). These criteria led to the development of two main groups of modeling approaches; Empirical approach and Hydrodynamic approach.

In this chapter, we shall discuss these approaches in terms of their methodology, data requirements, application, merits and demerits as this will serve as basis for a sensible model choice to implement during the research.

### **2.1 Empirical Approaches**

Empirical approaches are based on observations from past flooding events. These models are developed locally based on observations done through field surveying, remote sensing, satellite imagery, areal photogrammetry, etc. and statistical models have been developed from these datasets (M. Amadio et al., 2019; Carisi, Schröter, Domeneghetti, Kreibich, & Castellarin, 2018; J. Teng et al., 2017). The development of these models is based on certain assumptions and often involve uncertainties due to the nature of the methods used to generate these datasets (Carisi et al., 2018; J. Teng et al., 2017). Empirical models have been developed for flood damage loss or flood inundation, however, a major limitation of these models, in addition to uncertainty, is their transferability (M. Amadio et al., 2019; Carisi et al., 2018). These models are

usually region-specific and do not perform well in other regions (Mattia Amadio et al., 2016; M. Amadio et al., 2019; Carisi et al., 2018; Jongman et al., 2012; Scorzini & Frank, 2017). These models, however, often find their application in the decision-making process, as inputs to other models/approaches, and most notably, as reference for calibration and validation of hydrodynamic models (J. Teng et al., 2017).

## **2.2 Hydrodynamic Approach**

Hodges (2014) defines hydrodynamic modeling as “the art and science of applying conservation equations for momentum, continuity, and transport to represent evolving velocity, density, and scalar fields.” The Hydrodynamic approach is based on Newtonian continuum mechanics, developed for incompressible fluids, which is: (i) Principle of conservation of mass (Continuity) and (ii) Principle of conservation of momentum. Hydrodynamic models are mathematical models, founded on aforementioned principles of Physics, which attempt to simulate the fluid flow by solving the math (J. Teng et al., 2017).

Hydrodynamic models can be categorized as one, two or three-dimensional (Caletka, Šulc Michalková, Koli, & Trizna, 2019; Hodges, 2014; J. Teng et al., 2017). These models differ in their mathematics and input data requirements, as furtherly discussed. The choice of hydrodynamic modeling approach is outcome specific as well as dependent on input data, computational expense and accuracy requirements (J. Teng et al., 2017).

### **2.2.1 1-D Hydrodynamic Models**

One-dimensional hydrodynamic models are the simplest way to simulate hydraulic processes in rivers and streams. These models find their application predominantly in large river networks extending over hundreds of kilometers in length (Hodges, 2014), or in cases such as pipe flow where, 1-D flow is

dominant (*i.e.* flow parallel to the centerline of the channel) (Pender, 2006), or where a coarse output is required and 1-D flow assumption can be justified (J. Teng et al., 2017).

These models are founded on 1-D Saint-Venant equations conserving mass and momentum between two cross-sections (Gary W. Brunner, 2016a). The one-dimensional St. Venant equations are given as follows:

$$\begin{array}{l} \text{Conservation} \\ \text{of Mass} \end{array} \quad \frac{\partial Q}{\partial x} + \frac{\partial A}{\partial t} = 0 \quad (1)$$

$$\begin{array}{l} \text{Conservation} \\ \text{of Momentum} \end{array} \quad \frac{1}{A} \frac{\partial Q}{\partial t} + \frac{1}{A} \frac{\partial \left( \frac{Q^2}{A} \right)}{\partial x} + g \frac{\partial h}{\partial x} - g(S_o - S_f) = 0 \quad (2)$$

Where,

Q = Discharge

A = Area of flow

t = time step

g = gravitational acceleration

S<sub>o</sub> = Channel bed slope

S<sub>f</sub> = Friction slope

h = Water depth

Equations (1) and (2) are Partial differential equations and have no analytical solution. The 1-D models make use of numerical methods to solve these equations. The implicit finite difference scheme is most commonly employed in these models (Gary W. Brunner, 2016a).

The advantage that 1-D hydrodynamic models have is that they are computationally inexpensive and efficient, however, they are unable to

simulate lateral flood wave diffusion, use cross-section average velocity, and cross-section topography is discrete rather than continuous (J. Teng et al., 2017).

### 2.2.2 2-D Hydrodynamic Models

Two-dimensional hydrodynamic models are based on 2-D Saint Venant Equations, also known as shallow water equations (SWE), which are derived from the Navier-Stokes equations considering simplifications that the third dimension (*i.e.* depth) is much smaller (or shallow) as compared to the other two dimensions; pressure is hydrostatic; fluid is incompressible with uniform density and the parent equations (Navier-Stokes equations) are Reynold averaged over depth (Gary W. Brunner, 2016a; S. Neelz, 2009; J. Teng et al., 2017). The 2-D SWE in simplified vector form are expressed as follows:

$$\frac{\partial U}{\partial t} + \frac{\partial F}{\partial x} + \frac{\partial G}{\partial y} = H \quad (3)$$

Where,  $x$  and  $y$  are the two spatial dimensions. The vectors  $U$ ,  $F$ ,  $G$  and  $H$  are defined as:

$$\begin{aligned} U &= \begin{pmatrix} h \\ hu \\ hv \end{pmatrix}, F = \begin{pmatrix} h \\ g \frac{h^2}{2} + hu^2 \\ huv \end{pmatrix}, G = \begin{pmatrix} hv \\ huv \\ g \frac{h^2}{2} + hv^2 \end{pmatrix}, H \\ &= \begin{pmatrix} 0 \\ gh(S_{ox} - S_{fx}) \\ gh(S_{oy} - S_{fy}) \end{pmatrix} \end{aligned} \quad (4)$$

Where,

$u$  = Depth average velocity in x-direction

$v$  = Depth average velocity in y-direction

$S_{ox}$  = Bed slope in x-direction

$S_{oy}$  = Bed slope in y-direction

$S_{fx}$  = Friction slope in x-direction

$S_{fy}$  = Friction slope in y-direction

Equation (3) also contains terms for viscosity, Coriolis (to consider the effect of Earth's rotation), wind shear stress, wall friction, inflow volume and momentum (Gary W. Brunner, 2016a; S. Neelz, 2009).

The two-dimensional SWEs do not have an analytical solution and, hence, numerical methods are employed to solve these equations. The numerical approach used to solve these equations can further categorize these models as solved based on Finite difference, Finite element and/or Finite volume methods (Gary W. Brunner, 2016a; S. Neelz, 2009; J. Teng et al., 2017). With respect to time discretization, the models can be explicit (*i.e.* individual units independent of entire domain computed at any time step) or implicit (*i.e.* entire computation domain be solved at each time step) (S. Neelz, 2009; J. Teng et al., 2017). The computation grid in these models can be either structured (*i.e.* rectangular) or unstructured (*i.e.* triangular) (J. Teng et al., 2017).

Further discretization schemes are introduced to overcome modeling challenges such as prediction of flood wave location and discontinuities (*i.e.* shocks) (Kvočka et al., 2017; S. Neelz, 2009). These schemes are commonly termed as shock capture schemes. Some of the most commonly used schemes are Total-Variation Diminishing (TVD) scheme (Kvočka et al., 2017), MacCormack method, Monotonic Upstream-centered Schemes for Conservation Laws (MUSCL) based on the Godunov approach, and Lax-Wendroff method (S. Neelz, 2009; E.F. Toro, 2001).

Two-dimensional hydrodynamic models have now become a common tool for flood modeling. These models accurately mimic the hydrodynamics of fluvial systems to a large extent and are capable of modeling velocities, water depths,

flood inundation extents, etc. (Néelz & Pender, 2013). However, these models are computationally more expensive (J. Teng et al., 2017), cannot represent channel-bend induced secondary circulation *i.e.* velocity currents generated transverse to flow direction as a result of unequal forces due to curvature or confluence of streams (Demissie, Soong, Bhowmik, Fitzpatrick, & Maxwell, 1986) and, unlike 1-D models, are not applicable to large scale systems of the order  $10^2$  km (Hodges, 2014).

### 2.2.3 3-D Hydrodynamic Models

Three-dimensional hydrodynamic models are based on the Navier-Stokes equations, which describe a fluid's hydrodynamics in 3-D. The compact form of these equations, for an incompressible fluid in the x-direction, is presented below:

$$\begin{array}{l} \text{Momentum} \\ \text{Equation} \end{array} \quad \frac{\partial u_i}{\partial t} + u_j \frac{\partial u_i}{\partial x_j} = \frac{-1}{\rho} \frac{\partial p}{\partial x_i} + \nu \frac{\partial^2 u_i}{\partial x_j \partial x_j} + g_i \quad (5)$$

$$\begin{array}{l} \text{Continuity} \\ \text{Equation} \end{array} \quad \frac{\partial u_i}{\partial x_i} = 0 \quad (6)$$

Where,

u = Velocity

$\rho$  = Fluid Density

p = Pressure

g = Gravitational acceleration

t = Time

The momentum equation is based on Newton's law of motion ( $\mathbf{F}=\mathbf{m}*\mathbf{a}$ ), while the continuity equation assumes incompressible fluid (White, 1991). Three-dimensional models can be broadly categorized as (i) Eulerian (grid-based) and

(ii) Lagrangian (particle-based) models (J. Teng et al., 2017). Particle-based approaches such as Smoothed Particle Hydrodynamics (SPH), are gaining more popularity as they don't need spatial discretization and can represent features smaller than grid sizes (Richards, Dove, Cleary, & Prakash, 2004).

Three-dimensional hydrodynamic models are usually applied to short river stretches to investigate specific hydrodynamic issues such as vertical turbulence, vortices (J. Teng et al., 2017), secondary circulation, bed mobilization, bank erosion, etc. (Hodges, 2014). The biggest downside of 3-D models is that they are complex; computationally expensive and have a larger scale limitation than 2-D models (*i.e.* <1 km) (Hodges, 2014; J. Teng et al., 2017; Zhang et al., 2018).

## **2.3 Terrain based Flood Modeling Approaches**

Terrain based approaches are non-physics-based approaches for modeling floods by employing methods that use topographic information obtained from Digital Terrain Models (DTMs) and simplified fluid mechanics to model flooding extents (Zhang et al., 2018). These models are also referred to as 0-D models (Pender, 2006). Their advantage is that they yield approximately satisfactory results for studies whose objectives are flood risk assessment, delineating inundation maps and land use planning with extremely low computational expense when compared with hydrodynamic modeling approaches (Néelz & Pender, 2013; S. Neelz, 2009).

Some of the terrain-based models are discussed below.

### **2.3.1 Rapid Flood Spreading Model (RFSM)**

The Rapid Flood Spreading Model (RFSM) was developed with the functional objectives of having a small runtime, appropriate grid size for estimation of economic damages, relatively accurate representation of flow processes, ability to run under different boundary conditions, numerical stability, and reliability

for economic risk assessment (Willingford, 2006). The developed model spreads flood volumes, discharged as a result of overtopped flood defenses, into floodplains based on the topography of the flood plains. The flood plains are divided into zones called Impact Zones (IZs) representing topographic depressions. The model spreads the flood by filling up the IZs adjacent to the breached defense section and spill the excess discharge to the neighboring IZ. This process of fill and spill is repeated as long as the discharge is in excess. The flood is considered to have reached its final state when no IZ has excess volume left (Gouldby, Sayers, Mulet-Marti, Hassan, & Benwell, 2008). In recent efforts to improve the model, the flood spreading algorithm was revised to be more representative of physical processes, such as dynamic effects while filling and friction effects (not considered in the original model) while spreading. These modifications have made the model more realistic and accurate yielding results comparable to results from hydrodynamic models (Julien Lhomme et al., 2008).

### **2.3.2 Teng Vaze and Dutta Inundation Model**

The Teng Vaze and Dutta floodplain inundation model was developed in 2013 (J Teng, Vaze, & Dutta, 2013) under efforts to establish a simplified methodology for flood inundation based on LiDAR DEM in order to have a quick assessment. The model takes into account LiDAR DEM, climate and soil hydraulic information to estimate flood inundation, volume and flow depths (J Teng et al., 2013). This model delineates floodplain inundation by using either of the following two inputs: (i) River Stage (Observed or Analytical) & Rating Curve; (ii) Overbank flow volume (Simulated) (J. Teng, Vaze, Dutta, & Marvanek, 2015). The model is based on the “Planar Method” or “Bathtub Method” (Priestnall, Jaafar, & Duncan, 2000). Under this approach, the model builds a database of planes representing water surface intersecting the DEM with rising river stage; a relationship between stage, overbank flow volume and



inundated area is established to estimate the extent of inundated floodplain. Dead storages are modelled as depressions in the DEM which are not connected to a river system and water stored is depleted through infiltration and evaporation to keep the model realistic (J. Teng et al., 2015). This model gives reasonably good estimates of flood inundation and saves computational time as compared to hydrodynamic approaches.

### **2.3.3 Height Above Nearest Drainage Model (HAND)**

Height Above Nearest Drainage model or simply HAND model is a drainage normalized form of a DEM (Nobre et al., 2011). This normalization is achieved by the HAND algorithm which first creates a hydrologically coherent DEM with flow path definition and stream delineation, and then produces a nearest drainage map. This map is then used to create the HAND raster by subtracting the elevation of each cell of the DEM from the elevation in the nearest stream cell (Nobre et al., 2011; Zhang et al., 2018). Flood inundation extents can be modelled with the HAND Contour method. HAND Contours are simple contour lines drawn for a HAND model (*i.e.* smooth polylines connecting points having same height from the nearest drainage). The HAND contour map can be utilized for modeling flood extents (Nobre et al., 2016). Stage data from hydrodynamic modeling or observations are coupled with the HAND Contour map; inundation extents are delineated based on cells that have HAND values smaller than the stage (Nobre et al., 2016; J. Teng et al., 2017; Zhang et al., 2018). Some limitations of this model are that it does not account for temporal dynamics of floods, its dependency on stage information and over-estimation of inundation extents in streams further from the flood wave (Nobre et al., 2016).

## **2.4 Recent Developments in Flood Modeling**

Flood modeling has remained an area of continuous development over the past two decades due to increasing number of events, uncertainty associated with available modeling techniques and precision at the cost of computational expense (J. Teng et al., 2017; Ticehurst, Dutta, Karim, Petheram, & Guerschman, 2015).

Empirical models are data-driven models, but historical data quality is often questionable. Further continuous data acquisition requires manpower and regular gauging station maintenance. This limitation has now been overcome with advances in remote sensing techniques which have become a handy tool in modern flood modeling techniques (J. Teng et al., 2017). For instance, satellite imagery based on Synthetic Aperture Radar (SAR) system is being used for modeling floods (Clement, Kilsby, & Moore, 2018). SAR systems emit radar pulses and returns are captured by the satellite. Returns from water smooth water surfaces to the satellite are minimal, this enables good delineation of flood extents. However, water surface roughening due to winds, turbulence, vegetation, etc. can lead to scattering of signals and ultimately inaccuracies in modeling (Clement et al., 2018; J. Teng et al., 2017). However, new and improved technologies in satellites with better sensors and improvements in data mining algorithms is bridging the gaps.

In hydrodynamic models, recent efforts have been focused on improving accuracy and reducing computational time. These efforts have led to not only improvements in individual models but also to new approaches where a combination of different spatial dimension models is being used such as 1-D combined with 2-D etc. (Gary W. Brunner, 2016a; Liu, Qin, Zhang, & Li, 2015; J. Teng et al., 2017). For 1-D hydrodynamic models this approach of combining them has been the highlight of recent advancements (Liu et al., 2015). One-dimensional models can be combined with 2-D models in a variety

of ways depending upon the objective of modeling however, two methods are commonly used. The first method involves stretching the domain of the 1-D and 2-D models to create an overlapping region and then setting up coupling of the two models in this area. The second method involves the linking of the two models at the junction of the individual model domain; the linkage is established on the principle that the water surface elevation and discharge computed by each model individually (*i.e.* 1-D and 2-D) should be equal at this junction (Liu et al., 2015). Other linking methods include lateral, longitudinal and vertical linkages (S. Neelz, 2009), with flow exchanges between different model domains bounded by certain restrictions such as no momentum exchange between floodplain and main channel, ignoring backflow from floodplain to channel, one dimensional flow assumption within main channel until bankfull condition and then 2-D flow conditions for floodplain (J. Teng et al., 2017). However, different linkage techniques and imposed limitations result in varied results; this variation is now the focus of contemporary research (Néelz & Pender, 2013; J. Teng et al., 2017).

Two-dimensional hydrodynamic models have received a greater research attention with regards to numerical techniques for solving the governing equations and shock (discontinuities) capturing algorithms. Among the various numerical techniques available such as Finite element, Finite difference and Finite volume methods, the latter has earned much recognition from the research community (Caleffi, Valiani, & Zanni, 2003; S. Neelz, 2009; J. Teng et al., 2017). The reason behind the success of Finite volume method lies in its ability to handle complex geometry of elementary volumes, structured and unstructured meshes, ability to conserve mass & momentum and conceptual simplicity of the method (ALCRUDO, 2004).

Further in 2-D models, topographic discontinuities (*e.g.* extreme slopes, large roughness, sharp geometrical changes etc.) present a big challenge in accurate

modeling of the hydrodynamics (Eleuterio F. Toro & Garcia-Navarro, 2007). The shallow water equations (SWEs) used for 2-D modeling have hyperbolic property, hence, their numerical solution experiences unphysical oscillations which increase over time step (J. Teng et al., 2017). Many methods have been developed to overcome the issue of shocks in hydrodynamic modeling. Godunov-type methods, first order discretization schemes, commonly used for this purpose, rely on non-oscillatory data reconstructions and solving the Riemann's problem ("governing equations subject to special initial conditions consisting of two constant states separated by a discontinuity" (Eleuterio F. Toro & Garcia-Navarro, 2007)). Hyperbolic systems such as shallow water equations have exact solution for Riemann's problem, however, practically approximate solutions provide simplicity and efficiency. Nonlinear second order Godunov type discretization schemes have also found successful application in shock capturing algorithms. These schemes are commonly known as Total Variation Diminishing (TVD). TVD schemes capture large solution gradients, or discontinuities, with little or none spurious oscillations (Eleuterio F. Toro & Garcia-Navarro, 2007).

One recent advancement in spatial discretization of 2-D models is the introduction of flexible meshes (*i.e.* network of triangles and quadrilaterals) whose size can be altered from fine to coarse depending on modeling requirements. This type of spatial discretization is computationally effective as it employs a fine mesh around complex areas and rather coarse mesh around large areas with minimal changes (J. Teng et al., 2017).

Time discretization in 2-D models is also a very relevant consideration from accuracy perspective (*e.g.* smaller time interval yields accurate results but computation time is increased). With respect to time discretization numerical techniques are implicit and explicit. Explicit techniques are more popular however, they too need to comply to model's numerical stability requirements,

these requirements are controlled by Courant Friedrichs-Lewy condition ( $\frac{\text{Flood wave Velocity} * \text{Time Step}}{\text{Cell size}} \leq 1$ ) (J. Teng et al., 2017).

In 3-D hydrodynamic modeling, the role of Smoothed Particle Hydrodynamics (SPH) is key to its development. Richards et al. (2004) showed that SPH could be used for flood modeling. Recently Prakash et al. (2014) employed an SPH based model for the simulations of a dam failure scenario thereby proving the applicability of SPH for rapidly varying flow cases. Particle-based methods (*i.e.* Lagrangian) have advantage over grid-based methods (*i.e.* Eulerian), such as higher accuracy, better representation of features smaller than grid sizes and non-diffusive prediction of convection (J. Teng et al., 2017).

## **2.5 1-D versus 2-D Hydrodynamic Models**

Hydrodynamic modeling is the most common approach for flood modeling since it helps simulate the physical processes and presents an accurate picture of the event. However, selection of the modeling approach and resolution is a significant part of the process. One-dimensional models are computationally efficient yet less accurate than two-dimensional models (S. Neelz, 2009; J. Teng et al., 2017).

Flood scenarios marked by extreme spatial variability and non-uniformity of flow present a great challenge in the application of 1-D models, such as urban flood modeling scenarios (S. Neelz, 2009). One-dimensional models are most suited in cases where the assumption for 1-D flows can be made reasonably, such as in the study by J. Lhomme, Bouvier, Mignot, and Paquier (2006) where a 1-D GIS-based model was applied to study deep flooding in narrow urban streets. One-dimensional models fall short at representing true hydrodynamics, such as lateral diffusion of flood wave and flow recirculation cases (such as bends). Moreover, 1-D modeling is subjective to cross-section spacing,

orientation and location as the topography is discretized over the cross-section rather than being a continuous surface (J. Teng et al., 2017).

Two-dimensional flood modeling has gained a lot of popularity among engineers and researchers primarily due to its accuracy in simulating the physical processes despite being computationally more intensive. Syme (2006) argued the suitability of 2-D models owing to their ability to represent local changes in velocities and flow depths as well as flow direction. These models do not need a predefined flow path and make better use of the topographic information unlike 1-D models. S. Neelz (2009) notes that 2-D modeling is an appropriate approach when modeling urban and coastal areas. Kvočka et al. (2017) have recently applied the 2-D flood modeling approach to steep rivers. Cases where wide floodplains are to be modelled or higher accuracy in determination of velocities, and water depths, are required 2-D models should be employed (Gharbi, Soualmia, Dartus, & Masbernat, 2016; J. Teng et al., 2017).

### **3 Methodology**

The main objective of this work is to determine linkages between topographical and hydraulic parameters in order to identify critical locations within a steep river. Thus, hydrodynamic modeling appears to be an appropriate approach to carry out this study since the nature of the work demands accuracy in the determination of hydraulic parameters.

This chapter explains in detail the methodology adopted for the study.

#### **3.1 Hydrodynamic Modeling**

Hydrodynamic modeling, which is based on the simulation of actual physical processes, is adopted for the study. Simpler approaches such as, the Empirical models and Terrain based models (also referred to as 0-D models) are based on the simplification of physical processes, observational data (which is bound to have uncertainties) and sometimes have model transferability issues. Hence, it is deemed appropriate to adopt a physical-based approach to determine the linkages between topography of the river and its hydraulics.

After selecting the modeling approach, the next question arises regarding the spatial dimensionality of the model. For this study, 2-D modeling was selected since flow in the floodplains is predominantly two-dimensional. Moreover, accurate determination of velocities, flow depth and water surface elevations are the focus of this study. The 2-D approach is, however, computationally intensive as compared to 1-D modeling, but it meets the output requirements of the work *i.e.* more precise fluid dynamics in lateral dimensions.

##### **3.1.1 Modeling package**

Many software packages, both commercial and open source, are available for 2-D hydrodynamic modeling. A summary of software packages based on review studies by J. Teng et al. (2017) is presented in Table 3-1:

Table 3-1 Summary of different software packages available for 2-D modeling

Developer	Package	Status
BMT	TUFLOW Classic 2D, TUFLOW HPC, TUFLOW FV	Commercial
Cardiff University	DIVAST, DIVAST-TVD	Research
DELTARES	SOBEK Suite	Commercial
Electricité de France	TELEMAC 2D	Open Source
DHI	MIKE21	Commercial
Nottingham University	TRENT	Research
University of California	BreZo	Research
US Army Corps of Engineers	HEC-RAS	Free

HEC-RAS is one of the most commonly used packages since it is free and has a user-friendly interface. Therefore, HEC-RAS was selected to execute the modeling process. Latest version of HEC-RAS (v. 5.0.7), released in March 2019, was used in this study.

### 3.1.2 HEC-RAS

HEC-RAS is developed by U.S. Army Corps of Engineers Institute of Water Resources Hydrologic Engineering Center. The package is capable of performing 1-D, 2-D and combined 1-D/2-D hydrodynamic modeling. The 2-D modeling in HEC-RAS solves the 2-D Saint-Venant equations or the 2-D Diffusion Wave equation (Gary W. Brunner, 2016b). The 2-D solver of HEC-RAS uses Implicit Finite Volume technique for improved stability. Further the algorithm is capable of handling sub-critical, super critical and mixed flow (*i.e.* flow at critical depth and transitions marked by hydraulic jumps) (Gary W.



Brunner, 2016b). Computational meshes in HEC-RAS are designed to be unstructured but structured meshes are also possible; a cell can have a maximum of eight faces. The program uses the terrain for flood computations and mapping. This means that some cells can be partially wet/dry instead of all wet or all dry thus, making the modeling process realistic. Moreover, the program can make use of multiple processors of a computer, hence, reducing computation time.

Some limitations associated with the 2-D modeling in this package include inability to carryout sediment transport analysis, bridge modeling in 2-D flow areas and water quality modeling (Gary W. Brunner, 2016b).

### **3.2 Idealized Rivers**

Idealized rivers with different constant bed slopes were created for hydrodynamic modeling. The concept of idealized river parameters was previously used by Kvočka et al. (2017) in their flood inundation modeling studies for steep rivers. In the current approach, idealized rivers were created from an existing river. For this purpose, a steep river catchment was selected and its Digital Elevation Model (DEM) was manipulated to achieve desired slopes along the reach length to be modeled. However, in order to study the effects of bends/curvature and cross-sectional changes, the cross-sectional geometry was not disturbed and only bed slope was changed. The slope range considered in this study is from 4% to 5.5% at an increasing interval of 0.5%.

#### **3.2.1 River Selection**

The river selected for idealization was river Byrteåi in Tokke municipality, Telemark, Norway. The river has a catchment area of 49.3 km<sup>2</sup>. The river has a small average annual discharge of 2.59 m<sup>3</sup>/s with mean flood discharge of 36 m<sup>3</sup>/s. The river length is 20.5 km with a river gradient of 4.5% (45.9 m/km)

(NVE), catchment report appended as **Appendix A**. The river drains into lake Byrtevatn. The catchment is shown below in Figure 3-1.

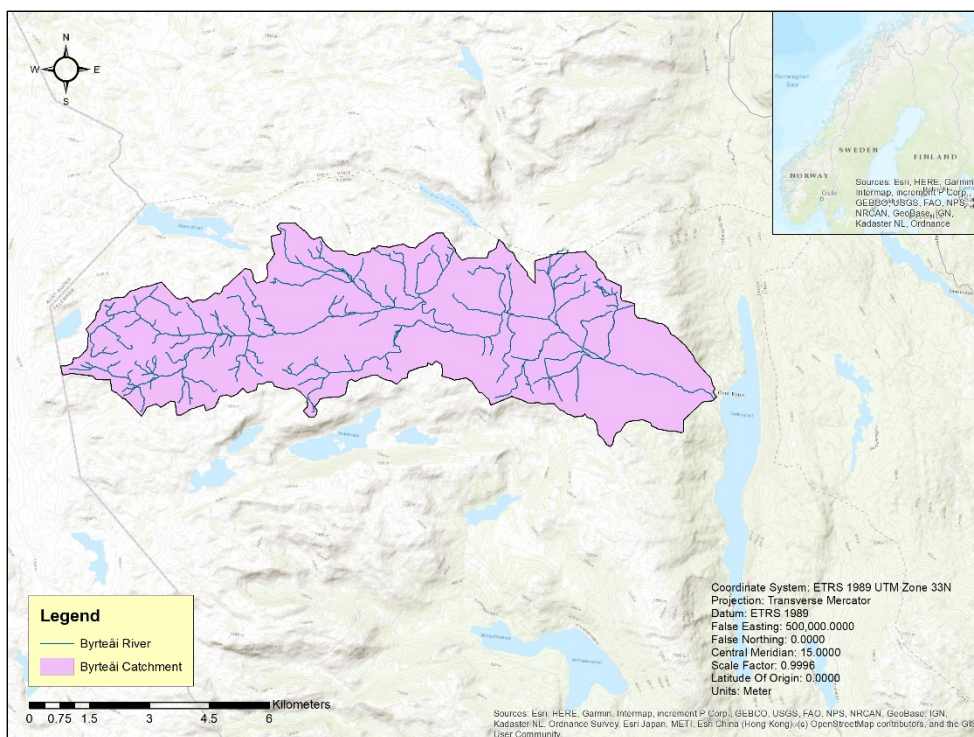


*Figure 3-1 Byrteåi River catchment, Tokke, Telemark*

The river had an active measuring station owned and maintained by Statkraft from January 1, 1967 to December 31, 2017. Time series for the due period is available for the measuring station under NVE’s Hydra II Project (NVE Hydra II). A short time series analysis from 2000 to 2017 was carried out to determine average annual discharge of the river, Figure 3-2. The station recorded a peak flood of 198.16 m<sup>3</sup>/s on July 30, 2009. This flood is well above NVE’s Q<sub>200</sub> calculations for the catchment which is 94.2 m<sup>3</sup>/s (**Appendix A**).

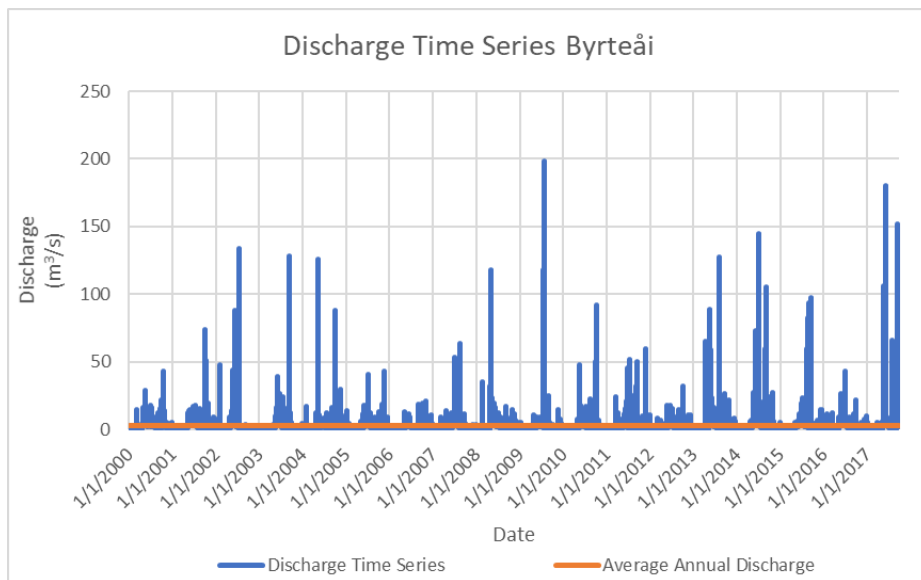


*Figure 3-2 Time Series of Byrteåi river. Average annual discharge 2.59 m<sup>3</sup>/s.*

### **3.2.2 Digital Elevation Model**

The DEM for the selected catchment was created from point cloud LiDAR data. The data was obtained from Høydedata (Norwegian Mapping Authority). The LiDAR point cloud data used, was collected as part of National Digital Elevation Model Project in 2017.

The point density of the data was 5 points/m<sup>2</sup>. Using this data set, a 1x1 m bare earth DEM was created in ArcMap (v. 10.6).

The LiDAR point cloud data was initially obtained in LAZ format, which was then converted to LAS format before it could be processed in ArcMap. The LAZ format being open source and having greater data compression abilities makes data storage and distribution easy as compared to LAS format and, therefore, is a preferred data storage format.

Since HEC-RAS has limitation in modeling bridges in 2-D environment, therefore, the point cloud data was refined for ground points only; bridges and noise (random inaccuracies in terrain values) were ignored in the creation of the raster. The LAS dataset was first converted into Triangulated Irregular

Network (TIN), which was then converted to raster format. The DEM was processed for gap filling and sinks before using it for modeling and manipulation. Figure 3-3 shows the processed DEM in raster format.

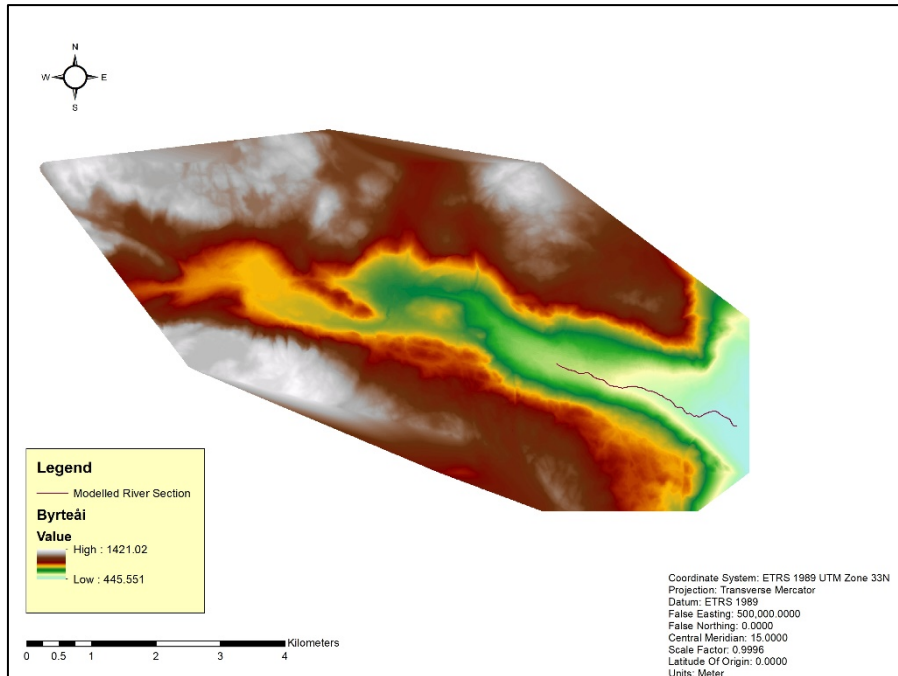


Figure 3-3 Digital Elevation Model of Byrteåi River Catchment

### 3.2.3 Terrain Manipulation

RAS Mapper tool in HEC-RAS allows to manipulate terrain by creating river cross-sections. The user is can define the width of the cross-sections as per their requirements while staying within the extents of the DEM. These cross-sections can then be edited to desired terrain values in the geometry editor tool in HEC-RAS. RAS Mapper then interpolates the terrain between the edited cross-sections. This modified part of the terrain can be exported as a raster dataset. This raster dataset is then superimposed on the original DEM raster dataset to create a new terrain which consists of user defined geometry. (Gary W. Brunner, 2016b).

The river length selected for manipulation was 3,150 meters. Equidistant cross-sections were defined at 50 meters spacing, with a cross-sectional width of 100 meters (50 meters on either side of the river centerline).

Figure 3-4 shows the original river section that was considered for manipulation of the terrain along with the equidistantly spaced cross-sections. Figure 3-5 shows the situation after the terrain was modified. A depression in DEM can be seen, which is due to difference in elevation once manipulated the sections. Figure 3-6 shows the river profile of before (left hand side) and after (right hand side) terrain manipulation, the idealized river has a constant slope throughout the length. Figure 3-7 shows that during terrain manipulation process the river cross sectional geometry was not altered besides the slope change.

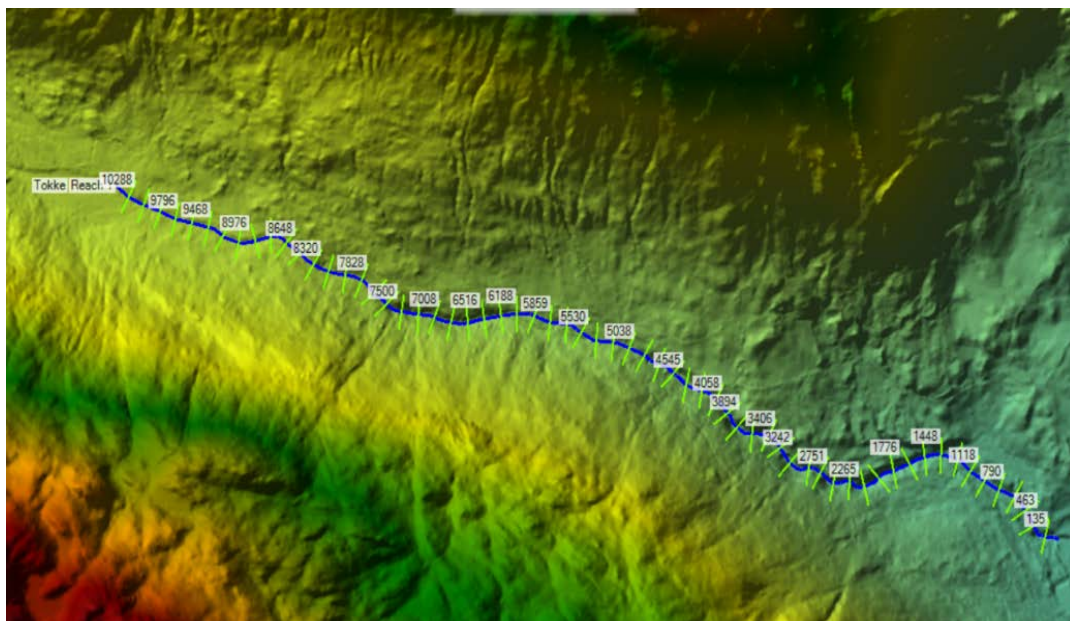


*Figure 3-4 Original River Section considered for Terrain Manipulation*



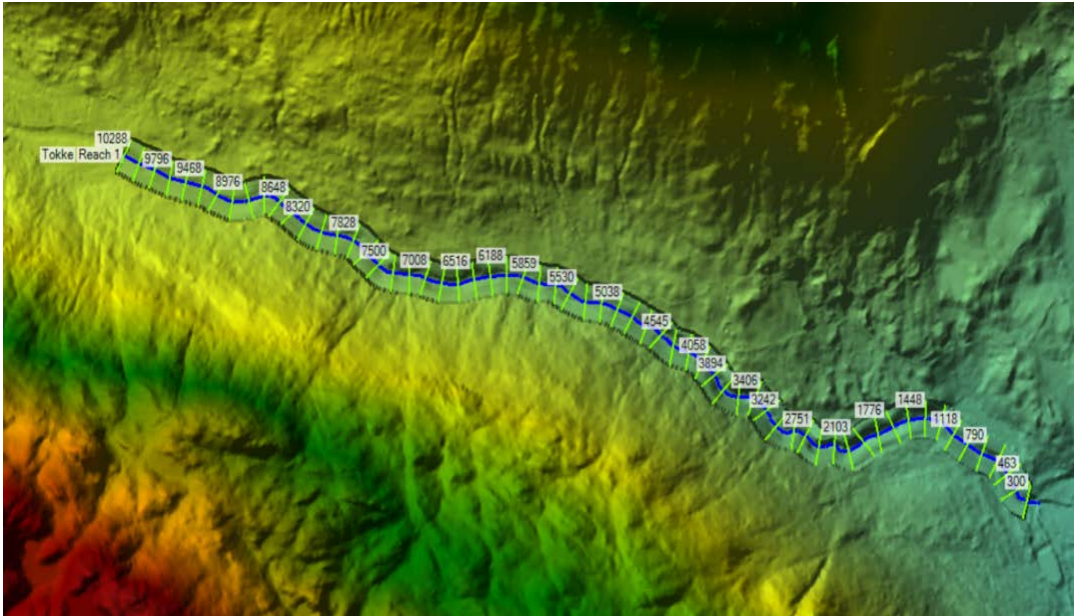


Figure 3-5 River section after Terrain Modification at a slope of 4.5%

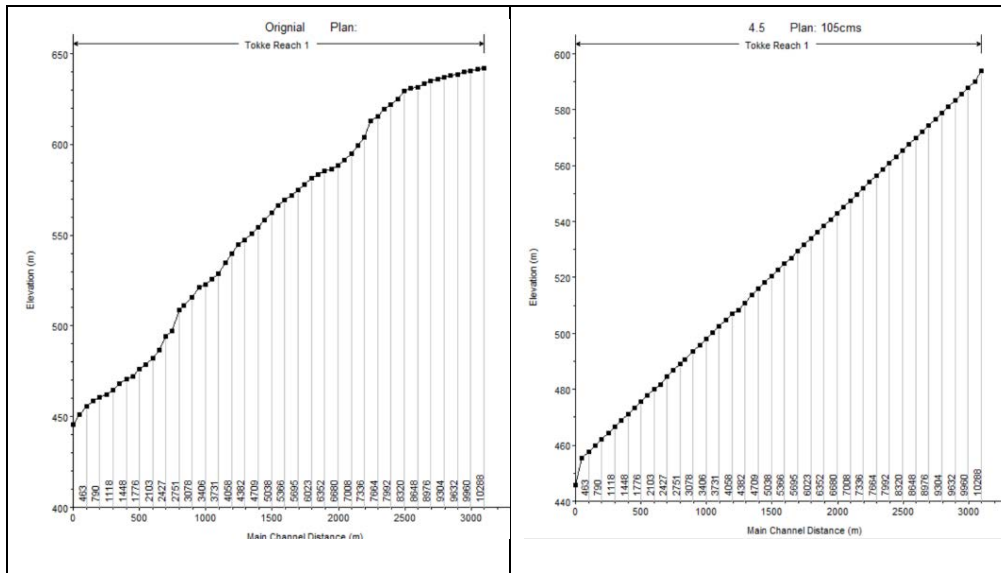
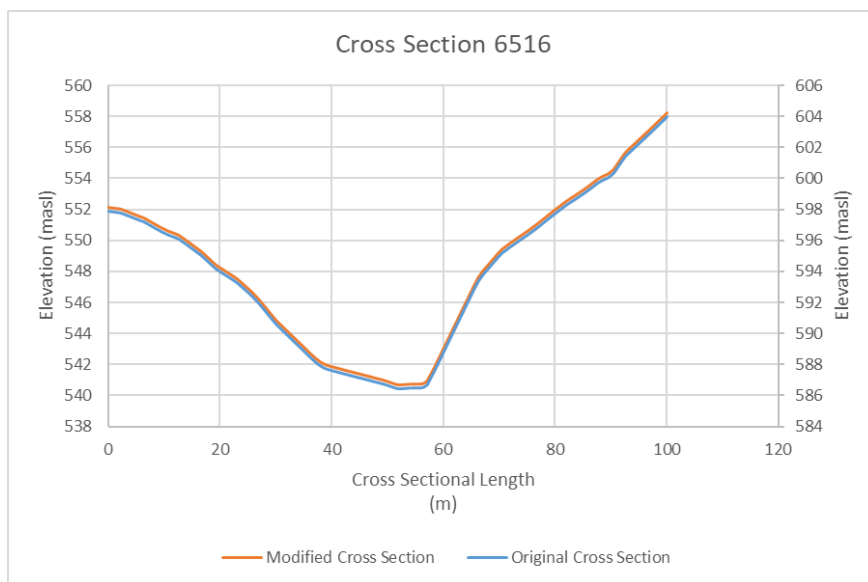


Figure 3-6 Original (Left) and Modified River (Right). The modified river has 4.5% slope



*Figure 3-7 Original and Modified Cross-Section*

### 3.3 Parameters for the Study

Hydraulic and Topographic parameters considered in the study are listed in Table 3-2. This section covers the definition of such parameters in the context of hydraulic modeling and monitoring river response to hydrologic and topographic changing conditions.

*Table 3-2 List of Parameters for the Study*

<b>Sr. No</b>	<b>Parameter</b>	<b>Symbol</b>	<b>Parameter Type</b>
1	Bed Slope	S	Topographic
2	Channel Width	W	Topographic/Hydraulic
3	Relative Section Width	$W_{xs}$	Topographic/Geometric
4	Lateral Confinement	$W_r$	Topographic
5	Channel Bends	$\underline{B}$	Topographic

<b>Sr. No</b>	<b>Parameter</b>	<b>Symbol</b>	<b>Parameter Type</b>
6	Discharge	Q	Hydraulic/Hydrologic
7	Flow Depth	D	Hydraulic
8	Flow Velocity	V	Hydraulic
9	Shear Stress	S	Hydraulic
10	Stream Power	SP	Hydraulic

It was also considered to study sediment transport. However, the lack of sediment data (*e.g.* material type, grain size, sediment volume, erosion volume, etc.) for the river used for idealization, the complexity of sediment transport processes in steep rivers and the limitation of the selected modeling package (HEC-RAS) to carryout 2-D sediment transport analysis induced to disregard morphodynamic analysis till future work.

### **3.3.1 Bed Slope (s)**

Bed slope is defined as the inclination of the river bed and is measured as the drop in elevation per unit length of the river. For instance, a 4% bed slope is a drop of 40 m over 1 km river reach. The idealization of this parameter, as well as the data used is furtherly described in **section 3.4.1**.

### **3.3.2 Channel Width (w)**

In this study, channel width is the lateral extent of water flow along a river/stream. Channel width is not a constant parameter along the length of the stream as it is a function of river discharge, slope and river bed roughness (Finnegan, Roe, Montgomery, & Hallet, 2005).



### **3.3.3 Relative Section Width ( $W_{xs}$ )**

Relative section width is a parameter defined in this study to collect information regarding contractions and expansions of cross-sections along the length of the river. This parameter is defined as follows:

$$W_{xs} = \frac{W_n}{W_{n-1}} \quad (7)$$

Where,

$W_{xs}$  = Relative Section Width

$W_n$  = Width of  $n^{\text{th}}$  cross-section

$W_{n-1}$  = Width of previous cross-section (or  $n-1^{\text{th}}$  cross-section)

$W_{xs} < 1$  represents contraction in flow path while  $W_{xs} > 1$  represents expansion in flow path.

### **3.3.4 Lateral Confinement Index ( $W_r$ )**

Lateral confinement is the confinement of the river in the longitudinal direction. It is defined as the percentage of the banks which is not in contact with the flood plain but in contact with the hillslope (Rinaldi et al., 2015). It is calculated as confinement index ( $W_r$ ) which is the ratio of flow width in the flood plains including the channel and the width of the channel at average discharge condition (Moraru, 2017; Rinaldi et al., 2015). Based on this index, channels can be categorized as (i.) high confinement ( $1 < W_r < 1.5$ ), (ii) medium confinement ( $1.5 < W_r < 5$ ) and low confinement ( $W_r > 5$ ) (Rinaldi et al., 2015).

In this study, the channel width at average discharge conditions was determined at a discharge of  $5 \text{ m}^3/\text{s}$  at each of the defined cross-sections. This width was then used to calculate lateral confinement index ( $W_r$ ) after determining the flow widths at flood discharges.

### 3.3.5 Channel Bend (B)

Channel bend is the deviation of channel course from the straight line along the channel axis. The overall effect of channel bends is reported in terms of sinuosity. Here in this study, bends are reported in terms of bend angles measured individually by fitting an arc to the bend and measuring the central angle of the arc as the bend angle, Figure 3-8.

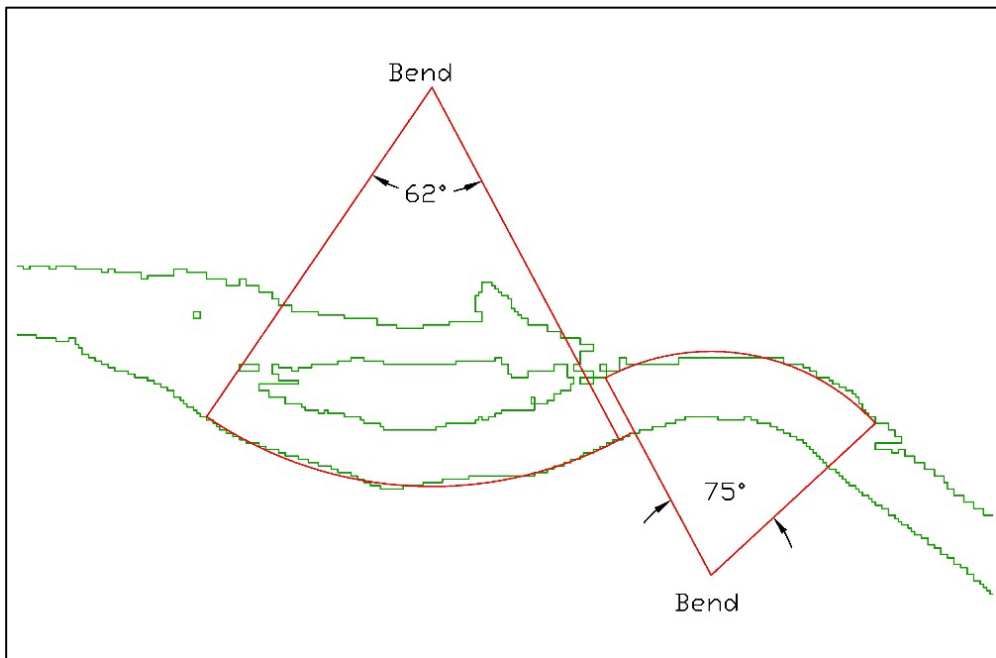


*Figure 3-8 Bend angle measurement methodology in the study*

### 3.3.6 Discharge (Q)

Discharge is the rate of flow of water through any cross section, typically expressed in  $\text{m}^3/\text{s}$ . The idealization of this parameter, as well as the data used is furtherly described in **section 3.4.2**.

### 3.3.7 Flow Depth (D)

Flow depth is defined as the height of water above the stream bed across any cross-section. The depth of flow is not constant all along the cross-section due to small variations in the river bed elevation from center of the river toward the

banks. In this study, flow depth will be obtained as an output from the hydrodynamic modeling.

### **3.3.8 Flow Velocity (V)**

Physically, flow velocity is the vector field used to describe the motion of fluid particles. In this study it will be obtained as an output from the hydrodynamic modeling. It is commonly expressed in m/s units.

### **3.3.9 Shear Stress (S)**

Shear stress is defined as the force exerted by water per unit area of the river bed or banks. It is expressed as (Gary W. Brunner, 2016a):

$$\tau_b = \gamma RS \quad (8)$$

Where,

$\tau_b$  = Bed Shear Stress (Pa)

$\gamma$  = Specific Weight of Water (9810 N/m<sup>3</sup>)

R = Hydraulic Radius

S = Energy line slope

In this study shear stress will be obtained as output from the hydrodynamic modeling.

### **3.3.10 Stream Power (SP)**

Stream power is defined as the ability to perform geomorphic work. It is a measure of the forces acting in a channel. It is a commonly used parameter for studying channel geomorphology and sediment transport (Bizzi & Lerner, 2015). It is calculated as follows (Gartner, 2016):

$$\Omega = \gamma QS \quad (9)$$

Where,

$\Omega$  = Stream Power (W/m)

$\gamma$  = Specific Weight of Water (9810 N/m<sup>3</sup>)

Q = Discharge

S = Channel bed slope

In this study stream power will be obtained as output from the hydrodynamic modeling.

### 3.4 Scenario Idealization

The process of scenario idealization was based on the two main input parameters *i.e.* slope (s) and discharge (Q). For slope four scenarios were idealized, further discussed in **section 3.4.1**, and corresponding to each slope scenario six scenarios for flood discharges were idealized, further discussed in **section 3.4.2**, this amounted for a total of 24 unique scenarios.

In this study, both slope and discharge are treated as discrete parameters in order to study their influence other parameters described in **section 3.3**.

#### 3.4.1 Slope Idealization

Rosgen (1994) classified rivers as steep in a slope range of 4% to 10%. Following the criteria laid down in literature, four slope scenarios were idealized for this study, ranging from 4% to 5.5% increasing at a constant interval of 0.5%. The purpose was to develop a strong correlation with other parameters reflecting the river response to changing conditions.

#### 3.4.2 Discharge Idealization

Steep rivers are characterized by low discharges as noted by Francesco Comiti and Mao (2012). The river Byrteâi also carries a low discharge ( $Q_{\text{avg}} = 2.59 \text{ m}^3/\text{s}$ ), as discussed in **section 3.2.1**, hence, the flood discharge scenarios were idealized from  $Q_{\text{Mean}} = Q_{\text{M}} = 30 \text{ m}^3/\text{s}$  to  $Q_{200} = 105 \text{ m}^3/\text{s}$ . A summary of the flood discharge cases tested is presented in Table 3-3:

*Table 3-3 Discharge scenarios considered for simulation*

<b>Flood Return Period</b>	<b>Discharge (m<sup>3</sup>/s)</b>
Q <sub>M</sub>	30
Q <sub>5</sub>	45
Q <sub>20</sub>	60
Q <sub>50</sub>	75
Q <sub>100</sub>	90
Q <sub>200</sub>	105

The idealized discharge values to corresponding return periods bear close resemblance to NVE's calculations for the corresponding return periods in the Byrteåi catchment although they are not exactly the same. A fixed interval of 15 m<sup>3</sup>/s was used to idealize these values in order to study the effect of discharge at a constant incremental rate. This is only logical as the study is based on idealized rivers and no actual data exists for such idealized cases.

### **3.5 Statistical Methods**

Various statistical methods were applied to analyze the data and determine correlations and interdependencies of hydraulic and topographical parameters. Statistical analysis was carried out using IBM SPSS Statistics (v. 25). The different statistical methods used are discussed below.

#### **3.5.1 Box Plots**

Box plots for different parameters were plotted in order to test the variation of data obtained for different parameters and identify the outliers. This helped in identifying unusual observations in data and rechecking the simulations at those points to inspect the cause of such results.

Box plots are created by drawing a box having a height equal to the difference between 75<sup>th</sup> and 25<sup>th</sup> Percentile of the data. The upper and lower datum is marked by data within 1.5 times the interquartile range (IQR). The interquartile range is determined as the difference between the third and first quartile. First quartile the middle value between the lowest value and the median while the third quartile is the middle value between the median and the maximum value (Weisstein). Points lying above or below the datum are termed as outliers.

### **3.5.2 Frequency Analysis**

Frequency analysis of parameters was carried out by plotting Histograms in order to see the distribution of data obtained from the analysis. This shall also help in sorting the parameters into various bands/classes.

### **3.5.3 Correlation Test**

Pearson correlation test was applied to the data to identify linkages between the hydraulic and topographic parameters. This test identifies the linear correlation between parameters in a range of -1 to 1, where “-1” means an inverse but perfectly correlated scenario and “1” means a direct and perfectly correlated scenario. “0” indicates that a linear correlation does not exist (Akoglu, 2018).

## 4 Simulations

Hydrodynamic simulations of the different idealized scenarios have been carried out in order to infer which parameters were more sensitive to changing conditions, thus, reflecting potential critical locations for further and more refined study. This chapter explains the model setup, input parameter and result extraction.

### 4.1 Model Set-up

The 2-D hydraulic model was set up in HEC-RAS (v. 5.0.7). In this section, the model set up is described in a stepwise manner.

#### 4.1.1 Terrain Creation

As explained in **section 3.2.2**, DEM was created in ArcMap and stored in raster format. The creation of idealized rivers through terrain manipulation has already been explained in **section 3.2.3**. The terrain model created in ArcMap was imported to HEC RAS mapping tool, *i.e.* RAS Mapper, where it was converted into a RAS Mapper compatible geometry format (Figure 4-1).

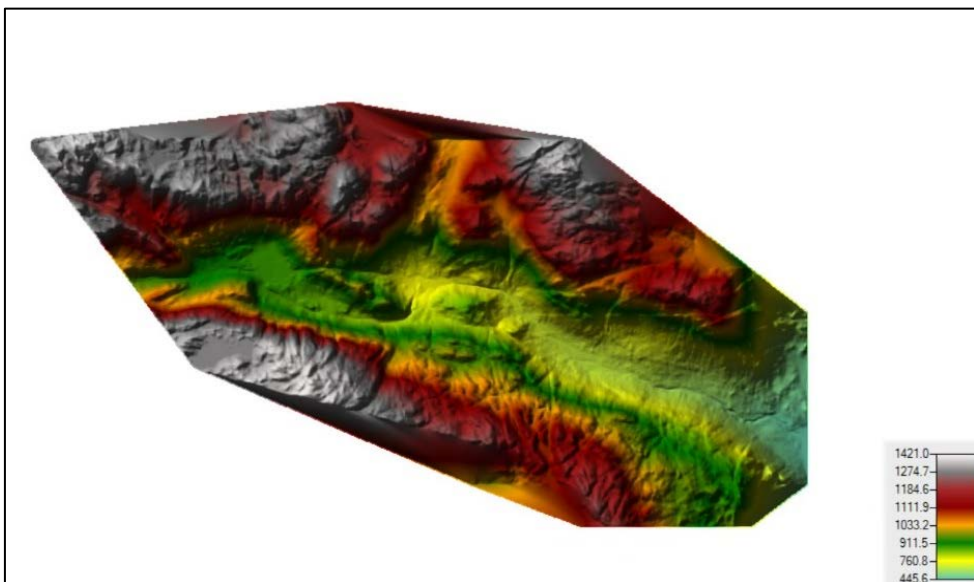


*Figure 4-1 Byrteâi River Catchment Terrain imported in RAS Mapper*

### 4.1.2 Geometry

Two-dimensional flow areas were defined along the portion of the river to be simulated. Initially, 3,150 m of river length was considered in the terrain manipulation phase. In order to keep the desired slopes constant along the river reach, some artificial drops at the start and end of the river reach under consideration were created. Furthermore, in order to optimize the computation time, the simulated river length was reduced to 2525 m. Figure 4-2 shows the simulated river section. The resolution of the 2-D flow area mesh was set to be 2x2 m. The computation grid generated from the flow area mesh was, consequently, also set as 2x2 m *i.e.* one computation point in each grid cell. The computation grid can be refined to a finer resolution over the 2-D flow area mesh *i.e.* creating multiple computation points within a single grid cell. The disadvantage of this refinement is computational expense. The HEC-RAS 2-D User Manual recommends to use a fine mesh for steep terrains in order to achieve greater accuracy in computations. Different mesh sizes were tried before choosing 2x2 m as the appropriate mesh size for simulations. Coarser mesh sizes tend to reduce computation time, but results were significantly less accurate. Finer meshes than 2x2 m, on the other hand, significantly increased the computational time and the results were not significantly different.



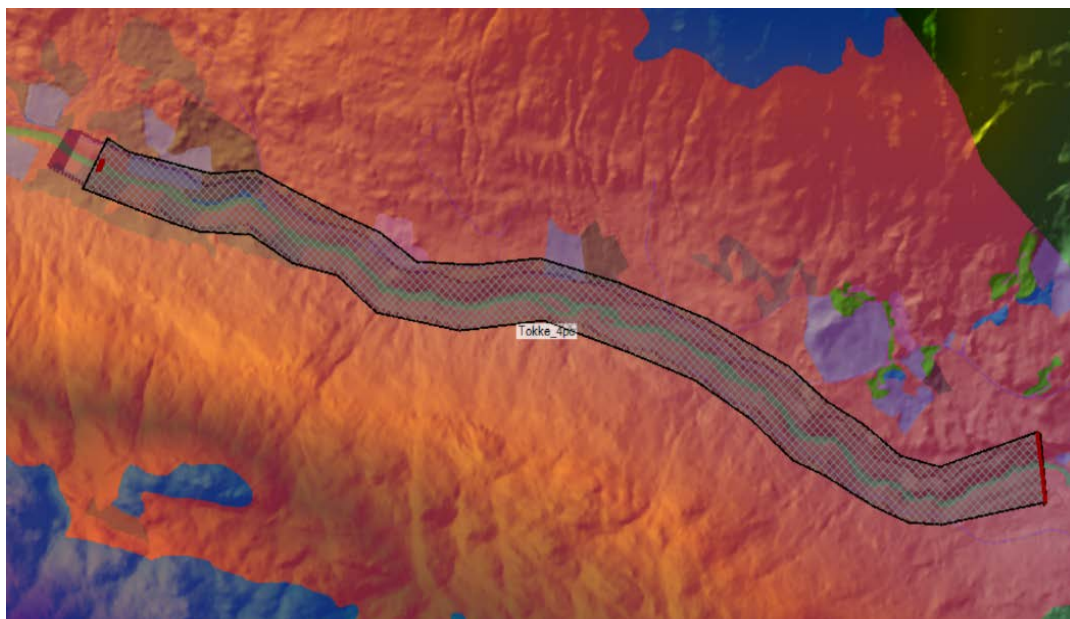


*Figure 4-2 2-D Flow Area Defined for Simulation*

### **4.1.3 Roughness Coefficients**

In two-dimensional hydrodynamic modeling, Manning's coefficient  $n$  is an important input parameter, as it is a quantitative representation of a channel's (bed and banks included) resistance to flow (Coon, 1998). Hence, its accurate estimation is essential as the resistance to flow influences the hydraulic parameters and the flow regime (sub-critical or super-critical) significantly. Accurate measurement or estimation of Manning's  $n$  in steep rivers is extremely difficult due to larger particle-size of bed material and complex hydraulics (*e.g.* step-pool morphology) (Marcus, Roberts, Harvey, & Tackman, 1992; Andrew C Wilcox et al., 2011).

In order to assign the roughness characteristics to terrain, land use maps, prepared by The Norwegian Institute for Bio-economy Research (NIBIO), were used. The land use of the catchment is presented in Figure 4-3. Most of the area corresponds to forest and open land. Close to the river the land use is characterized by forest, full grown soil and

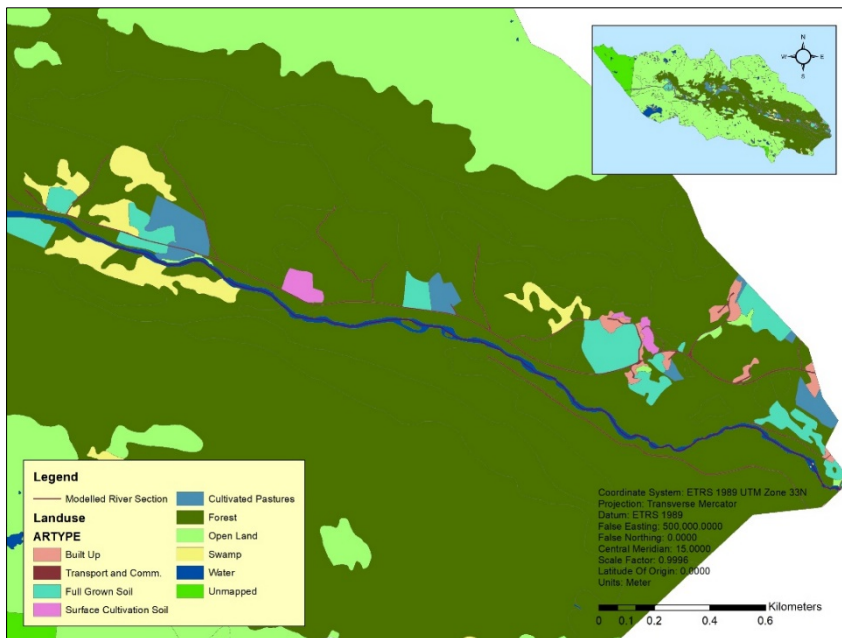


Figure 4-3 Byrteåi Catchment Land use Map

The values for Manning’s  $n$  used were adopted from HEC RAS 2-D User Manual (Gary W. Brunner, 2016b) and table published by Chow (1959). Table 4-1 presents the adopted values for Manning’s  $n$  in this study. The land use map was imported in the RAS Mapper as Manning’s layer with a pixel size of 1x1 m so that the resolution of the Manning’s layer is concurrent with the resolution of the underlying DEM.

Table 4-1 Manning’s  $n$  Values adopted for different land use features

Land use	Description	Manning’s $n$
Built up	Area that has been demolished or built up significant degree, as well as adjacent areas which in function is closely linked to settlement	10

<b>Land use</b>	<b>Description</b>	<b>Manning's <i>n</i></b>
Transport & Communication	Area used for transport, in mainly roads and railways.	0.04
Full Grown Soil	Area that is cultivated at regular plow depth, and which can be used for field crops or for meadow that can be renewed by plowing	0.045
Surface Cultivation Soil	Area that is mostly tidy and even surface, so that mechanical harvesting is possible	0.04
Cultivated Pastures	Inland area that can be used as pasture, but that cannot be harvested mechanically. Smallest 50% of the area shall be covered by grasses	0.035
Forest	Area with at least 6 trees per. acres that are or can be 5 m high	0.12
Open Land	Area resource mapped area that is not agricultural area, forest or marsh.	0.06
Swamp	Area with at least 30 cm thick peat layer as on the surface has the mark of marsh	0.06
Water	Lake and river	0.05
Not Mapped	Area that has unknown nature	0.12

#### **4.1.4 Boundary Conditions**

In HEC-RAS 2-D modeling, boundary conditions (BCs) are broadly classified into two main categories, namely internal and external BCs.

Internal boundary condition is a flow condition defined entirely inside the 2-D flow area. In HEC-RAS, an internal boundary condition is often a flow hydrograph. The internal boundary condition was defined as the upstream inflow boundary condition in the model, for which an idealized flow hydrograph (furtherly discussed in **section 4.1.4.1**) was entered.

External boundary condition, on the other hand, is defined as the flow condition outside the 2-D flow area. There are five ways to define the external boundary condition in HEC-RAS. These include Stage Hydrograph, Flow Hydrograph, Rating Curve, Normal Depth and Precipitation (Gary W. Brunner, 2016b). For this study, Normal Depth was selected as the external boundary condition since data for any of the other four conditions was unavailable. The Normal Depth condition is defined as the downstream boundary condition. The input for this condition is the friction slope value, which is used in the Manning's equation to compute the Normal Depth. In steady state flow (*i.e.* flow condition where no change occurs over time), the friction slope is equal to the bed slope therefore, bed slope was entered as the input for this condition.

##### **4.1.4.1 Flood Discharge**

After setting up the rest of the modeling parameters, flow conditions were defined. This comprised of a flood hydrograph, corresponding to the internal (namely inflow in the model) boundary condition. In HEC-RAS, a longer hydrograph takes longer time to simulate and is computationally expensive.

In order to save computation time, a Restart file was created. A Restart file can be generated after a scenario has been modeled and this can be used as the

initial condition of the river for the next simulation with different inflow boundary conditions. For each slope scenario, six different discharge scenarios were idealized so in order to make the simulations computationally less expensive, a 7-hr long low flow hydrograph was run and stored as a Restart file (Table 4-2 and Figure 4-4).

*Table 4-2 Hydrograph Data showing initial flow conditions in the river*

<b>Simulation Time</b>	<b>Discharge (Q) m<sup>3</sup>/s</b>
00:00	1
01:00	2
02:00	3
03:00	4
04:00	5
05:00	5
06:00	5
07:00	5

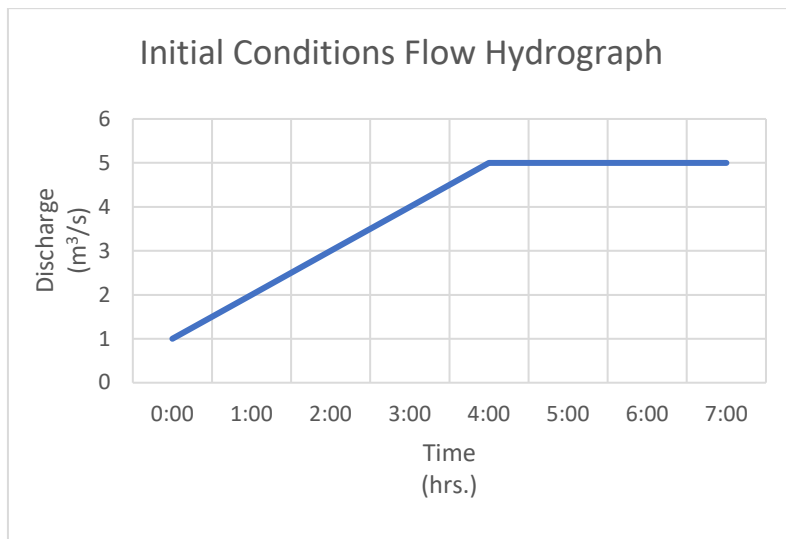


*Figure 4-4 Flow Hydrograph showing Initial flow Conditions in the River*

An example of flow condition in the channel is shown in Figure 4-5. Figure 4-6 shows the different flood hydrographs input for various scenarios. As the flood discharge parameter was discrete in nature, it was found through simulations that running the hydrograph for a long duration of time did not change any hydraulic parameters. Therefore, each flood discharge scenario was simulated for a period of 2 hours, this time was found to be sufficient to fill up the channel and achieve steady flow condition with a reasonable computation time.

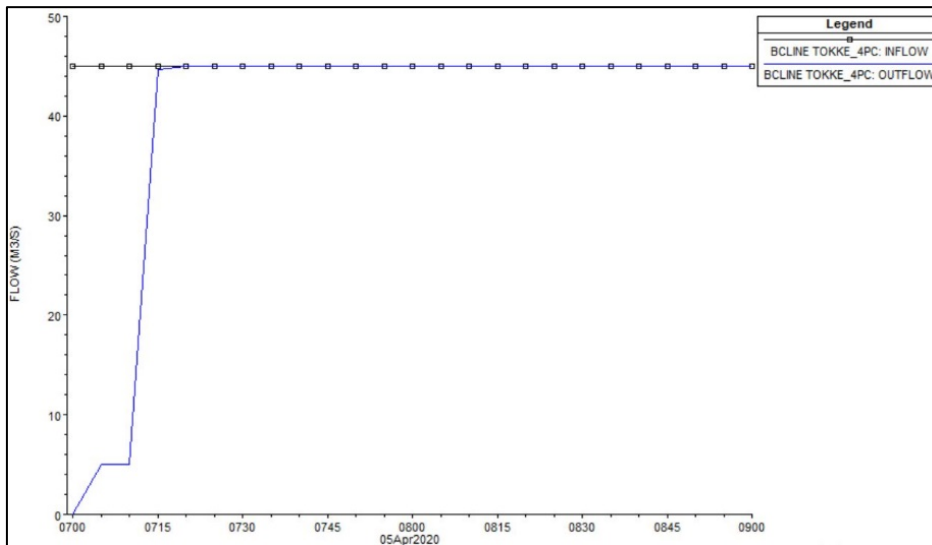


*Figure 4-5 Flow condition at inflow and outflow boundaries*

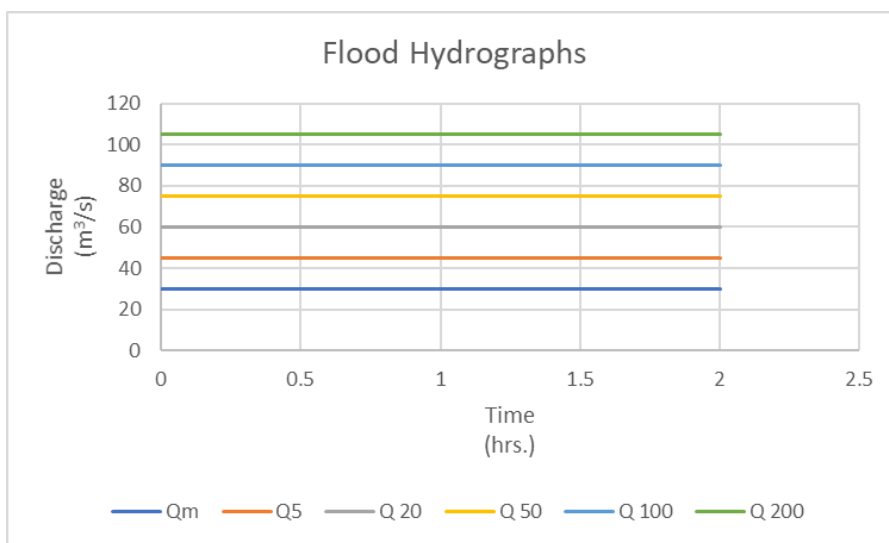


*Figure 4-6 Input Flood Hydrographs for different slope Scenarios*

## 4.2 Computation Parameters

HEC-RAS provides a few computation settings to fine tune the model. Two settings are important to discuss here: i) the equation set, ii) the computation time step.

### 4.2.1 Equation Set

HEC RAS offers two different sets of equations for 2-D flow modeling namely; Diffusion Wave equation and Full Momentum (or Shallow Water Equations). The HEC-RAS 2-D User Manual suggests using both sets of equations one by one and comparing the results. If no significant difference is found in the simulation results then, Diffusion Wave equation can be used, as it is numerically more stable and encounters less instabilities with a larger computational time step. However, if significant difference is observed in the results, Full Momentum approach is preferred as it is more accurate (Gary W. Brunner, 2016b).

A scenario (slope 4.5% &  $Q = Q_M$ ) was modelled using both sets of equations one by one. A significant difference was observed in the water surface profiles (Figure 4-7), hence, it was decided to use the Full Momentum equation set.

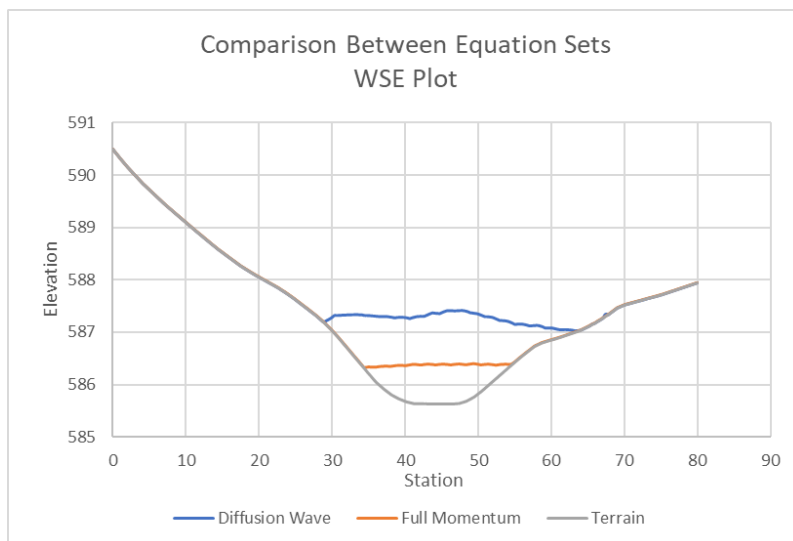


Figure 4-7 Comparison between Diffusion Wave and Full Momentum Equation Sets

### 4.2.2 Computation Time Step

The appropriate selection of time step is very important when using the Full Momentum approach. A too large time step can lead to numerical diffusion and instabilities, while a too small time step can increase computation time as



well as may lead to instabilities (Gary W. Brunner, 2016a). Computational time step can be kept to a fixed/constant value or it may be kept variable, where computations are carried out according to a defined condition of numerical stability (*i.e.* Courant condition). The problems with fixed computation time steps are that the numerical solution may not be stable at the predefined computation time step which will lead to erroneous results, numerical model convergence issues and in some severe cases the instabilities due to computation time step may lead to the crashing of the model. Hence, it is recommended to use a variable time step. This variable computation time step is determined by defining the Courant condition.

The Courant condition is a condition for stability of any unstable numerical method which is applied to solve wave or convective phenomenon (*e.g.* partial differential equations of hyperbolic nature, such as 2-D SWEs) (Caminha, 2019). The condition is expressed as follows (Gary W. Brunner, 2016b):

$$C = \frac{V\Delta T}{\Delta X} \leq 1 \quad (10)$$

Where,

C = Courant Number

V = Flood Wave velocity

$\Delta T$  = Computation Time Step

$\Delta X$  = Average cell size

The Maximum Courant Number is recommended to be set less than or equal to 1 for Full Momentum equation whereas, it can be kept as high as 3 when using Diffusion Wave equation.

For this study, the computation time step was chosen to be 15 seconds with Courant number was set as 1.

### 4.3 Simulation of Scenarios

Idealized scenarios (as discussed in **section 3.4**) were simulated using the settings described above. In 2-D simulations HEC-RAS provides output as map layers for Water Depth, Velocity, Water Surface Elevation, Shear Stress, Stream Power, etc. The mapping output interval was selected as 5 minutes for all the scenarios. Depending upon the parameter and time of interest, output maps can be generated and exported to GIS for post processing (*i.e.* extraction of required data at desired locations, comparison between different scenarios, etc.). Figure 4-8 is an example of the output from these simulations, where the red lines represent the inflow and outflow BCs, and the Water Surface Elevation (WSE) was calculated for a  $Q_{50}$  flowing on a constant slope of 4.5%.

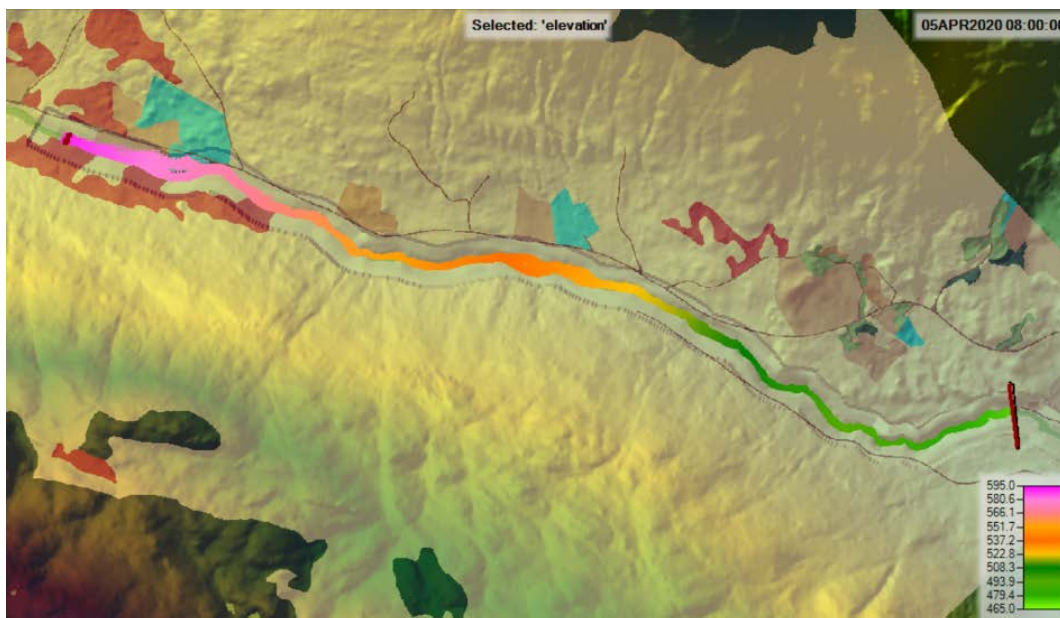


Figure 4-8 WSE for Simulated Scenario ( $s=4.5\%$ ,  $Q_{50}$ ). Values go from 465 m (green tones) to 595 m (pink tones)

For this study, output maps for the following parameters were generated:

- i. Water Surface Elevation (WSE)
- ii. Water Depth
- iii. Velocity

- iv. Shear Stress
- v. Stream Power
- vi. Froude Number

These maps were then exported to ArcMap for post processing.

#### **4.4 Comparison of Simulations**

Two-dimensional hydrodynamic simulations for steep rivers are recommended to be carried out to be carried out in modeling packages that make use of TVD discretization schemes (Kvočka et al., 2017). HEC-RAS (v. 5.0.7) does not include this discretization scheme. Therefore, it was considered rational to compare the simulations carried out in HEC-RAS with simulations from a modeling package that uses TVD discretization to ensure the accuracy of the output from HEC-RAS and its applicability to steep rivers. For comparison, TELEMAC 2-D was selected as the modeling package since it incorporates TVD discretization scheme and is an open source code. A short reach of the river was selected for modeling in both HEC-RAS (v. 5.0.7) and TELEMAC 2-D (Figure 4-9). The length of the selected reach was 325 m.

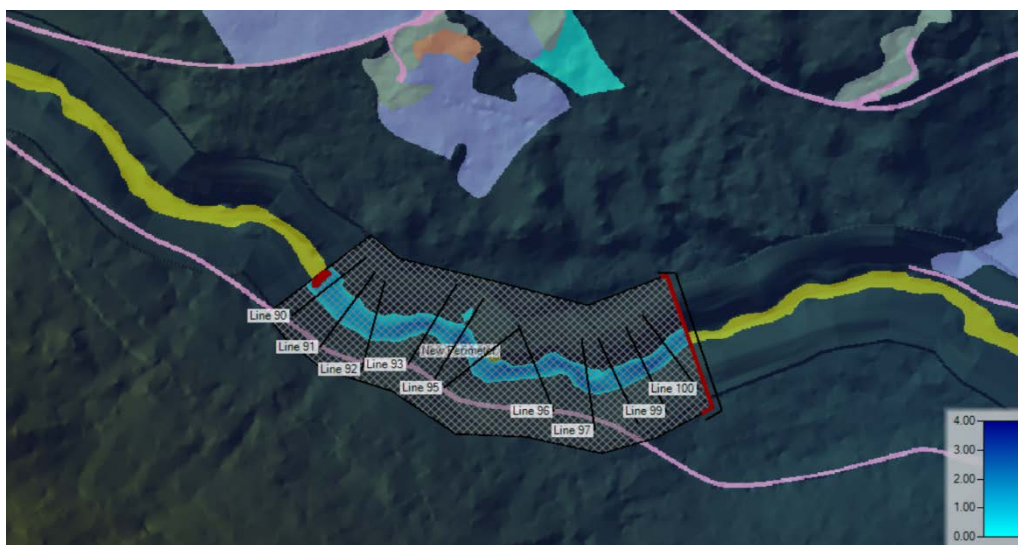


*Figure 4-9 Reach Selected for Comparison with TELEMAC 2-D (Water Depth layer turned in HEC-RAS). Scenario  $s = 5.5\%$ ,  $Q = Q_{200}$*

The modeling conditions were kept same as described in **section 454.2**. The scenario selected for modeling was  $Q = Q_{200}$ ,  $s = 5.5\%$ .

#### **4.5 Result Extraction**

In order to identify relationships between different topographical and hydraulic parameters and quantify these relationships through correlations by carrying out the statistical analysis, it was essential to obtain the results for different parameters in numerical terms instead of mapping extents. Therefore, all the maps obtained from HEC-RAS were transferred to ArcMap for point data extraction.

New cross-sections, at a constant interval of 25 m, were defined along the simulated length. Three points were defined in each of these cross-sections. The points were defined based on the flow extents for scenario  $Q = Q_M$  and  $s = 4\%$  *i.e.* the first scenario. The first scenario was selected as it gave the lowest flow extents as compared to other discharge scenarios. These points were then kept the same for all the modeled scenarios so that the comparison between points is logical and true.

One point was defined at the center of the channel and one at each bank. The banks were defined as right bank and left bank from the upstream perspective such as an observer standing at upstream and looking towards downstream the bank to his right is the right bank and the bank to his left is the left bank. Figure 4-10 shows the three-point scheme for data extraction.

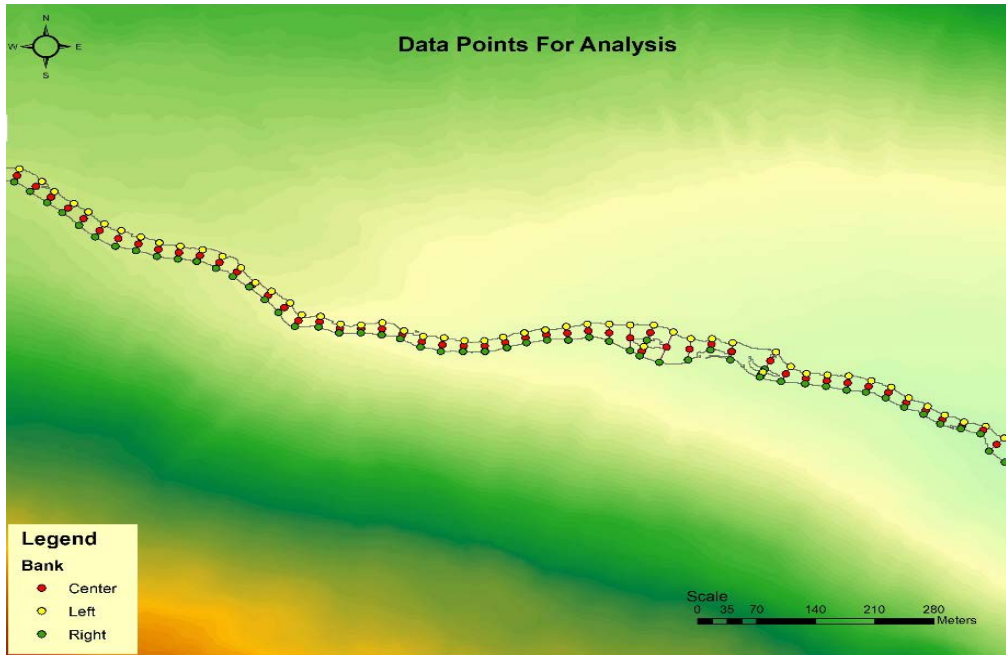


*Figure 4-10 Data Extraction scheme for results*



## 5 Results

In this chapter the results obtained from the 2-D hydrodynamic analysis are presented. Different statistical analysis tests were applied to determine the correlation between parameters under consideration.

### 5.1 Longitudinal Variation of Hydraulic Parameters

The longitudinal variation of hydraulic parameters, such as Water Depth, Velocity, Shear stress and Stream Power, was studied to identify trends in these parameters with respect to discharge (Q), slope (s) and relative section width ( $W_{xs}$ ).

#### 5.1.1 Water Depth Variation

The variation of water depth along the stream at different data points is presented from Figure 5-1 to 5-3.

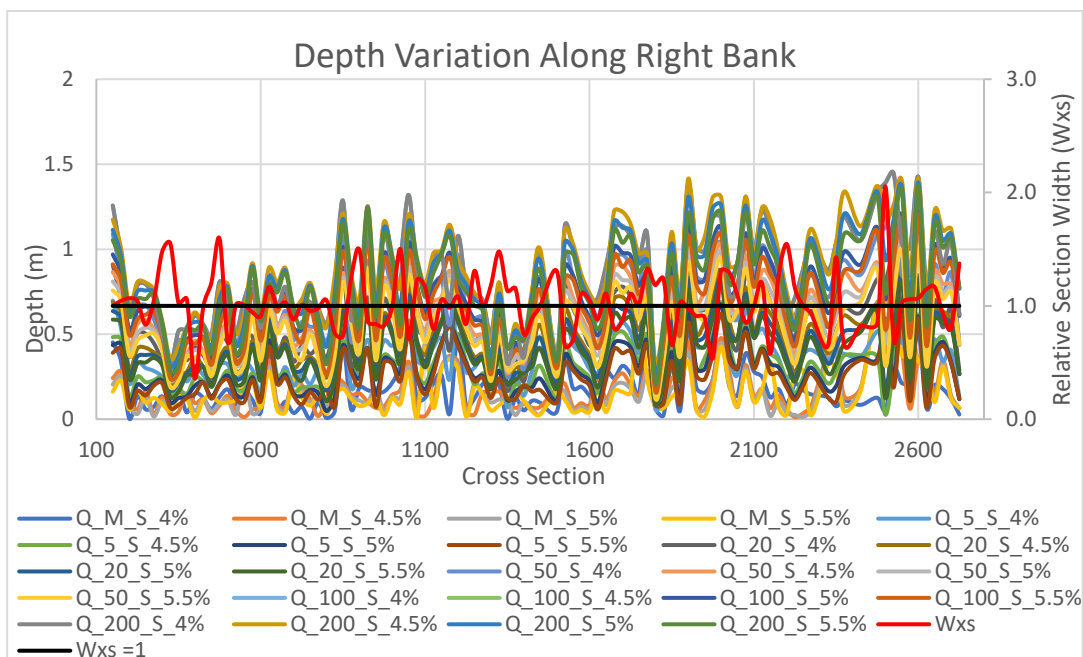


**Figure 5-1 Water Depth Variation along River Right Bank**

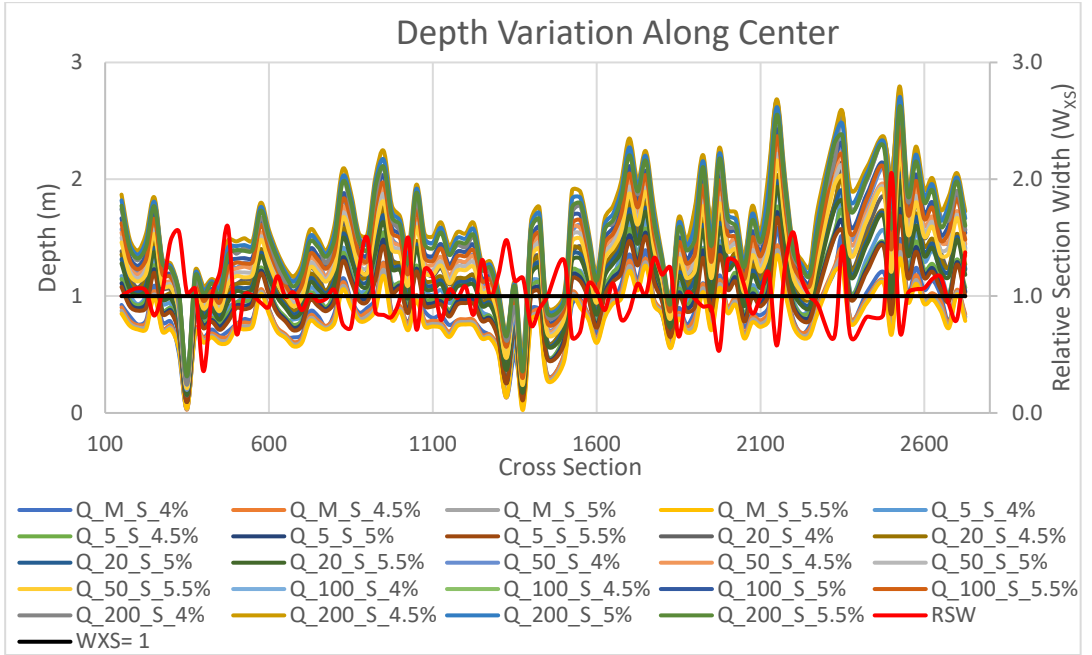


Figure 5-2 Water Depth Variation along River Center

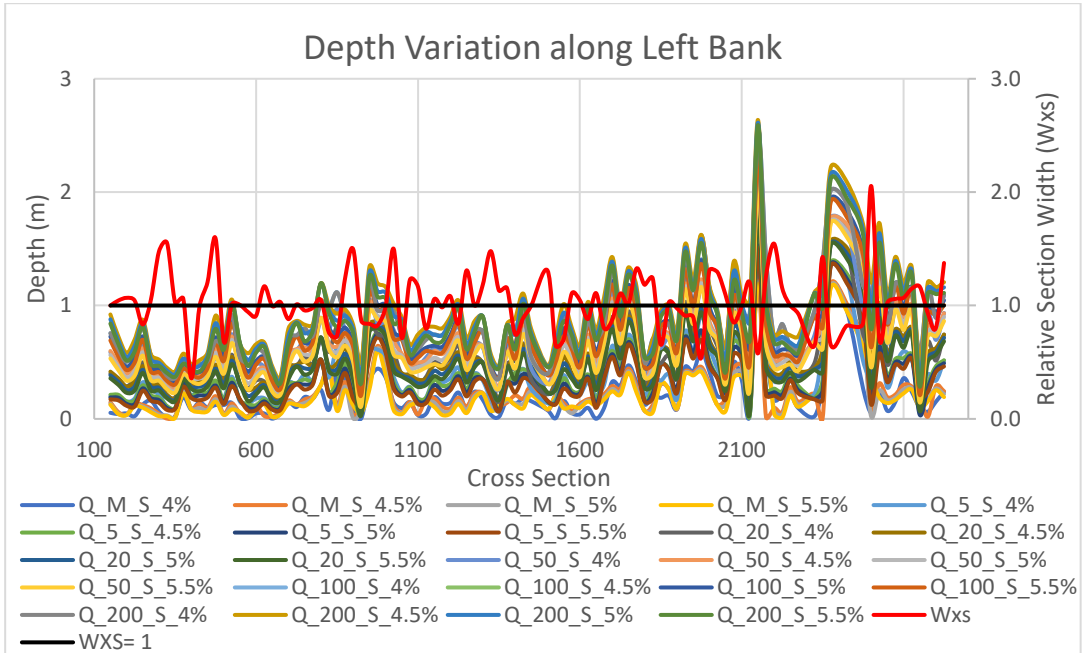


Figure 5-3 Depth Variation along River Left Bank



Water depth along banks and river center show a clear pattern that cross-sections where a contraction ( $W_{xs} < 1$ ) occurs water depth rises whereas, at cross-sections with expansions ( $W_{xs} > 1$ ) reduction in water depth is observed. Another trend observed is the variation in water depth with discharge ( $Q$ ) and slope ( $s$ ). With increase in discharge ( $Q$ ), at a particular slope ( $s$ ), water depth increases, indicating a direct proportionality relationship whereas, increase in slope tends to reduce water depth for a constant discharge ( $Q$ ), indicating an inverse proportionality relationship between slope and water depth.

### **5.1.2 Velocity Variation**

The variation of velocity along the stream at different data points is presented from Figure 5-4 to 5-6.

Higher velocities are observed in the center of the channel as compared to the banks. This behavior is largely due to increased roughness at the banks than in the channel center.

Cross-sections with contractions ( $W_{xs} < 1$ ) experience increased velocities while cross-sections with expansion ( $W_{xs} > 1$ ) experience reduction in velocity.

At a particular slope ( $s$ ), the increase in discharge leads to increase in velocity, a direct proportionality relationship. The same trend is observed for increasing slope at a constant discharge.

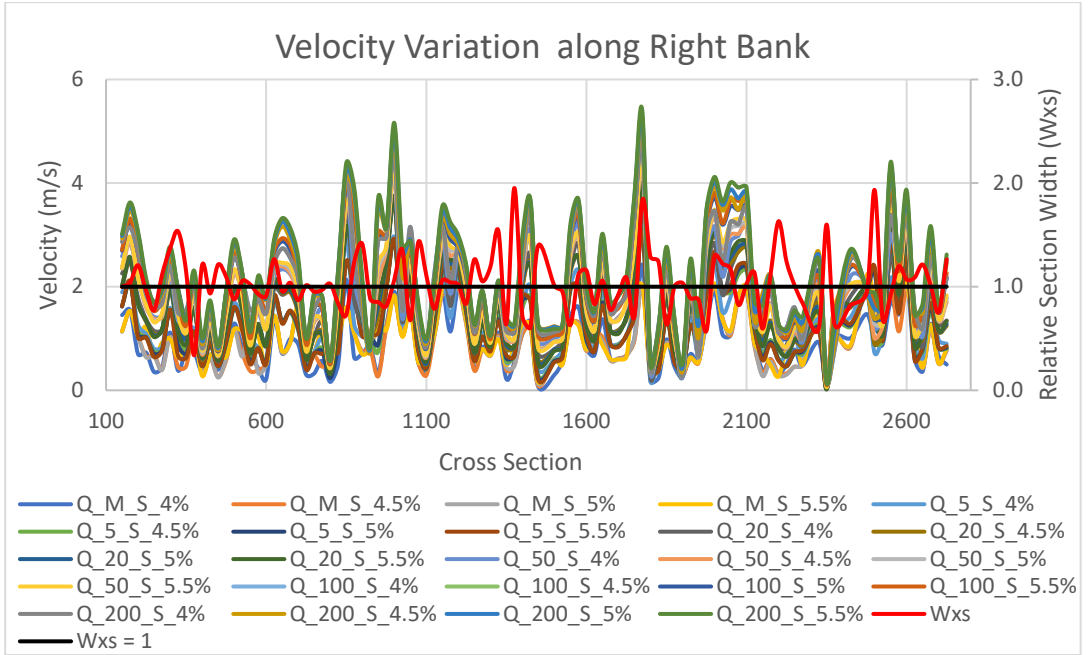


**Figure 5-4 Velocity Variation along the River Right Bank**

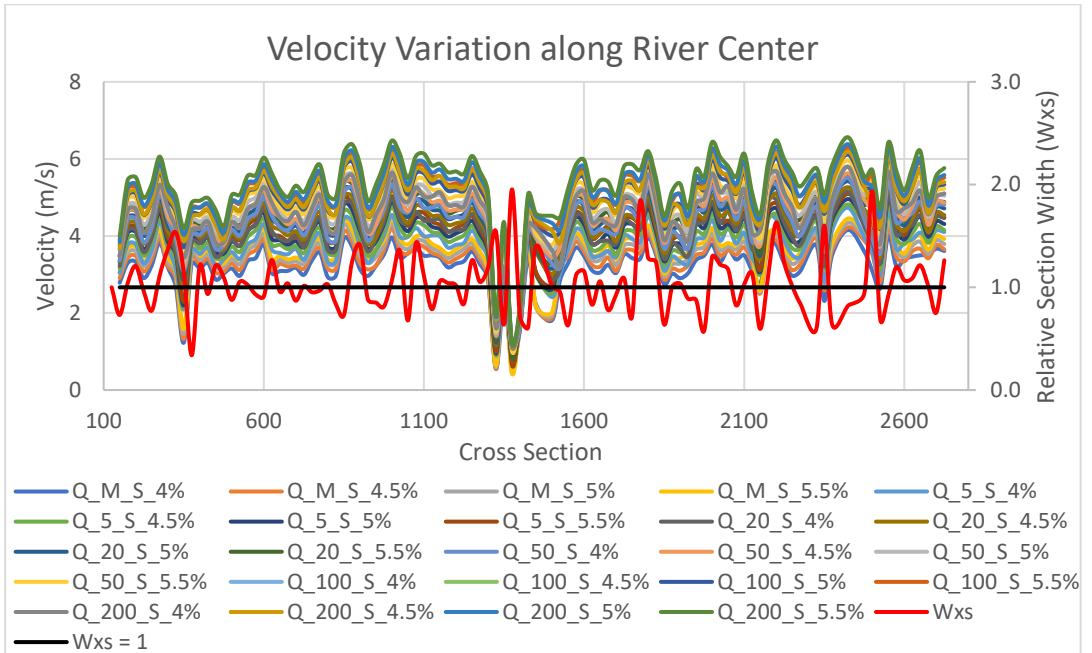


**Figure 5-5 Velocity Variation along the River Center**

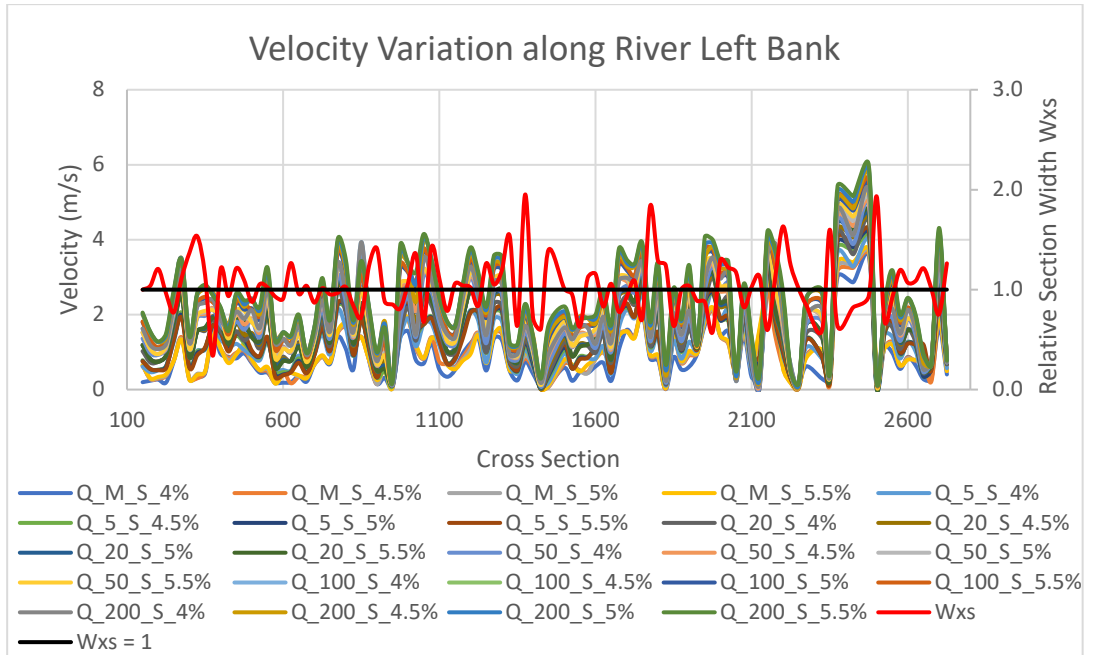


**Figure 5-6 Velocity Variation along the River Left Bank**

### **5.1.3 Shear Stress Variation**

The variation of shear stress along the stream at different data points is presented from Figure 5-7 to 5-9.

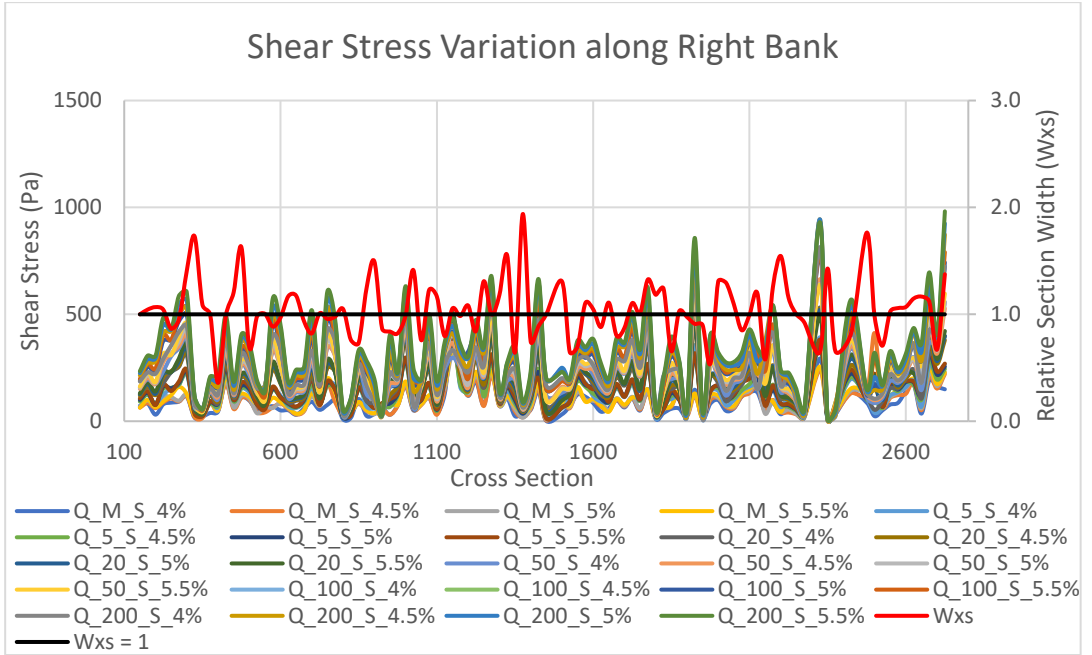


**Figure 5-7 Shear Stress Variation along the River Right Bank**

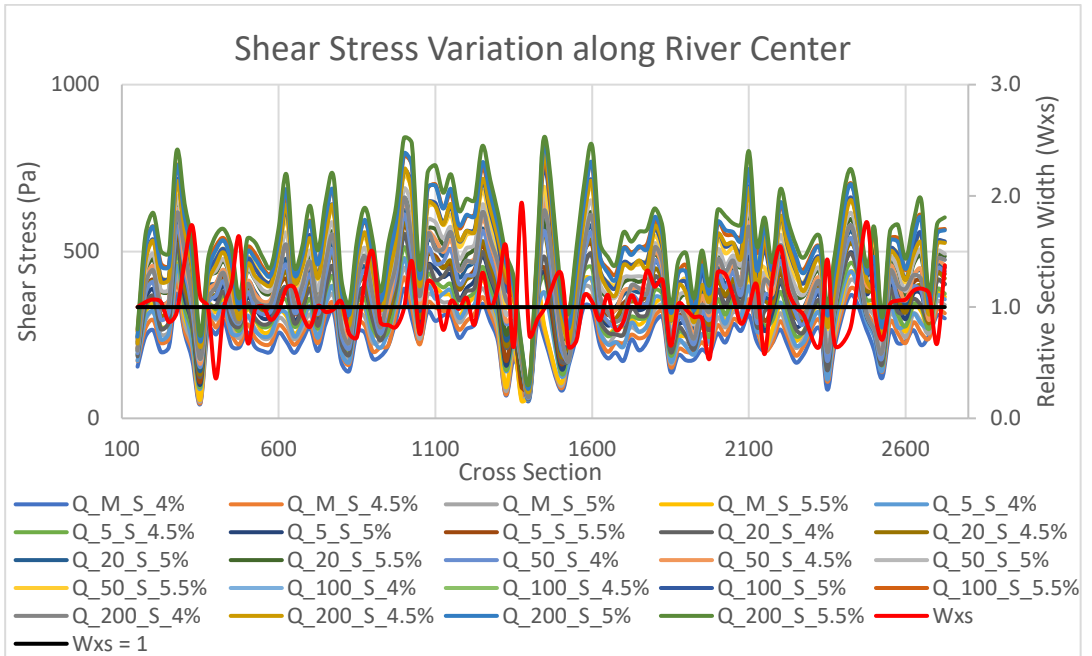


**Figure 5-8 Shear Stress Variation along the River Center**

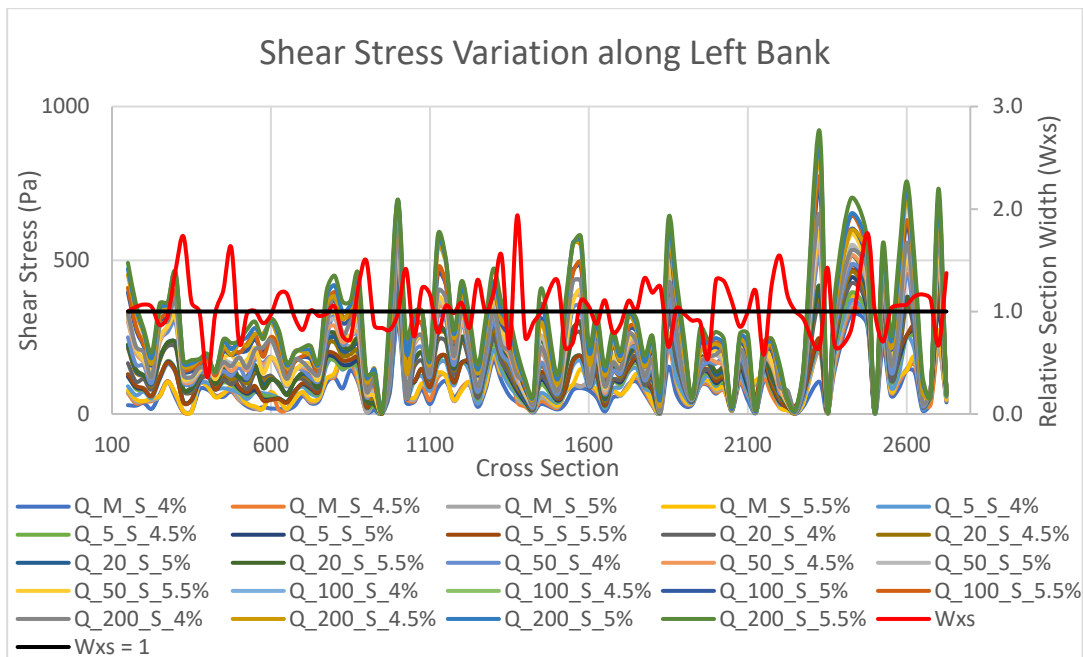


**Figure 5-9 Shear Stress Variation along the River Left Bank**

The data does not show any notable trend of shear stress variation along the stream with respect to the relative section width ( $W_{xs}$ ) parameter. The trend is quite random with respect to contractions and expansion in the cross-sections which indicate an independence of shear stress from this parameter.

A direct proportionality trend can be observed between shear stress and discharge ( $Q$ ) *i.e.* increase in discharge leads to increase in shear stress in the channel and the banks. Similarly, an increase in slope ( $s$ ) leads to an increase in shear stress at a particular discharge.

Channel experiences higher shear stress at the center as compared to the banks where the shear stress is relatively low. This variation in shear stress can be explained by the reduced water depths and velocities at the banks.

### 5.1.4 Stream Power Variation

The variation of Stream Power along the stream at different data points is presented from Figure 5-10 to 5-12.

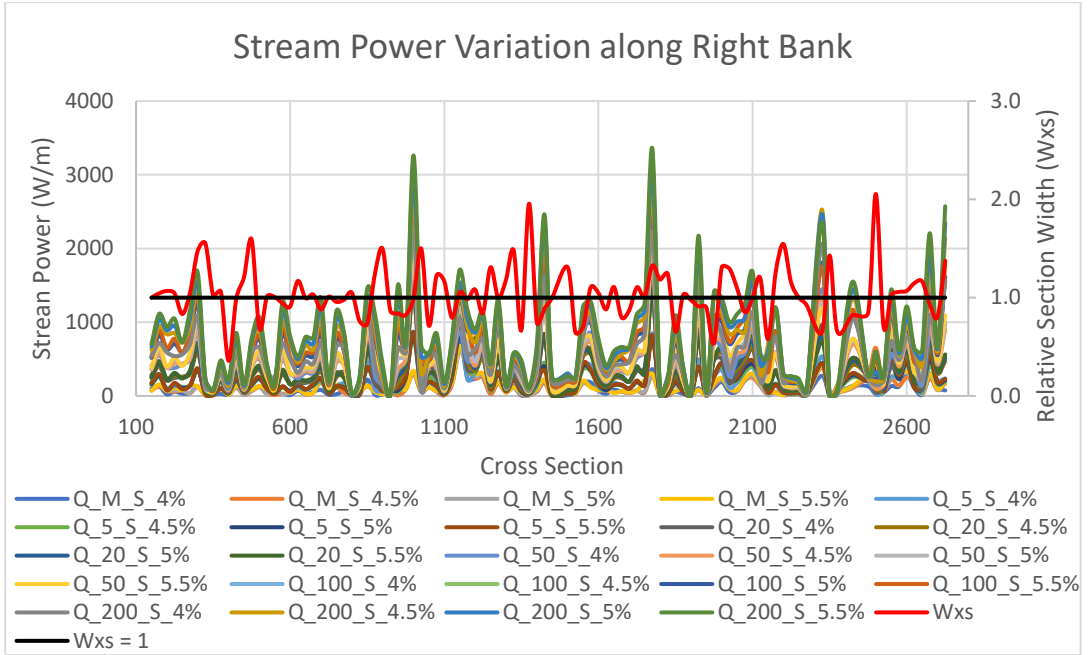


**Figure 5-10 Stream Power Variation along the River Right Bank**

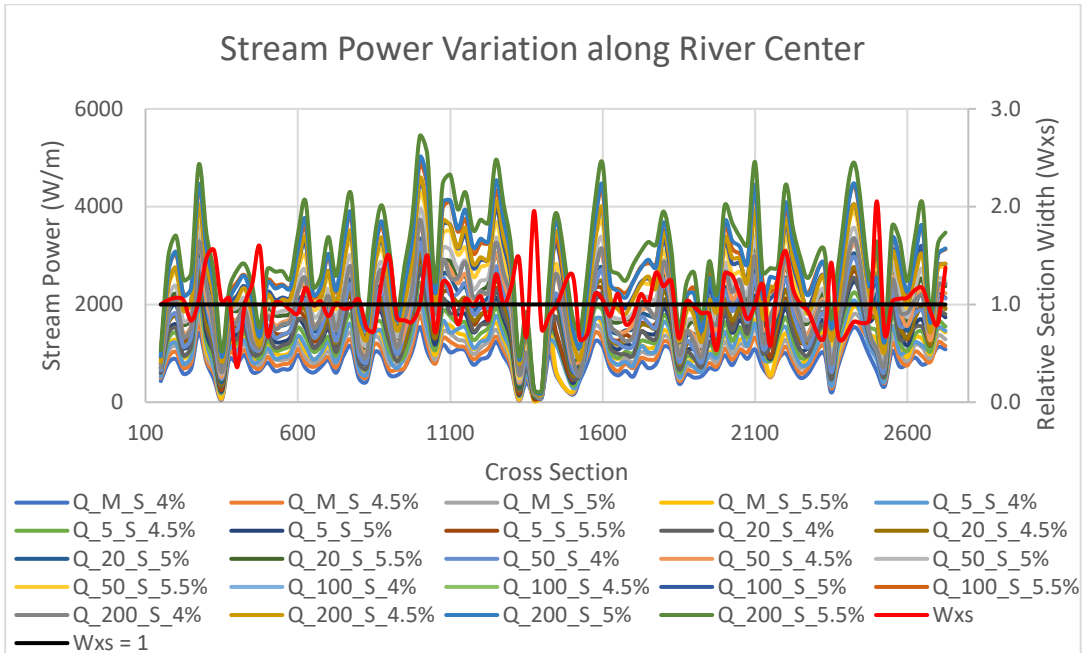


**Figure 5-11 Stream Power Variation along River Center**

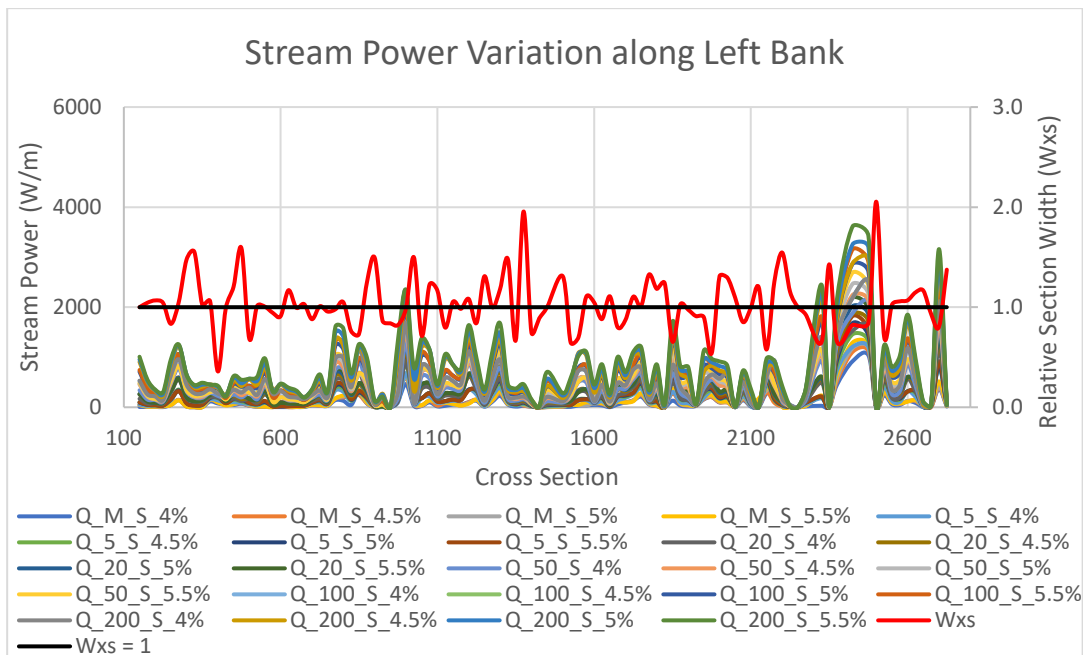


**Figure 5-12 Stream Power Variation along River Left Bank**

The plots show that stream power is independent of variations in the relative section width ( $W_{xs}$ ) and responds randomly to channel contractions and expansion.

Stream Power bears a direct relationship with discharge ( $Q$ ) and slope ( $s$ ). At a constant slope ( $s$ ), stream power increases with increasing discharge. Similarly, at a constant discharge ( $Q$ ) stream power increases with increasing slope.

Stream Power is high at the river center and relatively low at the banks. This variation can be attributed to the lower velocities at the banks.

## **5.2 Variation of Hydraulic Parameters with Varying Slope**

The variation of different hydraulic parameters at a constant discharge was studied to quantify the effect of slope variation.

### 5.2.1 Depth

The average percentage difference in Depth at a point by the variation in slope at a constant discharge is presented from Figure 5-13 to 5-15. The general trend is negative indicating that an inverse relationship between flow depth and slope. However, the variation at banks, especially at  $Q_M$  and  $Q_{200}$  is random and very small (close to zero). This can be explained by the fact that slope changes in steep rivers also affects the flow width, this makes the depth of flow at the banks quite sensitive as it remains a function of the underlying terrain.

The effect of slope change at a constant discharge is well pronounced at the stream center. It follows a constant trend and indicates that the average change in depth caused by slope change is constant. Anomaly is observed in case of  $Q_M$  and  $Q_{200}$ , where the depth increases for slope variation from 4% to 4.5% and 4% to 5% at the Left bank, while at the right bank an increase in depth is observed for  $Q_M$  and  $Q_{200}$  at slope variation from 4% to 4.5%. Also, at right bank for  $Q_M$  there is an increase in water depth when slope changes from 4% to 5%.

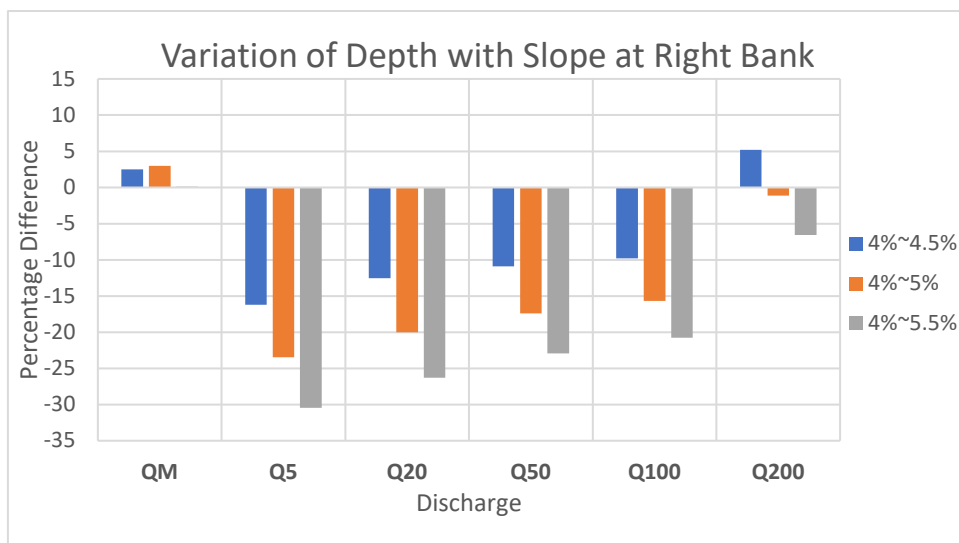


*Figure 5-13 Average Percentage Variation of Depth with Slope at Constant Discharge at River Right Bank*



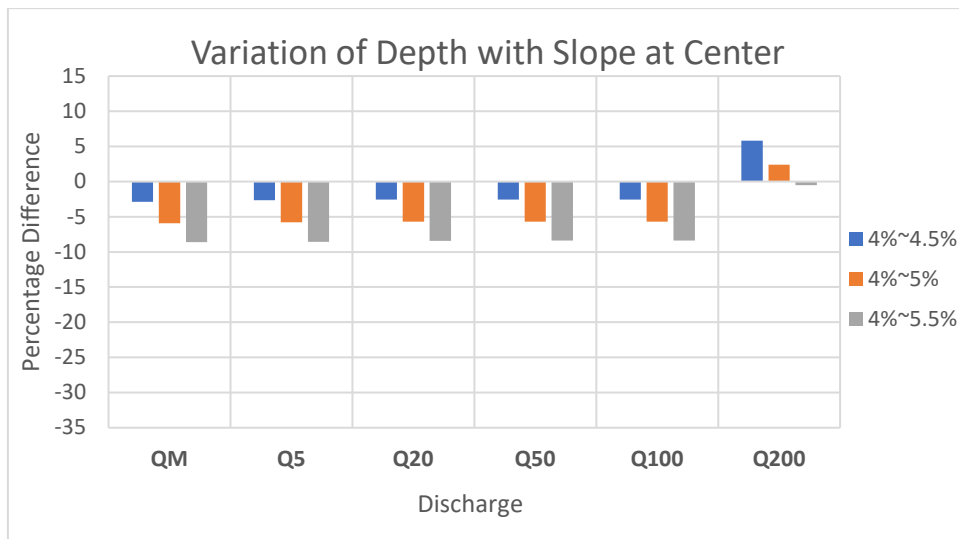


**Figure 5-14 Average Percentage Variation of Depth with Slope at Constant Discharge at River Center**

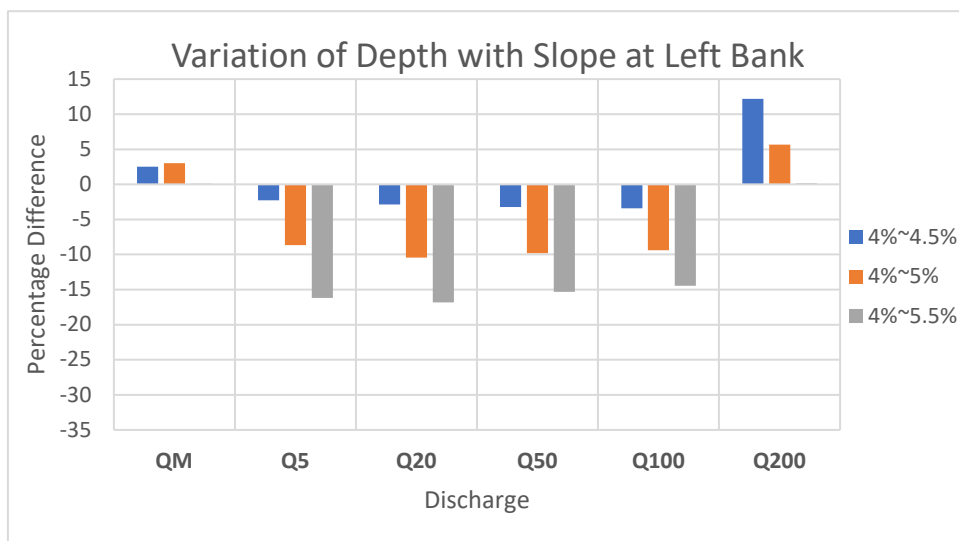


**Figure 5-15 Average Percentage Variation of Depth with Slope at Constant Discharge at River Left Bank**

Table 5-1, Figure 5-16 present the percentage change in depth (averaged over the cross-sections and further averaged over the discharge scenarios for each slope case) resulted from slope variation.

Table 5-1 Average Change in Water Depth with Slope Variation

Slope Change Case	Change in Slope (%)	Percent Change in Depth at Right Bank (%)	Percent Change in Depth at Center (%)	Percent Change in Depth at Left Bank (%)
4%~4.5%	12.5	-5.83	-2.5	1.14
4%~5%	25	-12.44	-5.7	-4.94
4%~5.5%	37.5	-17.82	-8.4	-10.42

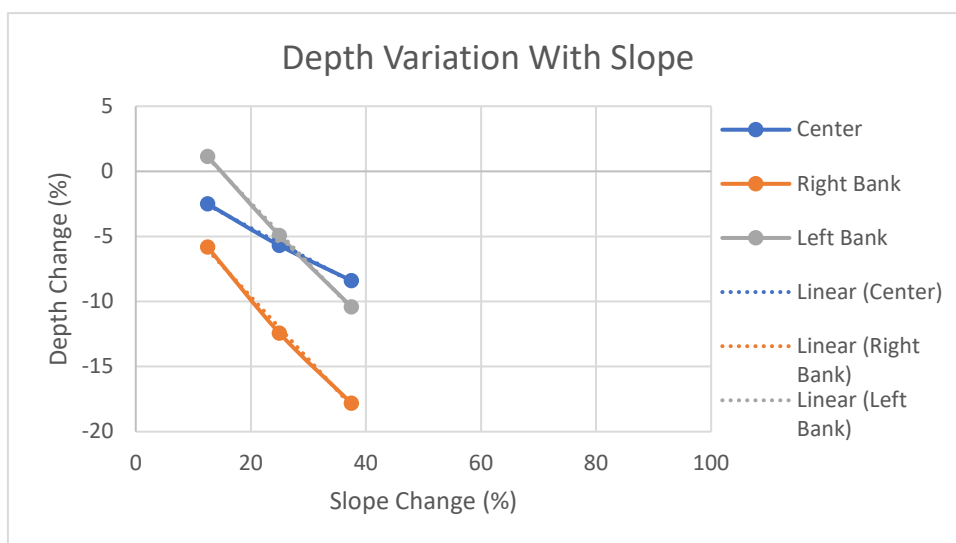


Figure 5-16 Relationship Between Slope Change and Depth Change

### 5.2.2 Velocity

The average percentage difference in Velocity at a point by the variation in slope at a constant discharge is presented from Figure 5-17 to 5-19.

The overall trend at the banks and center indicates a direct relationship between velocity and slope but abnormalities can be seen in velocity variations at the

banks especially at the right bank. These abnormalities can be caused by the changing channel width and the computational mesh size & shape at the banks. The variations at the center are consistent with the trend and show a moderate increase in average velocity change with increase in slope. The behavior at the left bank shows consistency with the trend but variations among discharge cases show abnormal behavior.

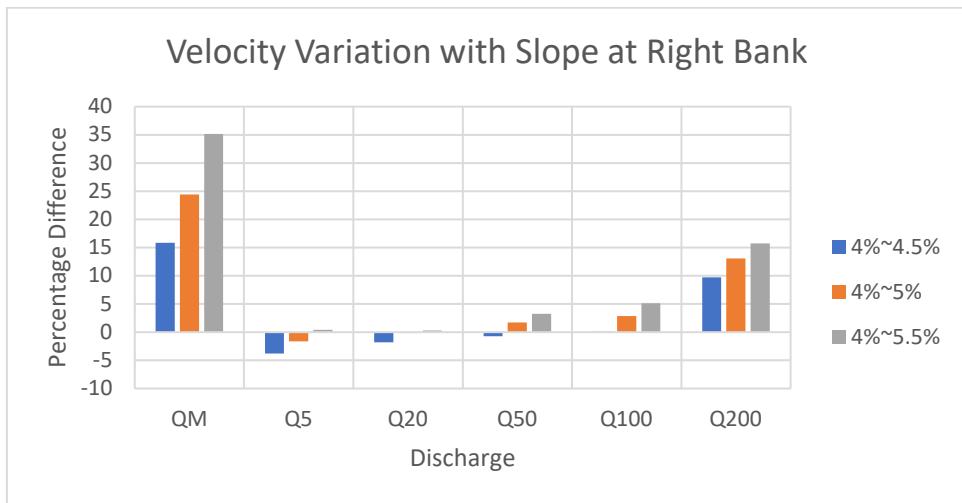


**Figure 5-17 Average Percentage Variation of Velocity with Slope at Constant Discharge at River Right Bank**

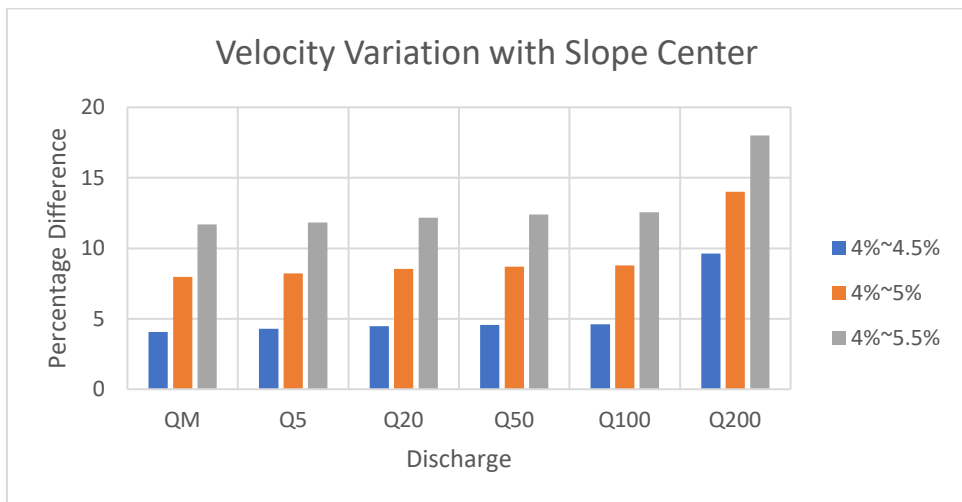


**Figure 5-18 Average Percentage Variation of Velocity with Slope at Constant Discharge at River Center**

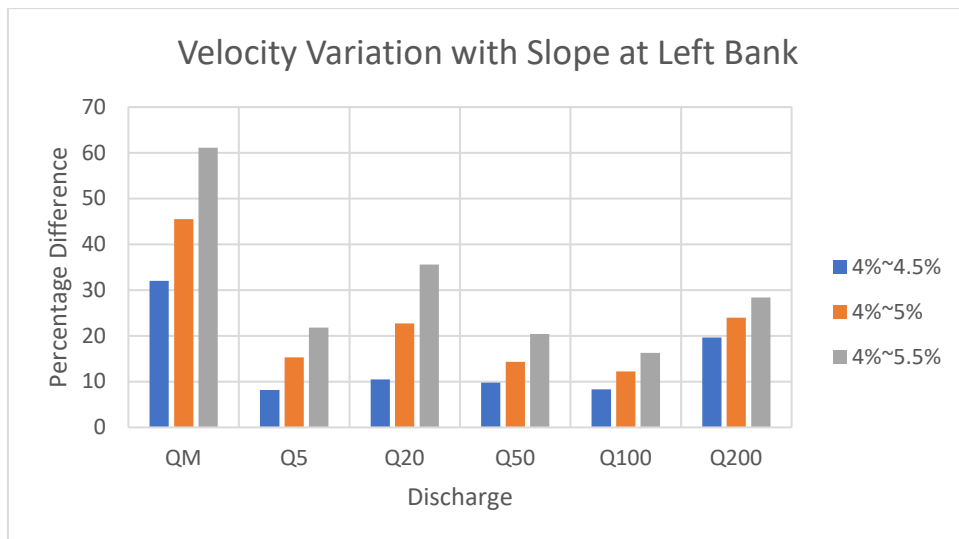
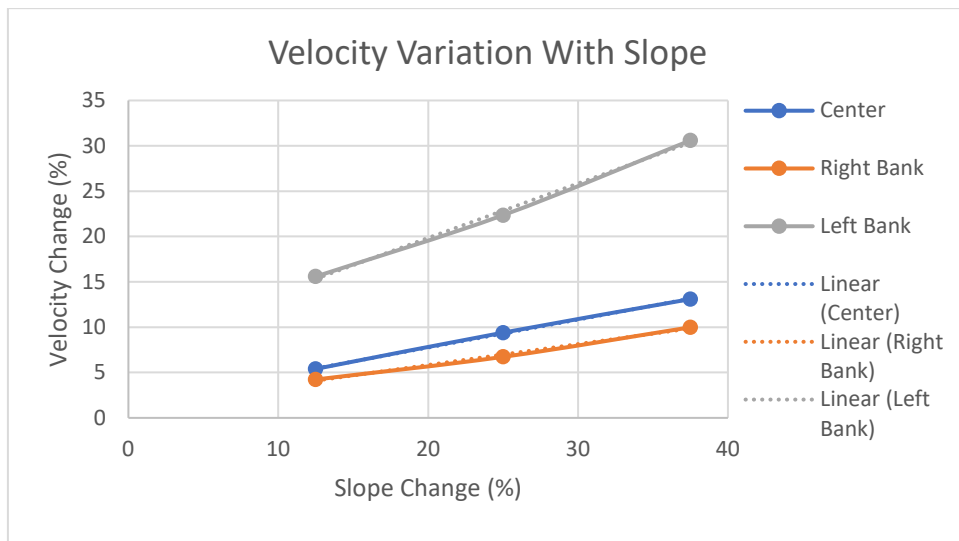


Figure 5-19 Average Percentage Variation of Velocity with Slope at Constant Discharge at River Left Bank

Table 5-2 and Figure 5-20 represent the percentage change in velocity (averaged over the cross-sections and further averaged over the discharge scenarios for each slope case) resulted from slope variation.

Table 5-2 Average Change in Velocity with Slope Variation

Slope Change Case	Change in Slope (%)	Percent Change in Velocity at Right Bank (%)	Percent Change in Velocity at Center (%)	Percent Change in Velocity at Left Bank (%)
4%~4.5%	12.5	4.23	5.40	15.59
4%~5%	25	6.73	9.40	22.36
4%~5.5%	37.5	9.99	13.10	30.60



*Figure 5-20 Relationship Between Slope Change and Velocity Change*

### **5.2.3 Shear Stress**

The average percentage difference in Shear stress at a point by the variation in slope at a constant discharge is presented from Figure 5-21 to 5-23.

Shear stress also varies directly with changing slope. The trend at banks and center is consistent however, the percentage difference among different discharge cases at banks is inconsistent. The change in shear stress at left bank is higher than the center and the right bank.

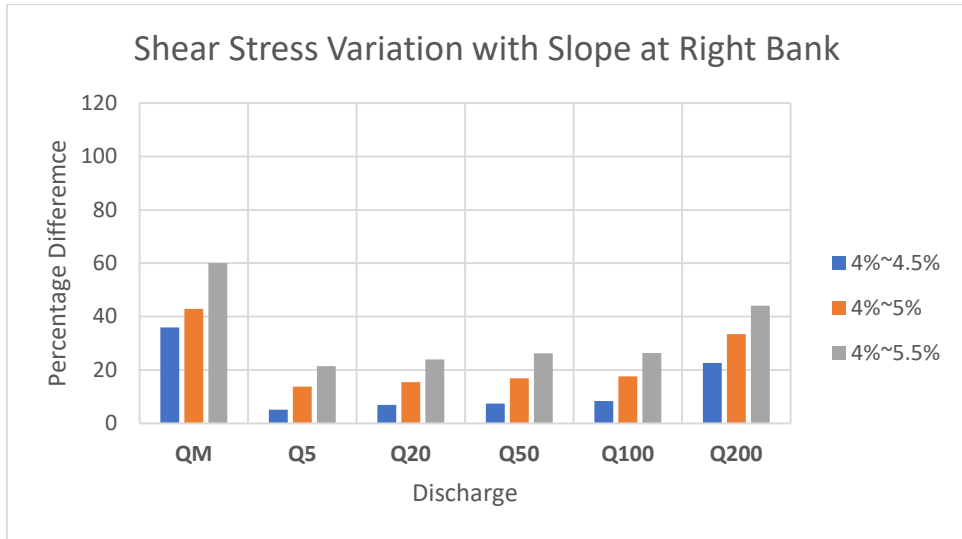


**Figure 5-21 Average Percentage Variation of Shear Stress with Slope at Constant Discharge at River Right Bank**

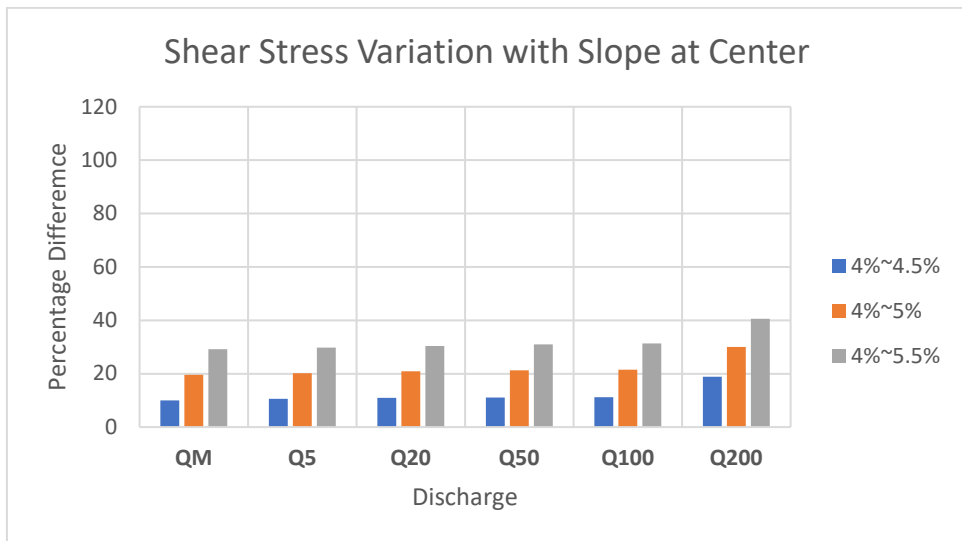


**Figure 5-22 Average Percentage Variation of Shear Stress with Slope at Constant Discharge at River Center**

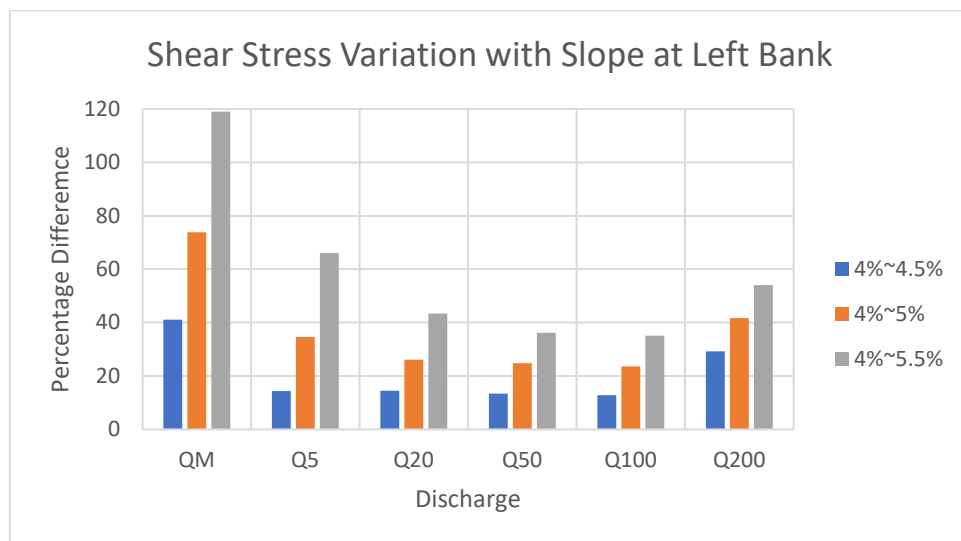


*Figure 5-23 Average Percentage Variation of Shear Stress with Slope at Constant Discharge at River Left Bank*

Table 5-3, Figure 5-24 represent the percentage change in shear stress (averaged over the cross-sections and further averaged over the discharge scenarios for each slope case) resulted from slope variation..

*Table 5-3 Average Change in Shear Stress with Slope Variation*

<b>Slope Change Case</b>	<b>Change in Slope (%)</b>	<b>Percent Change in Shear Stress at Right Bank (%)</b>	<b>Percent Change in Shear Stress at Center (%)</b>	<b>Percent Change in Shear Stress at Left Bank (%)</b>
4%~4.5%	12.5	15.88	12.30	22.20
4%~5%	25	23.36	22.20	37.44
4%~5.5%	37.5	33.70	32.00	58.97

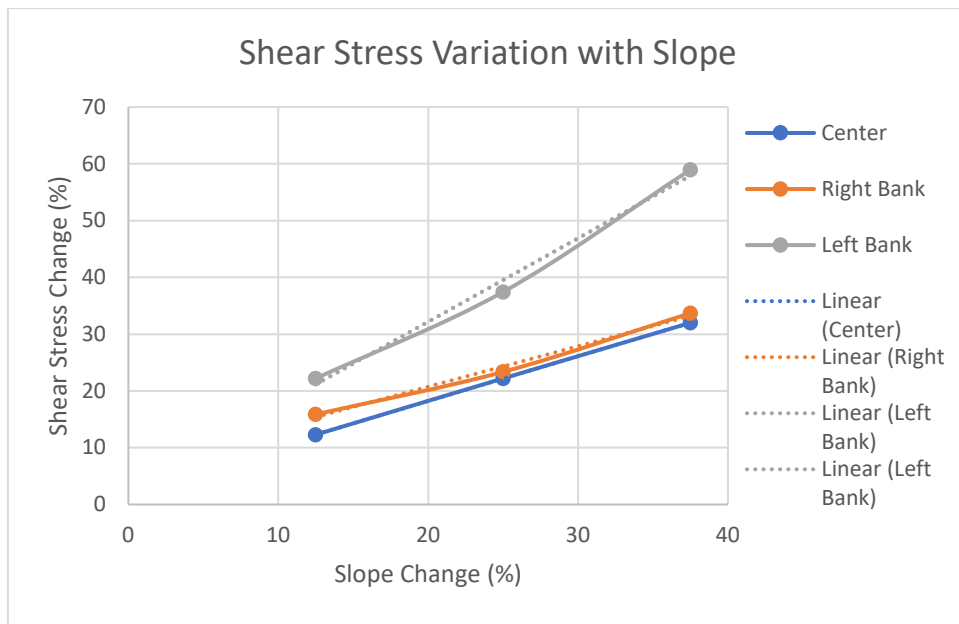


*Figure 5-24 Relationship Between Slope Change and Shear Stress Change*

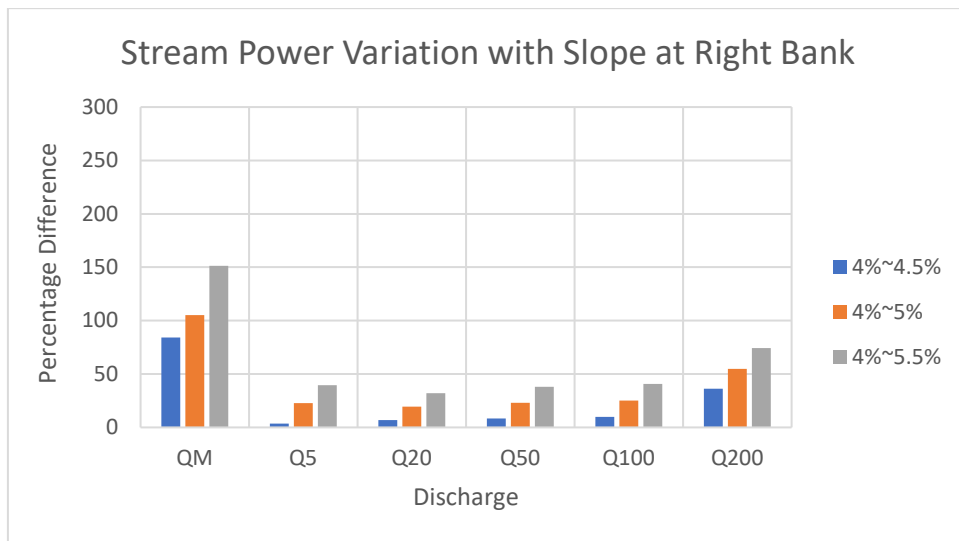
#### 5.2.4 Stream Power

The average percentage difference in Stream Power at a point by the variation in slope at a constant discharge is presented from Figure 5-25 to 5-27.

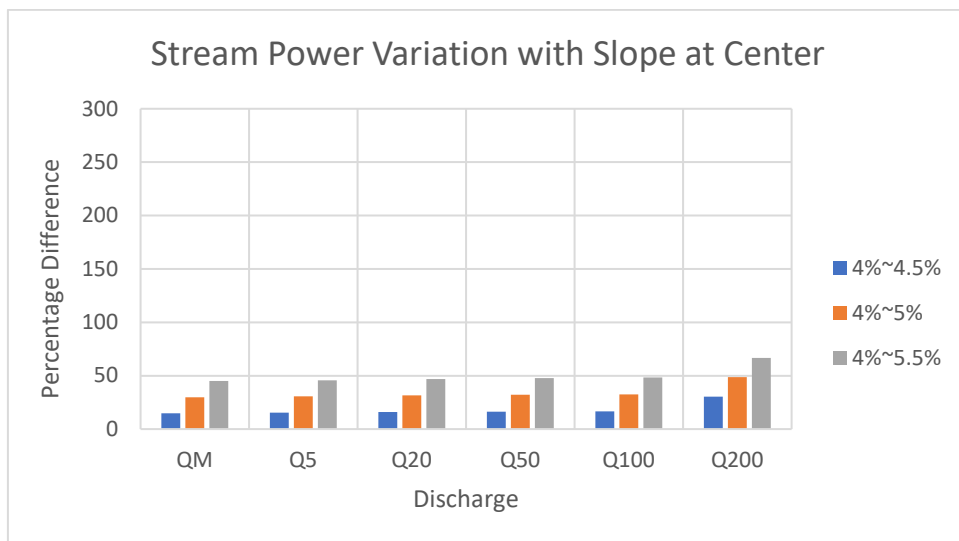
Stream Power also varies directly with changing slope at center and banks. Similar to shear stress, Stream Power changes with slope are higher at the left bank as compare to right bank and center. The trend among the different discharge cases with changing slope is consistent at the center as compared to the banks, where the rising trend is distributed randomly among the different discharge cases.

Table 5-4 and Figure 5-28 represent the percentage change in stream power (averaged over the cross-sections and further averaged over the discharge scenarios for each slope case) resulted from slope variation..





**Figure 5-25 Average Percentage Variation of Stream Power with Slope at Constant Discharge at River Right Bank**



**Figure 5-26 Average Percentage Variation of Stream Power with Slope at Constant Discharge at River Center**

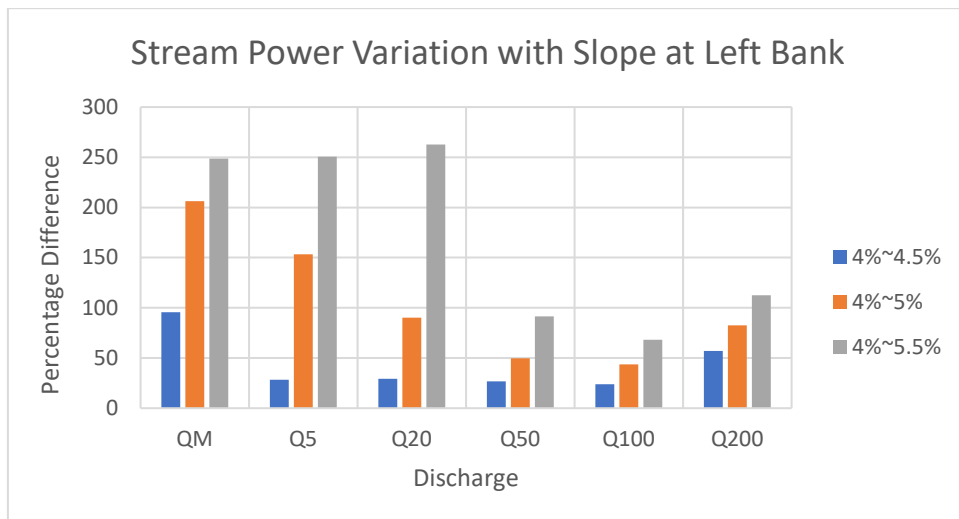
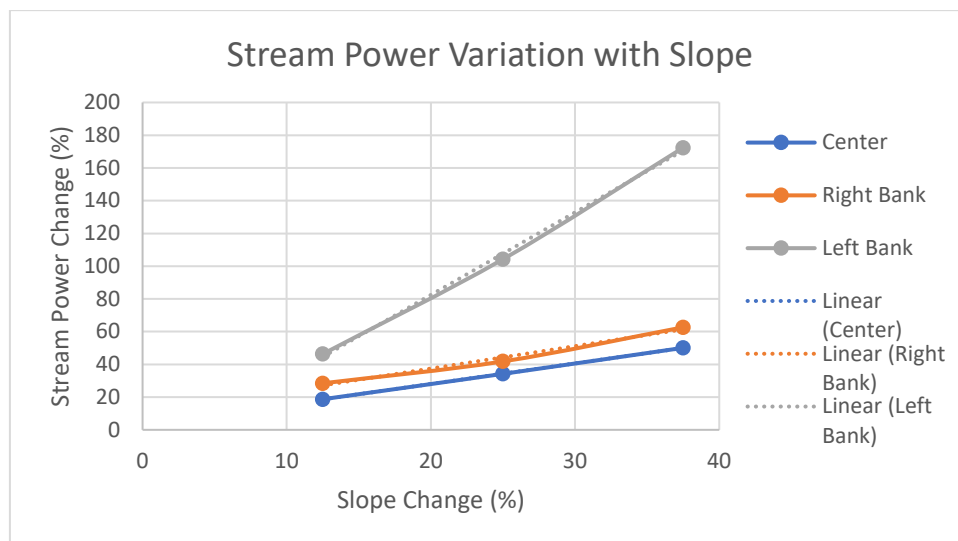


Figure 5-27 Average Percentage Variation of Stream Power with Slope at Constant Discharge at River Left Bank

Table 5-4 Average Change in Stream Power with Slope Variation

Slope Change Case	Change in Slope (%)	Percent Change in Shear Stress at Right Bank (%)	Percent Change in Shear Stress at Center (%)	Percent Change in Shear Stress at Left Bank (%)
4%~4.5%	12.5	28.43	18.7	46.33
4%~5%	25	41.80	34.2	104.26
4%~5.5%	37.5	62.66	50.1	172.40



*Figure 5-28 Relationship Between Slope Change and Stream Power Change*

### **5.3 Variation of Hydraulic Parameters at Varying Discharge**

The variation of different hydraulic parameters at a constant slope was studied to evaluate the effect of discharge variation.

#### **5.3.1 Depth**

The average percentage difference in Depth at a point by the variation in discharge at a constant slope is presented from Figure 5-29 to 5-31.

The variation of water depth with discharge follows a directly proportional relationship at constant slope *i.e.* increasing water depth with increasing discharge. The banks show extremely high depth changes while confirming the general rising trend with increasing discharge. This trend at the banks is due to the fact that increasing discharge will increase the channel width accordingly the bank points will experience flows with greater depths. The analysis of depth change at these points shows that the effect of discharge on depth is much more significant than the effect of slope on depth, where an inverse relationship exists (**section 5.2.1**).

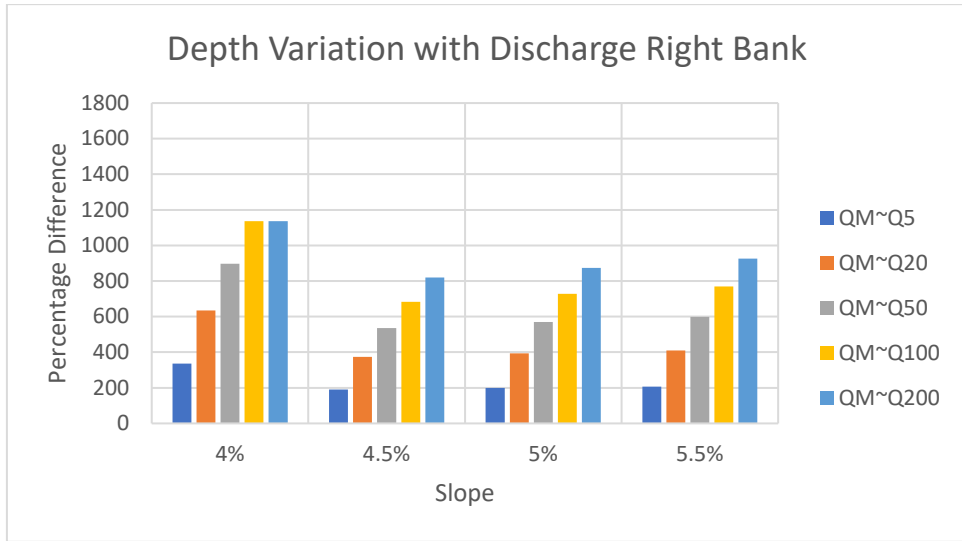


**Figure 5-29 Average Percentage Variation of Depth with Discharge at Constant Slope at River Right Bank**

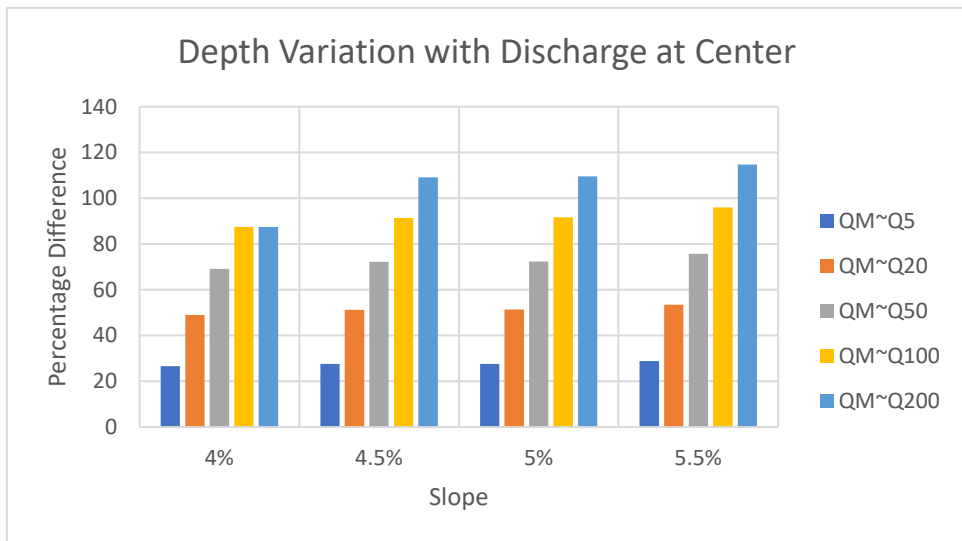


**Figure 5-30 Average Percentage Variation of Depth with Discharge at Constant Slope at River Center**

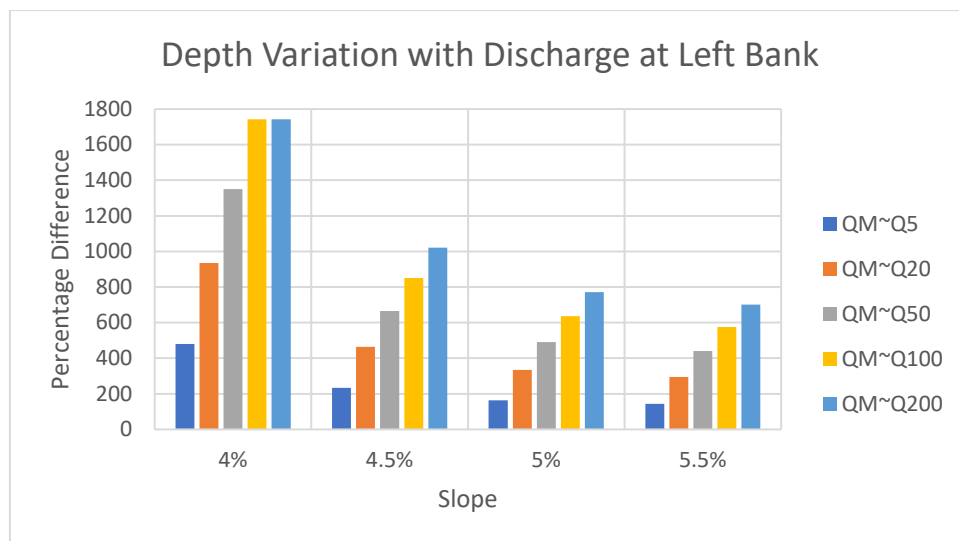


*Figure 5-31 Average Percentage Variation of Depth with Discharge at Constant Slope at River Left Bank*

Table 5-5 and Figure 5-32 present the percentage change in depth (average over the cross-sections and further averaged over the slope scenarios) change with changing discharge.

*Table 5-5 Average Change in Depth with Discharge Variation*

<b>Discharge Change Case</b>	<b>Change in Discharge (%)</b>	<b>Percent Change in Depth at Right Bank (%)</b>	<b>Percent Change in Depth at Center (%)</b>	<b>Percent Change in Depth at Left Bank (%)</b>
QM~Q5	50	232.80	27.69	255.47
QM~Q20	100	452.82	51.28	506.71
QM~Q50	150	650.36	72.38	736.69
QM~Q100	200	829.50	91.64	951.01

Discharge Change Case	Change in Discharge (%)	Percent Change in Depth at Right Bank (%)	Percent Change in Depth at Center (%)	Percent Change in Depth at Left Bank (%)
Q <sub>M</sub> ~Q <sub>200</sub>	250	938.86	105.25	1059.23

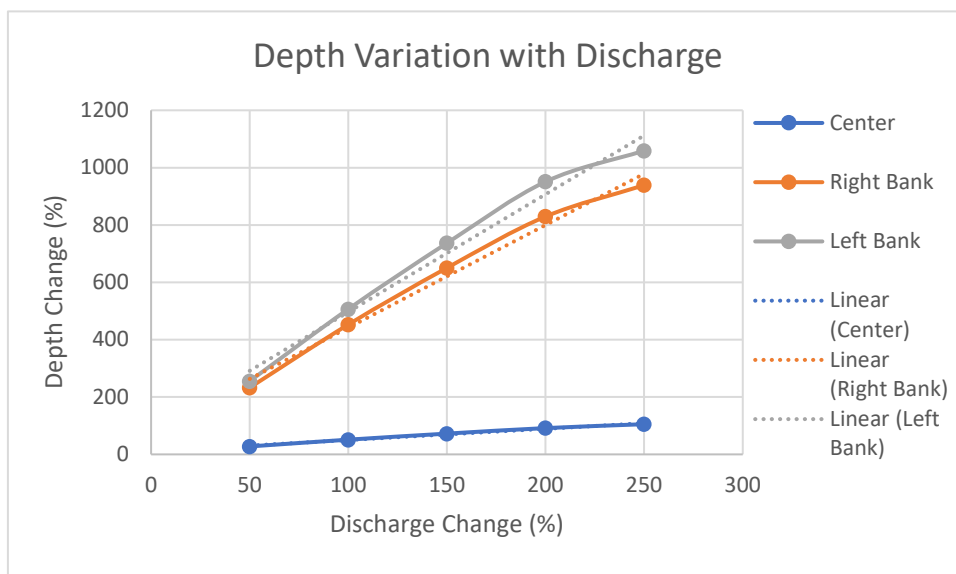


Figure 5-32 Relationship Between Discharge Change and Depth Change

### 5.3.2 Velocity

The average percentage difference in Velocity at a point by the variation in discharge at a constant slope is presented from Figure 5-33 to 5-36.

The trend suggests an increase in velocity with increasing discharge. The increase at the banks is extremely high as compared to the river center. The reason being increased flow width due to increased discharge and hence greater velocities. Moreover, velocity changes at the left bank are higher than the right bank. The velocity changes in the center of the river are also higher as compared to those observed when discharge was constant and slope was

varied, confirming that velocities in the river are more responsive to discharge changes.

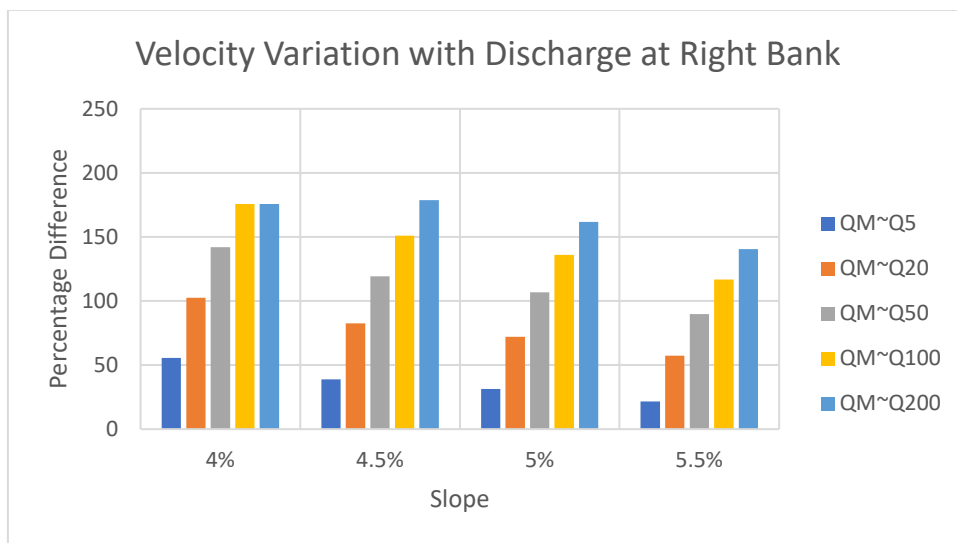


**Figure 5-33 Average Percentage Variation of Velocity with Discharge at Constant Slope at River Right Bank**

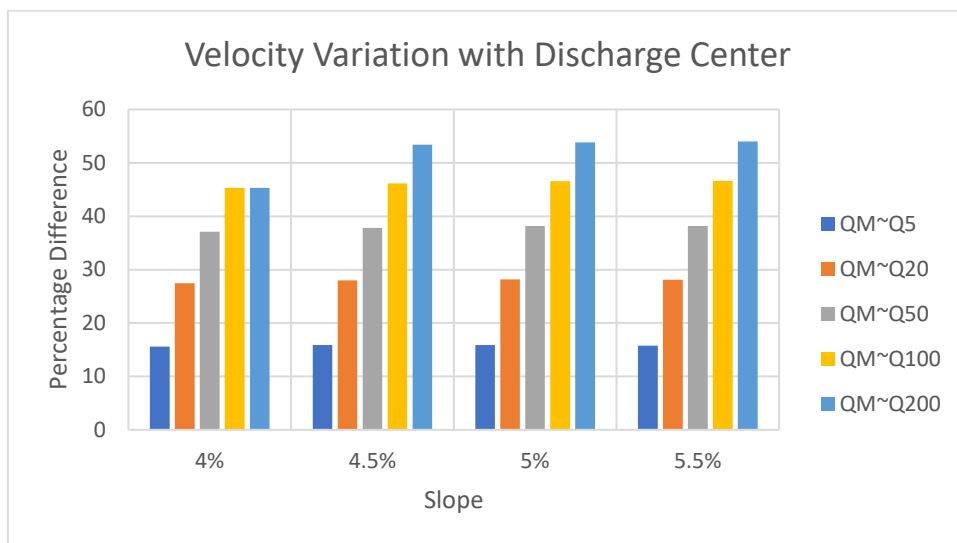


**Figure 5-34 Average Percentage Variation of Velocity with Discharge at Constant Slope at River Center**

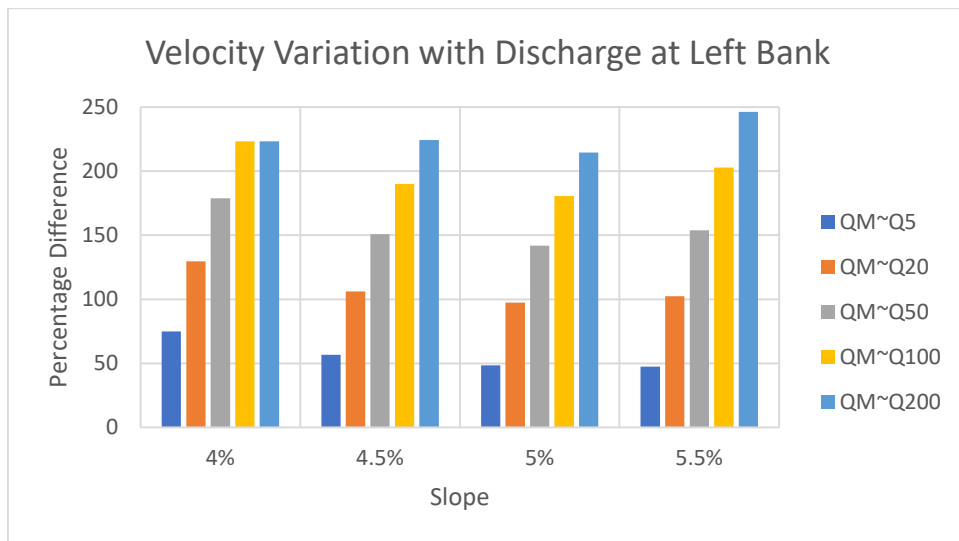


Figure 5-35 Average Percentage Variation of Velocity with Discharge at Constant Slope at River Left Bank

Table 5-6 and Figure 5-36 the percentage change in velocity (average over the cross-sections and further averaged over the slope scenarios) change with changing discharge.

Table 5-6 Average Change in Velocity with Discharge Variation

Discharge Change Case	Change in Discharge (%)	Percent Change in Velocity at Right Bank (%)	Percent Change in Velocity at Center (%)	Percent Change in Velocity at Left Bank (%)
Q <sub>M</sub> ~Q <sub>5</sub>	50	36.82	15.80	56.91
Q <sub>M</sub> ~Q <sub>20</sub>	100	78.65	27.94	108.88
Q <sub>M</sub> ~Q <sub>50</sub>	150	114.51	37.82	156.36
Q <sub>M</sub> ~Q <sub>100</sub>	200	144.84	46.19	199.18



Discharge Change Case	Change in Discharge (%)	Percent Change in Velocity at Right Bank (%)	Percent Change in Velocity at Center (%)	Percent Change in Velocity at Left Bank (%)
Q <sub>M</sub> ~Q <sub>200</sub>	250	164.09	51.66	227.05

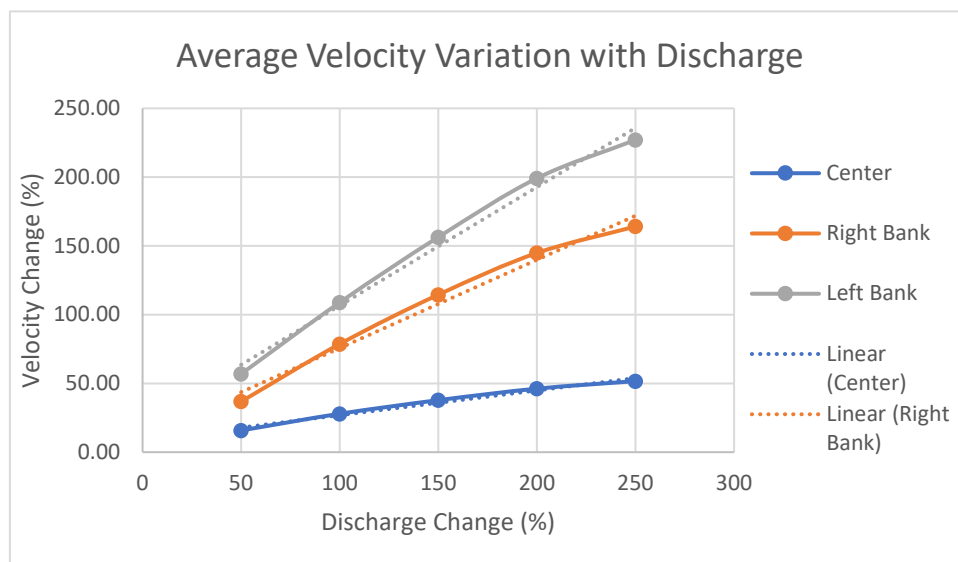
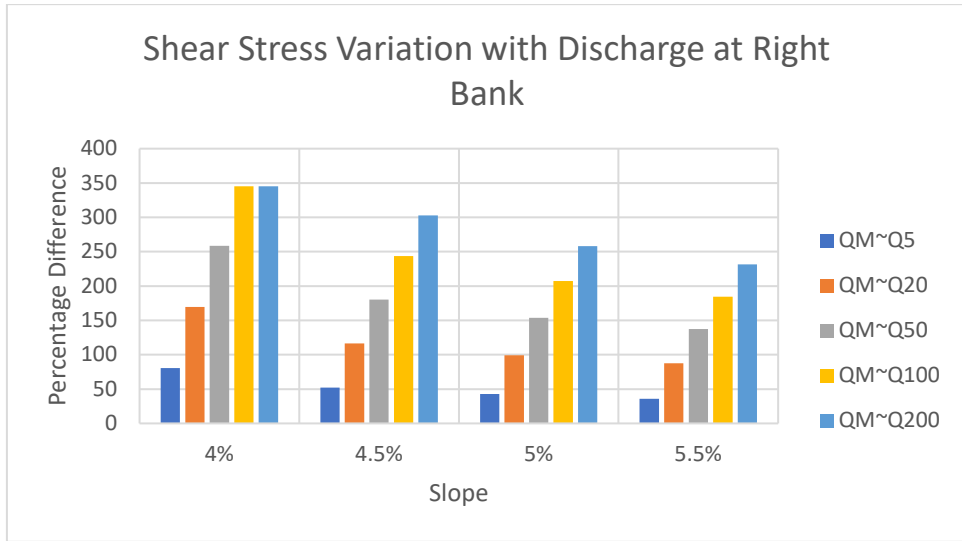


Figure 5-36 Relationship Between Discharge Change and Velocity Change

### 5.3.3 Shear Stress

The average percentage difference in Shear stress at a point by the variation in discharge at a constant slope is presented from Figure 5-37 to 5-39.

Shear stress varies directly with discharge *i.e.* increasing discharge increases the shear stress both at banks and river center. The variation in shear stress is extremely high at the banks as compared to the center of the river however, the rising trend is consistent in all cases with increasing discharge. The shear stress changes at the left bank are slightly higher than the changes at right bank.



**Figure 5-37 Average Percentage Variation of Shear Stress with Discharge at Constant Slope at River Right Bank**

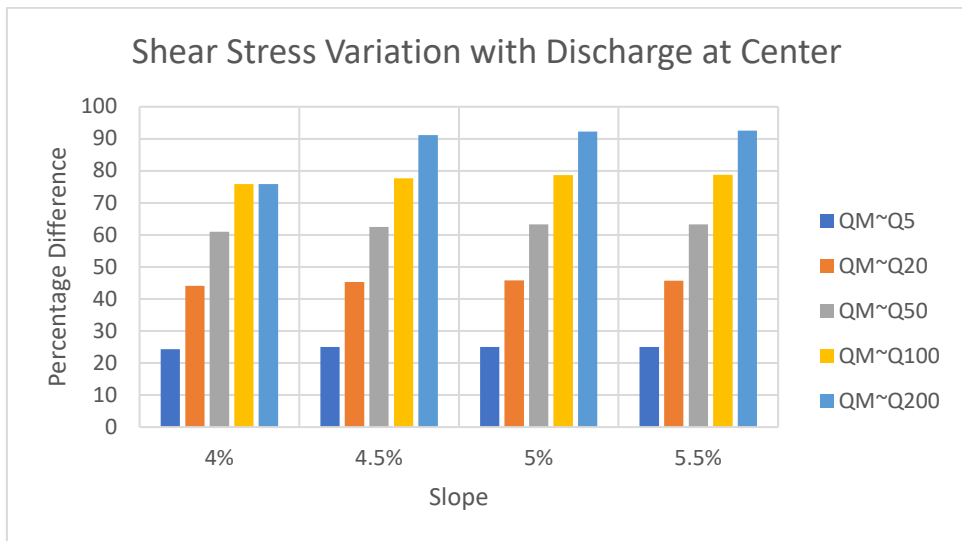


**Figure 5-38 Average Percentage Variation of Shear Stress with Discharge at Constant Slope at River Center**

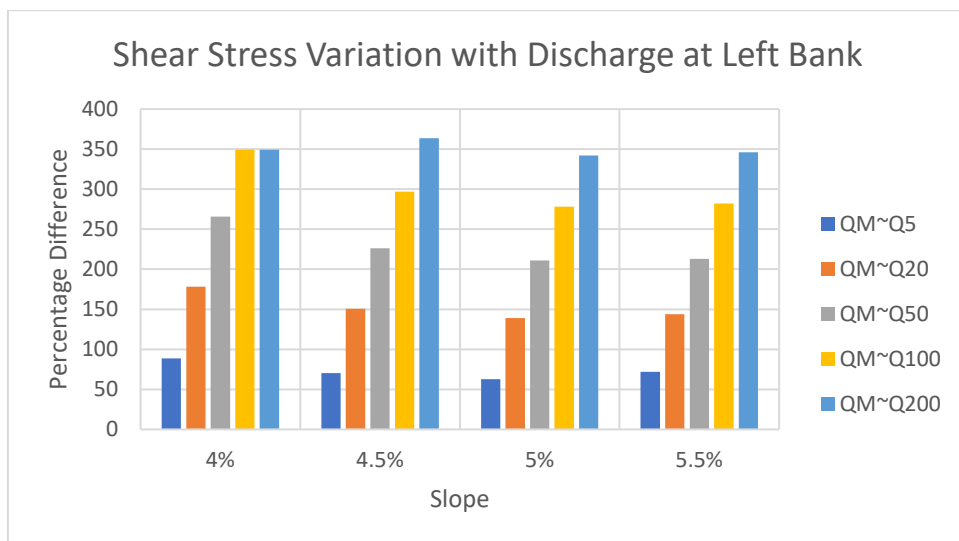


*Figure 5-39 Average Percentage Variation of Shear Stress with Discharge at Constant Slope at River Left Bank*

Table 5-7 and Figure 5-40 the percentage change in shear stress (average over the cross-sections and further averaged over the slope scenarios) change with changing discharge.

*Table 5-7 Average Change in Shear Stress with Discharge Variation*

<b>Discharge Change Case</b>	<b>Change in Discharge (%)</b>	<b>Percent Change in Shear Stress at Right Bank (%)</b>	<b>Percent Change in Shear Stress at Center (%)</b>	<b>Percent Change in Shear Stress at Left Bank (%)</b>
Q <sub>M</sub> ~Q <sub>5</sub>	50	52.81	24.86	73.30
Q <sub>M</sub> ~Q <sub>20</sub>	100	118.13	45.21	152.87
Q <sub>M</sub> ~Q <sub>50</sub>	150	182.55	62.52	229.05

<b>Discharge Change Case</b>	<b>Change in Discharge (%)</b>	<b>Percent Change in Shear Stress at Right Bank (%)</b>	<b>Percent Change in Shear Stress at Center (%)</b>	<b>Percent Change in Shear Stress at Left Bank (%)</b>
Q <sub>M</sub> ~Q <sub>100</sub>	200	244.98	77.72	301.52
Q <sub>M</sub> ~Q <sub>200</sub>	250	284.42	87.95	350.17

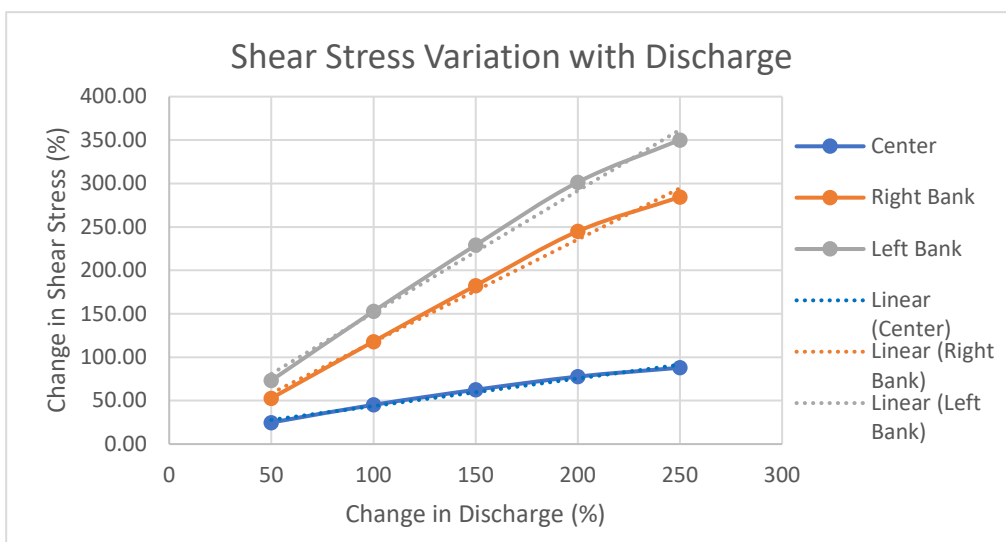


Figure 5-40 Relationship Between Discharge Change and Shear Stress Change

### 5.3.4 Stream Power

The average percentage difference in Stream Power at a point by the variation in discharge at a constant slope is presented from Figure 5-41 to 5-43.

Stream Power increases with increase in discharge. The trend is consistent at banks and river center. The increase in Stream Power at the banks, especially at the left bank, is significantly large as compared to the river center. This is

due to large variations in shear stress and velocities at these points (*i.e.* in HEC-RAS, Stream Power is computed as the product of Velocity and Shear Stress at a point).

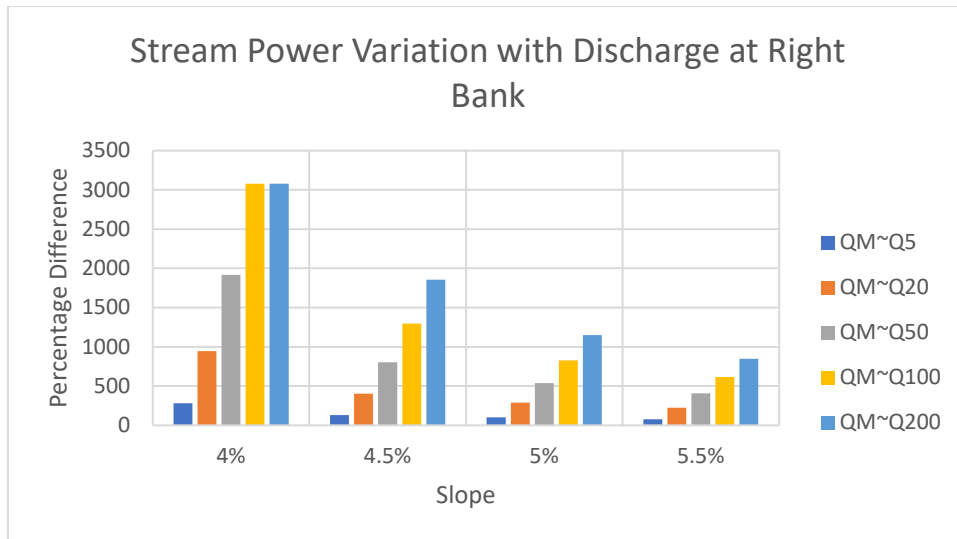


**Figure 5-41 Average Percentage Variation of Stream Power with Discharge at Constant Slope at River Right Bank**

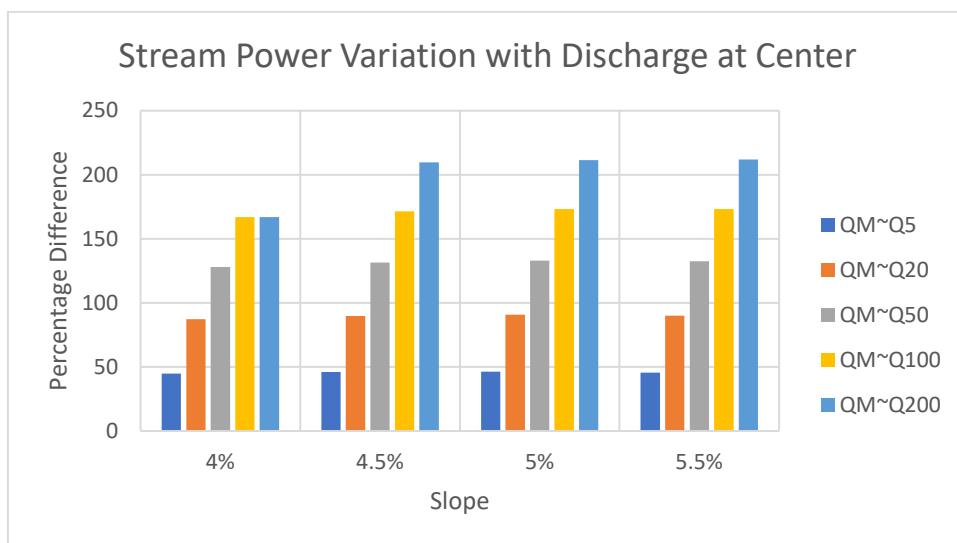


**Figure 5-42 Average Percentage Variation of Stream Power with Discharge at Constant Slope at River Center**

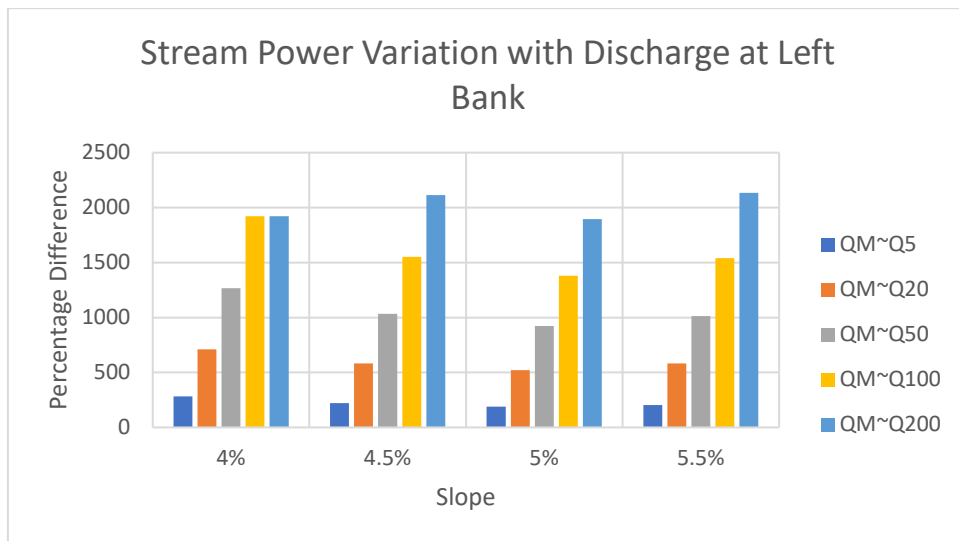


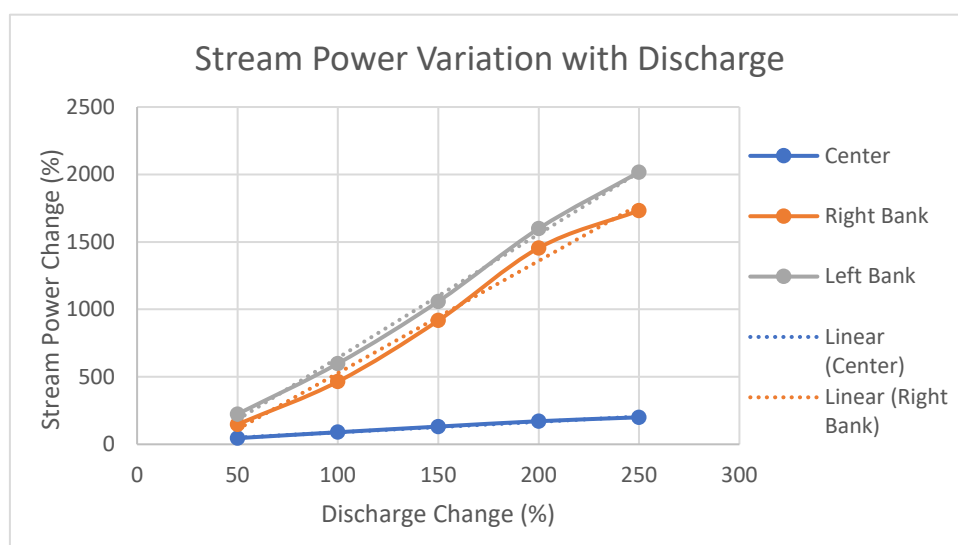
Figure 5-43 Average Percentage Variation of Stream Power with Discharge at Constant Slope at River Left Bank

Table 5-8 and Figure 5-44 the percentage change in stream power (average over the cross-sections and further averaged over the slope scenarios) change with changing discharge.

Table 5-8 Average Change in Stream Power with Discharge Variation

Discharge Change Case	Change in Discharge (%)	Percent Change in Stream Power at Right Bank (%)	Percent Change in Stream Power at Center (%)	Percent Change in Stream Power at Left Bank (%)
QM~Q5	50	147.90	45.73	224.21
QM~Q20	100	464.65	89.51	598.74
QM~Q50	150	916.94	131.22	1058.83

<b>Discharge Change Case</b>	<b>Change in Discharge (%)</b>	<b>Percent Change in Stream Power at Right Bank (%)</b>	<b>Percent Change in Stream Power at Center (%)</b>	<b>Percent Change in Stream Power at Left Bank (%)</b>
Q <sub>M</sub> ~Q <sub>100</sub>	200	1454.99	171.17	1598.41
Q <sub>M</sub> ~Q <sub>200</sub>	250	1732.65	200.05	2016.53



*Figure 5-44 Relationship Between Discharge Change and Stream Power Change*

### 5.4 Correlation Identification

The data obtained from the simulations was further subjected to different statistical tests in order to find correlations and interdependencies of different parameters. This section discusses in detail the different statistical tests applied on the data.

A total of 100 cross-sections were analyzed under the three-point data scheme. The number of scenarios modelled was 24. This resulted in 2400 observations for each parameter along each observational strip (for example 2400 observations for water depth along river right bank). With three observational strips the total number of data point for a parameter were 7200.

While running the statistics, scenarios discretization was maintained. The data was organized from lowest to highest scenario ( $Q=Q_M$  &  $S=4\%$  being lowest scenario and  $Q=Q_{200}$  &  $S=5.5\%$  being highest scenario) and observations were numbered from 1 to 2400 respectively.

### 5.4.1 Box Plots

As a preliminary statistical test box plots were plotted for the different hydraulic parameters under consideration.

#### 5.4.1.1 Depth

The box plot for water depth is shown in Figure 5-45. The outliers are identified in this test as observation number (the numbering process being explained in section 5.4).

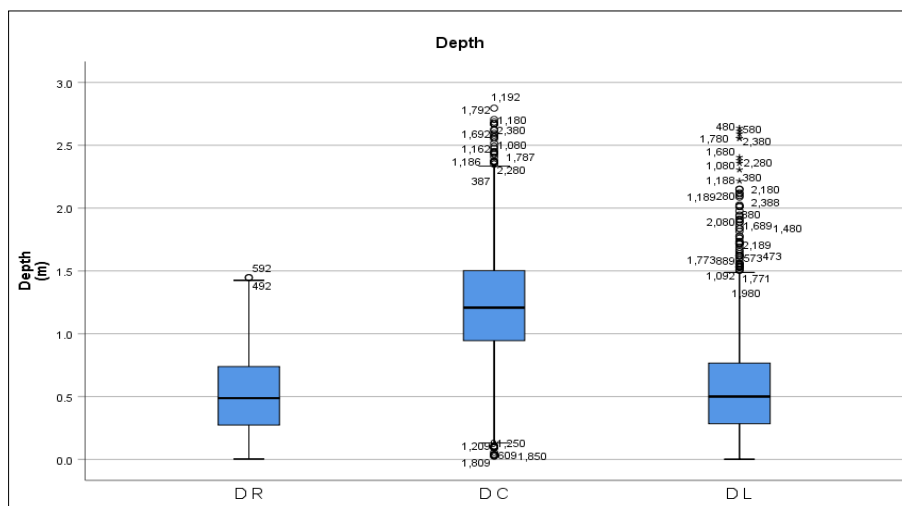


Figure 5-45 Box Plot for Depth (DR= Depth at Right Bank, DC= Depth at Center, DL= Depth at Left Bank)



The test shows good agreement between depths at the two banks with median lying at 0.48 m for right bank and 0.5 m for left bank. However, the number of outliers at the left bank is much higher than right bank. The inspection of topography at these points confirms the correctness of these values as the topography at the two banks is different and changes with flow width.

At the right bank 2 outliers were found above the highest datum. At the left bank 24 outliers were found above the highest datum. The median value of depth at the center lies at 1.2 m. A total of 4 outliers below lowest datum and 11 outliers above highest datum.

### 5.4.1.2 Velocity

The box plot for velocity is shown in Figure 5-46.

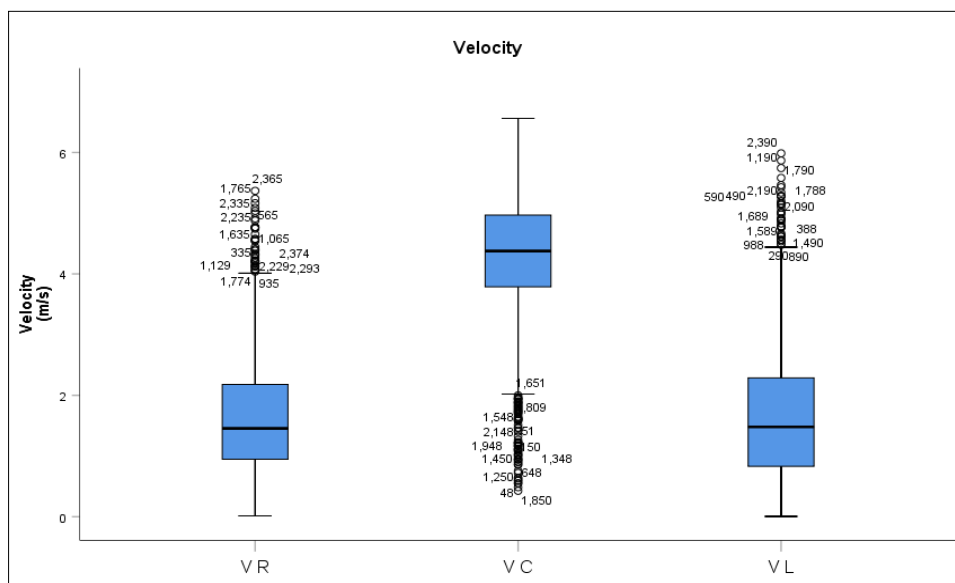


*Figure 5-46 Box Plot for Velocity (VR= Velocity at Right Bank, VC= Velocity at Center, VL= Velocity at Left Bank)*

The box plot shows that the range of velocities at left bank is slightly higher than the range at right bank.

The velocity data at right bank has a median of 1.45 m/s and 14 outliers above the highest datum. At the left bank the median value for velocity is 1.48 m/s with 15 outliers above the highest datum. At the center the median value for velocity is 4.38 m/s with 13 outliers below the lowest datum.

### 5.4.1.3 Shear Stress

The box plot for shear stress is shown in Figure 5-47.

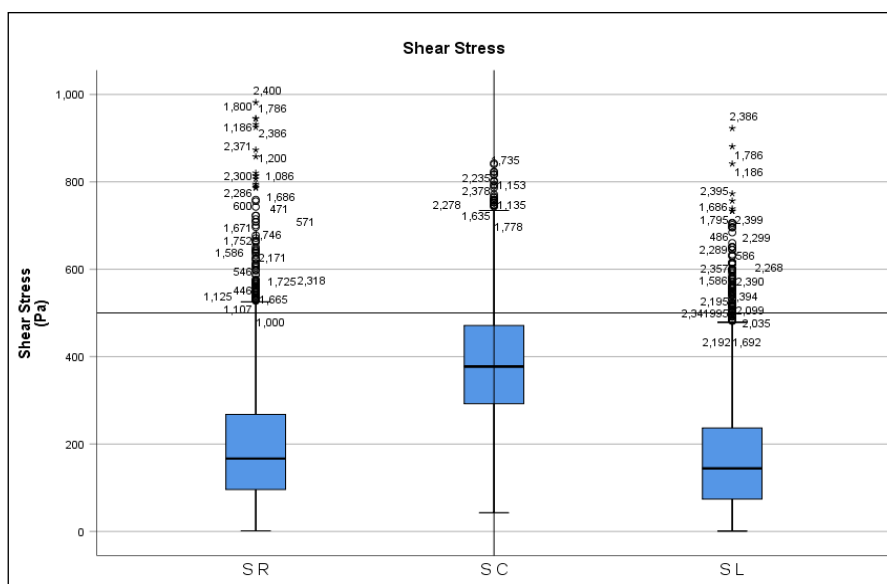


Figure 5-47 Box Plot for Shear Stress (SR= Shear Stress at Right Bank, SC= Shear Stress at Center, SL= Shear Stress at Left Bank)

The variation in shear stress data is large at the center points with 8 outliers above the highest datum. The number of outliers at the right and left bank are 27 and 23, respectively and they are all above the highest datum. The median value of shear stress at the right and left bank is 166.66 Pa and 144.19 Pa respectively, while the median value at the center is 377.5 Pa.

### 5.4.1.4 Stream Power

The box plot for stream power is shown in Figure 5-48.

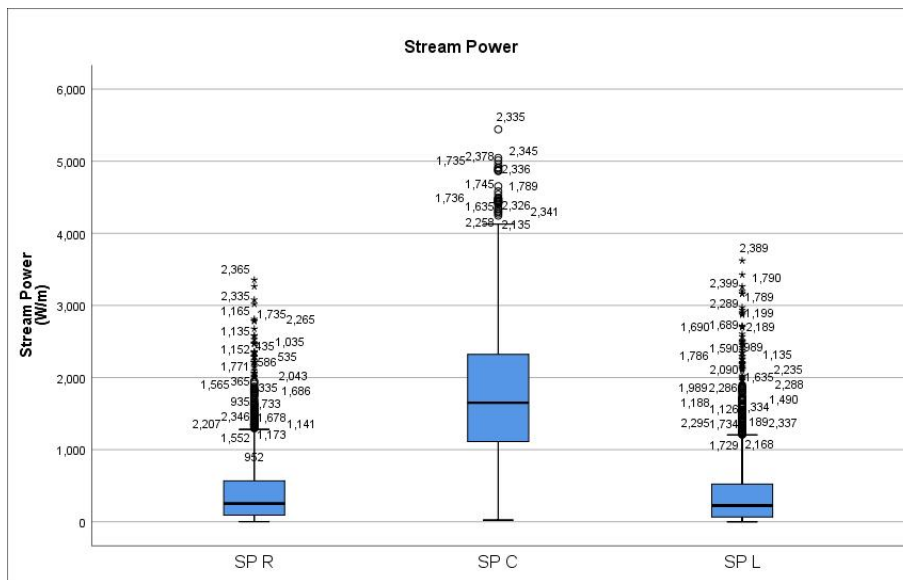


Figure 5-48 Box Plot for Stream Power (SP R= Stream Power at Right Bank, SP C= Stream Power at Center, SP L= Stream Power at Left Bank)

The variation of stream power at the center of the river is large as compared to the banks however, the number of outliers is low *i.e.* 8, while at the banks the number of outliers at the right and left bank is 20 and 25, respectively. Outliers in stream power at all three observation strips lye above the highest datum. The median value for stream power at right and left banks is 253.2 W/m and 224.73 W/m, respectively, whereas at the center the median value for stream power is 1650 W/m.

### 5.4.2 Frequency Analysis

Figure 5-49 to 5-54 show histograms for the parameters under consideration. The histograms were plotted to identify the ranges that exist for each parameter and relate them with one another.

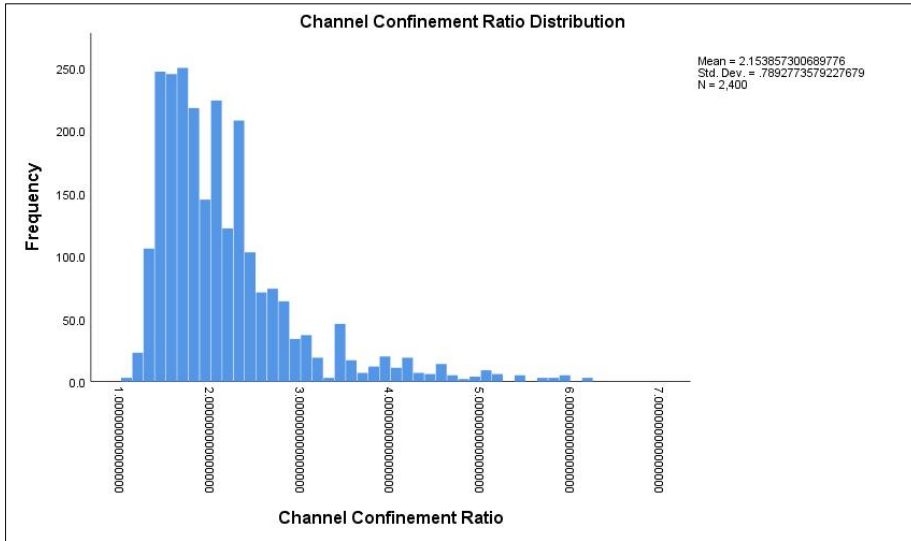


Figure 5-49 Lateral confinement ( $W_r$ ) Histogram

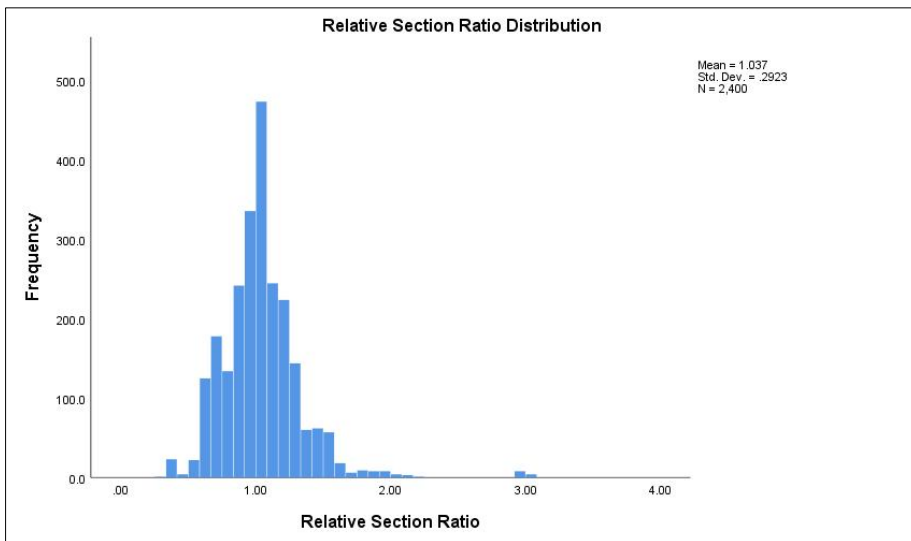


Figure 5-50 Relative Section Width Histogram

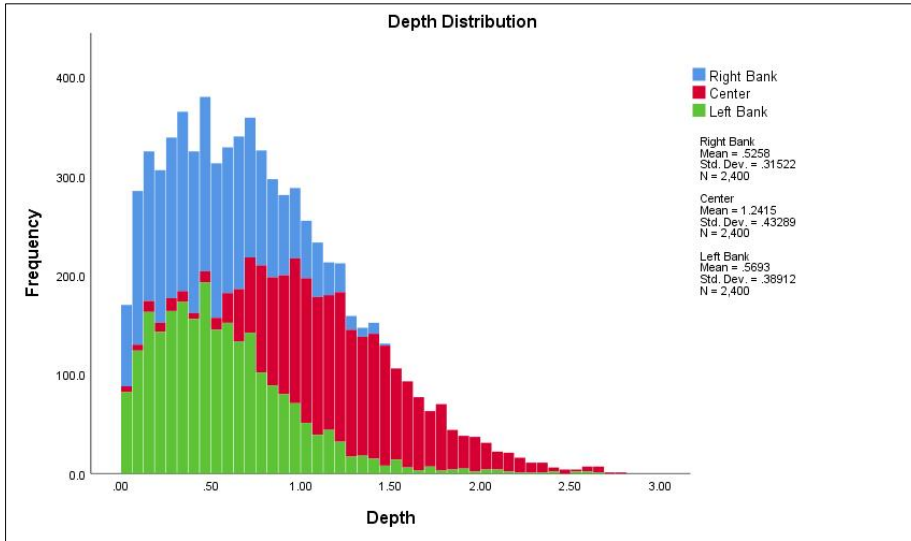


Figure 5-51 Depth Histogram

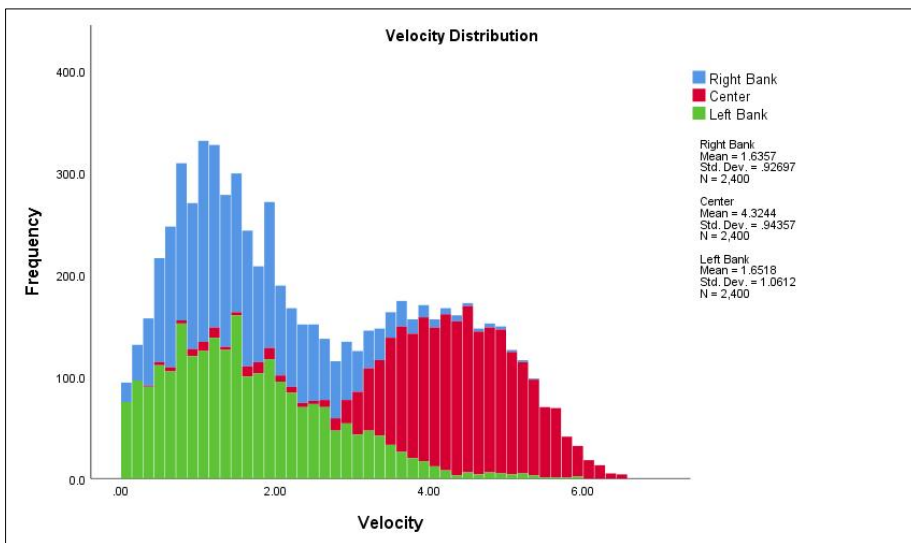


Figure 5-52 Velocity Histogram

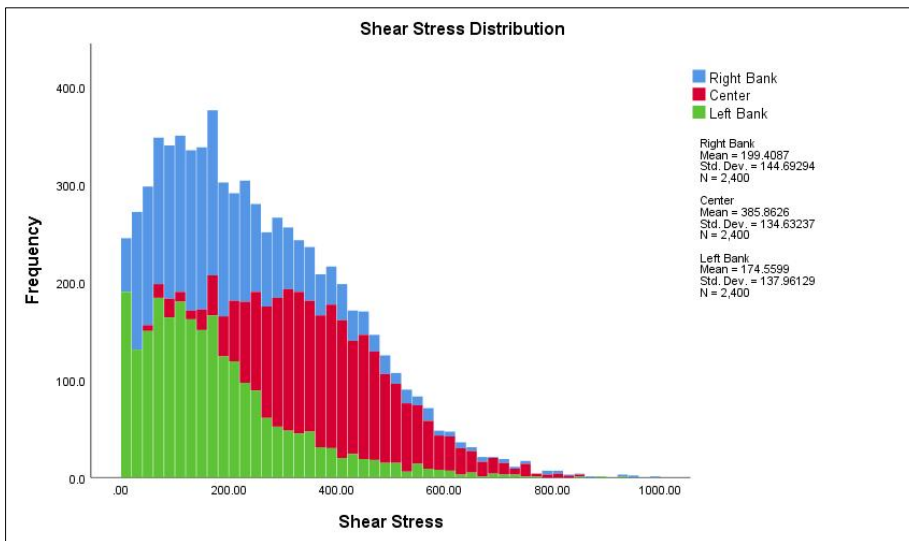


Figure 5-53 Shear Stress Histogram

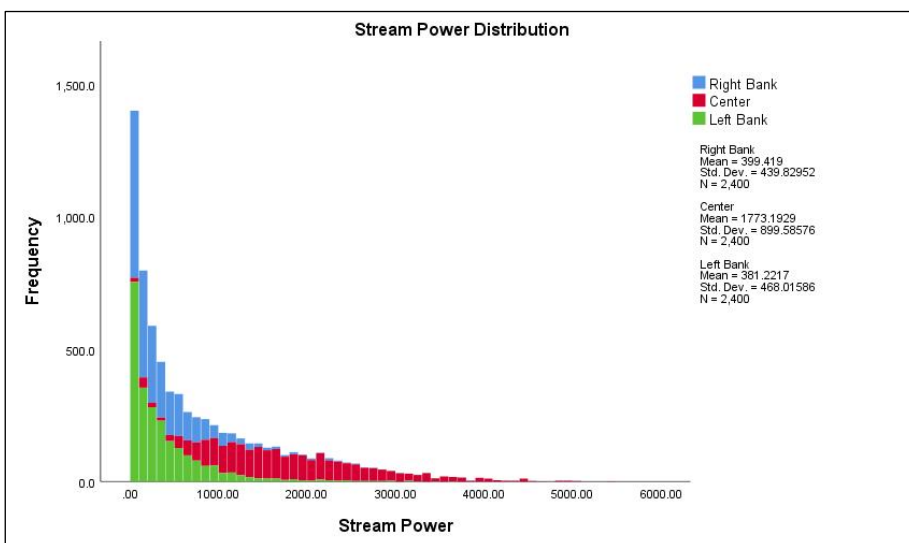


Figure 5-54 Stream Power Histogram

### 5.4.3 Correlation Test

Pearson correlation test was applied to test the correlation among various parameters. The correlation matrix is provided in Table 5-9 and the correlation matrix plot is provided in Figure 5-55.

**Table 5-9 Correlation Matrix for Different Parameters**

<b>Para.</b>	<b>SP</b>	<b>D</b>	<b>V</b>	<b>S</b>	<b>W<sub>xs</sub></b>	<b>W<sub>r</sub></b>	<b>s</b>	<b>Q</b>
<b>SP</b>	1	.689**	.905**	.897**	-.026*	.084**	.124**	.347**
<b>D</b>	.689**	1	.781**	.593**	-.141**	.113**	-.068**	.482**
<b>V</b>	.905**	.781**	1	.777**	-.068**	.088**	.065**	.298**
<b>S</b>	.897**	.593**	.777**	1	-.064**	.116**	.135**	.406**
<b>W<sub>xs</sub></b>	-.026*	-.141**	-.068**	-.064**	1	.143**	0.001	-0.004
<b>W<sub>r</sub></b>	.084**	.113**	.088**	.116**	.143**	1	0.012	.375**
<b>s</b>	.124**	-.068**	.065**	.135**	0.001	0.012	1	0.000
<b>Q</b>	.347**	.482**	.298**	.406**	-0.004	.375**	0.000	1

\*\* . Correlation is significant at the 0.01 level (2-tailed).

\* . Correlation is significant at the 0.05 level (2-tailed).

The correlation matrix Table 5-9 shows that discharge (Q) is positively related to all the hydraulic parameters and the correlation of discharge (Q) with water depth and shear stress is moderate. Discharge was weak correlation with velocity, stream power and lateral confinement. Whereas, its correlation with relative section width is zero.

Slope shows weak to zero correlations with all the other parameters. It has a weak correlation with shear stress and stream power. A very weak negative correlation with water depth. Very weak correlation with velocity. Slope shows zero correlation with discharge, relative section width and lateral confinement.

Lateral confinement shows weak to zero correlations with all the other parameters. Correlations of lateral confinement with discharge, relative section width, water depth, and shear stress are weak. Whereas, correlations with slope, stream power and velocity are very weak.

The relative section width ( $W_{xs}$ ) shows negative correlation with all the hydraulic parameters indicating that reduction in flow widths (contractions) leads to an increase in hydraulic parameters. The relative section width has a weak negative correlation with water depth. The correlation with lateral confinement is positive but weak. Relative section width's correlations with velocity, shear stress and stream power are very weak and negative. This parameter shows zero correlation with slope and discharge.

Shear Stress has a strong positive correlation with stream power, depth and velocity. It shows a moderate positive correlation with discharge. It has positive but weak correlation with slope and lateral confinement. The correlation between shear stress and relative section width is very weak and negative.

Velocity shows strong correlation with stream power, depth and shear stress. All these correlations are positive. It has a good positive correlation with discharge. The correlation of velocity with slope and lateral confinement is positive but weak. Velocity a very weak negative correlation with relative section width.

Water Depth has strong positive correlation with stream power and velocity. It has a moderate positive correlation with shear stress and discharge. Correlation of water depth with lateral confinement weak. The correlation of depth with relative section width ( $W_{xs}$ ) is negative and very weak. With slope water depth has a very weak negative correlation.

Stream power shows strong positive correlations with velocity, shear stress and water depth. It also has a moderate positive correlation with discharge. The correlation of stream power with slope is positive but weak. Stream power shows a very weak positive correlation with lateral confinement. Its correlation with relative section width is very weak and negative.



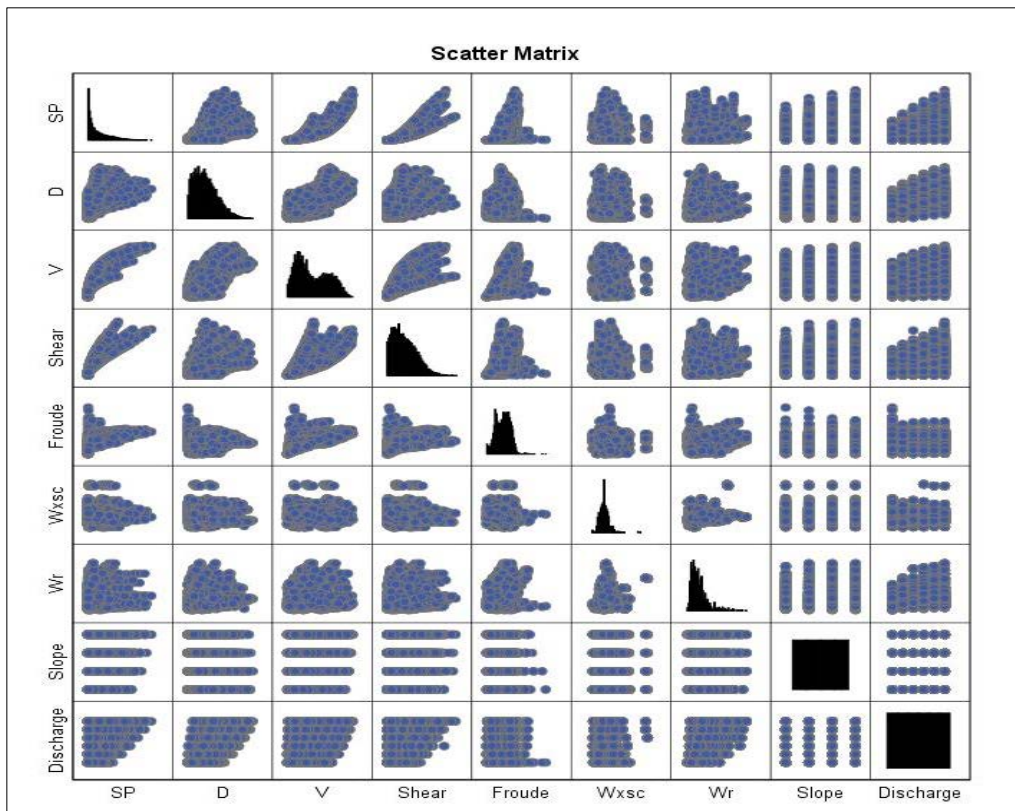


*Figure 5-55 Scatter Matrix Plot for Parameters*

## 5.5 Influence of Bends

Outliers identified in **section 5.4.1** were tracked back in the simulation results to cross-check incidence location as well as their legitimacy. It was observed that most of the high values for different hydraulic parameters appeared close to the channel bends, which indicated the influence of bends on these parameters. Figure 5-56 shows the locations and measurements of the bends in the modelled river reach. Table 5-10 presents the summary of these bends.

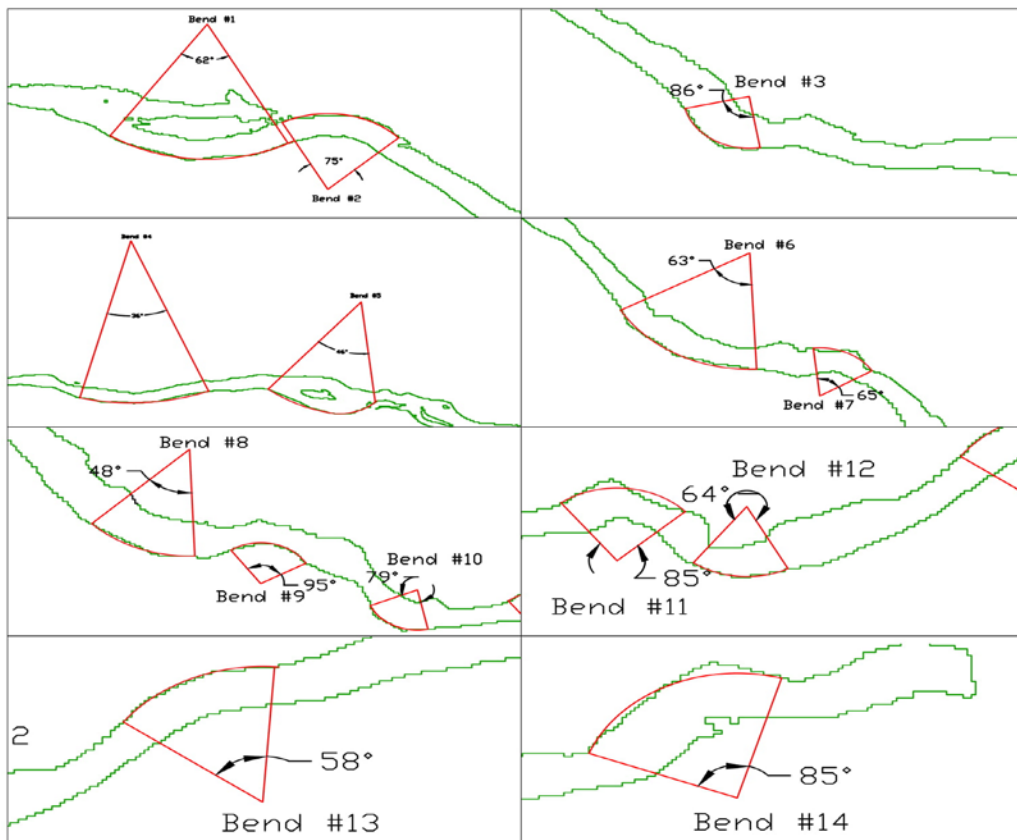


Figure 5-56 Bend Measurement in the Modelled River Reach

Table 5-10 Details of Bends in the Modelled River Reach

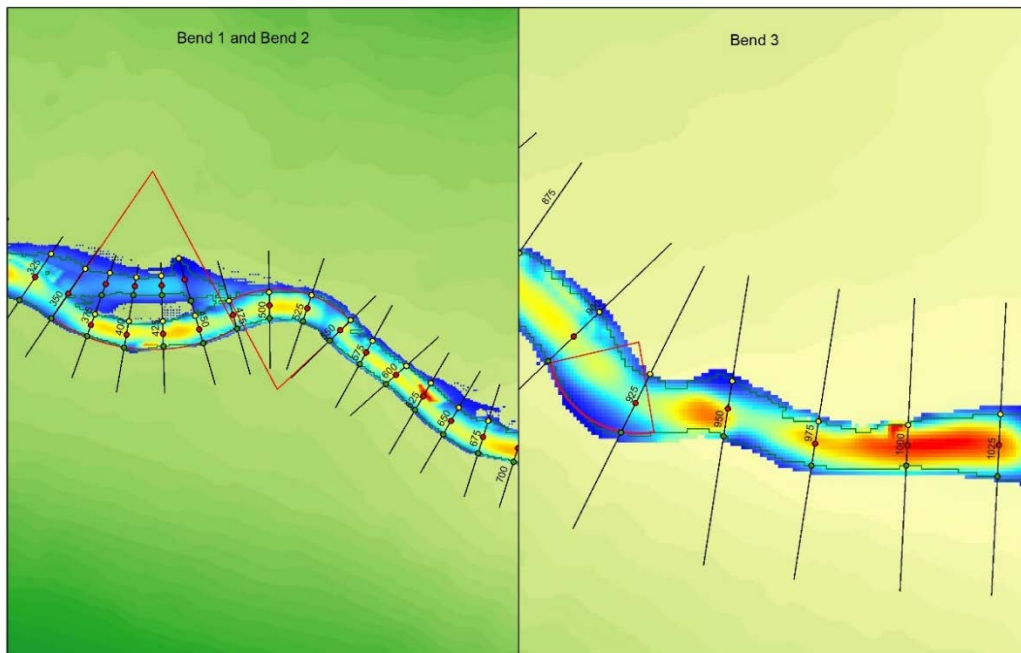
Bend #	Starting XS	Ending XS	Angle Degrees	$W_{xs}$	$W_{xs^*}$	$W_{xs^{**}}$
1	350	475	62°	1.07	0.698	1
2	475	550	75°	1.01	0.956	0.942
3	900	925	86°	0.839	0.857	0.827
4	1075	1225	36°	0.871	1.291	1.022
5	1300	1425	46°	0.815	1.127	1.216

<b>Bend #</b>	<b>Starting XS</b>	<b>Ending XS</b>	<b>Angle Degrees</b>	<b>W<sub>xs</sub></b>	<b>W<sub>xs*</sub></b>	<b>W<sub>xs**</sub></b>
6	2025	2100	63°	1.027	1.195	0.648
7	2125	2150	65°	0.648	1.104	1.537
8	2250	2275	48°	0.899	0.632	1.535
9	2300	2350	95°	1.535	0.637	0.828
10	2375	2400	79°	0.828	1.398	1.426
11	2425	2450	85°	1.398	1.426	0.698
12	2475	2500	64°	0.698	0.986	1.157
13	2550	2600	58°	1.066	1.106	0.745
14	2650	2700	85°	0.745	1.304	-

W<sub>xs\*</sub>. Relative Section width of First cross-section after bend

W<sub>xs\*\*</sub>. Relative Section width of Second cross-section after bend

Bends influence hydraulic parameters such as water depth, velocity, shear stress and stream power based on their angle and orientation. They cause recirculation of flow within and right after. The investigations also reveal that post-bend, channel morphology has an important role to play. The sharp rise in hydraulic parameters is also linked with the relative section width (W<sub>xs</sub>). The results from all simulated scenarios are consistent in the trend that bends followed by river section narrowing (or contractions *i.e.* W<sub>xs</sub> <1) tend to increase hydraulic parameters sharply, contrary to river cross-section expansions (W<sub>xs</sub> >1) where no sharp changes in hydraulic parameters are observed, (Figure 5-57).



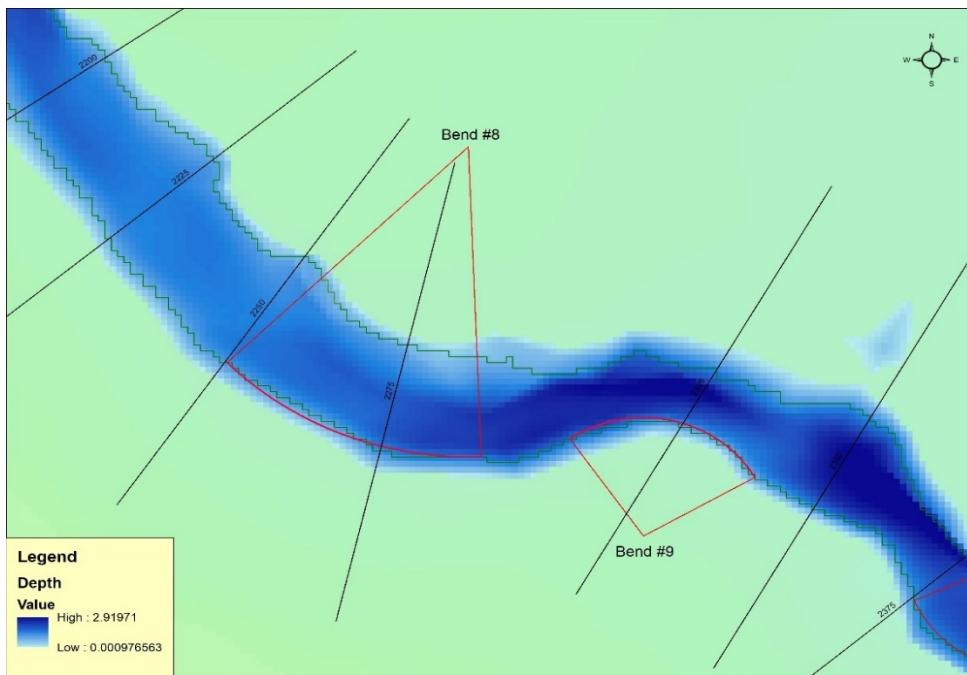


**Figure 5-58 Location of Bends under consideration within the modelled reach**

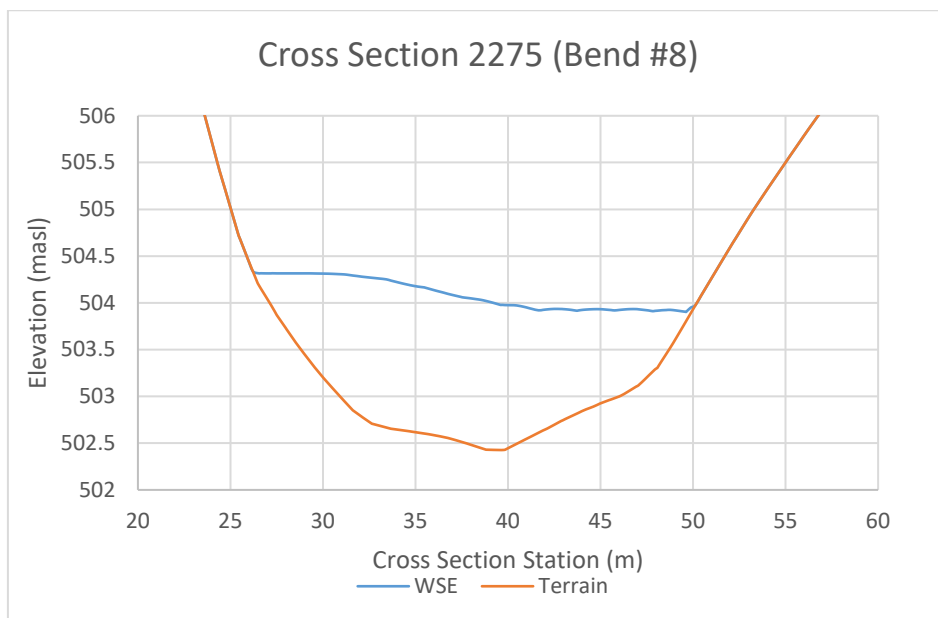


**Figure 5-59 Water Surface Elevation at Bend 8**

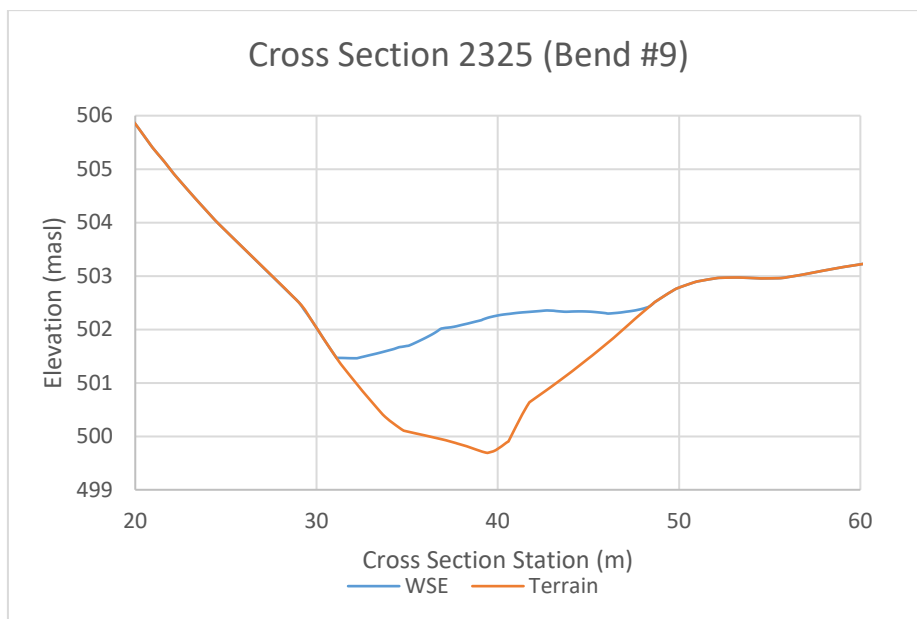


*Figure 5-60 Water Surface Elevation at Bend 9*

Figure 5-59 and Figure 5-60 show water surface profiles at bend #8 and bend #9, these figures correspond to scenario  $Q_{200}$ ,  $s = 5.5\%$ . It can be clearly seen that the water surface is tilted in the bends with lower end at the convex side of the bend and higher end at the concave side of the bend. Bend #8 has an angle of  $48^\circ$  while Bend #9 has an angle of  $95^\circ$ . The difference in water surface elevation between the concave and convex sides for Bend #8 and Bend #9 is 0.45 m and 1.03 m respectively.

Water depth comparison could not be made since it is dependent on the underlying terrain and the terrain on the two banks varies. Therefore, water depth was not a suitable parameter to demonstrate this effect of bends.

### **5.5.2 Influence of Bends on Velocity**

Within the bend, velocity tends to increase at the convex bank of the bend while it remains low at the concave banks. The bend angle influences the degree of increase and distribution of velocities within the bend. Sharp bends (bends having large angles) increase velocities significantly as compared to mild

bends. Figure 5-61 shows the comparison of a mild and sharp bend. Bend #4 can be seen to have high velocities concentrated mostly at the center of the river, while at bend #13 high velocities are distributed from center to the convex bank of the bend.

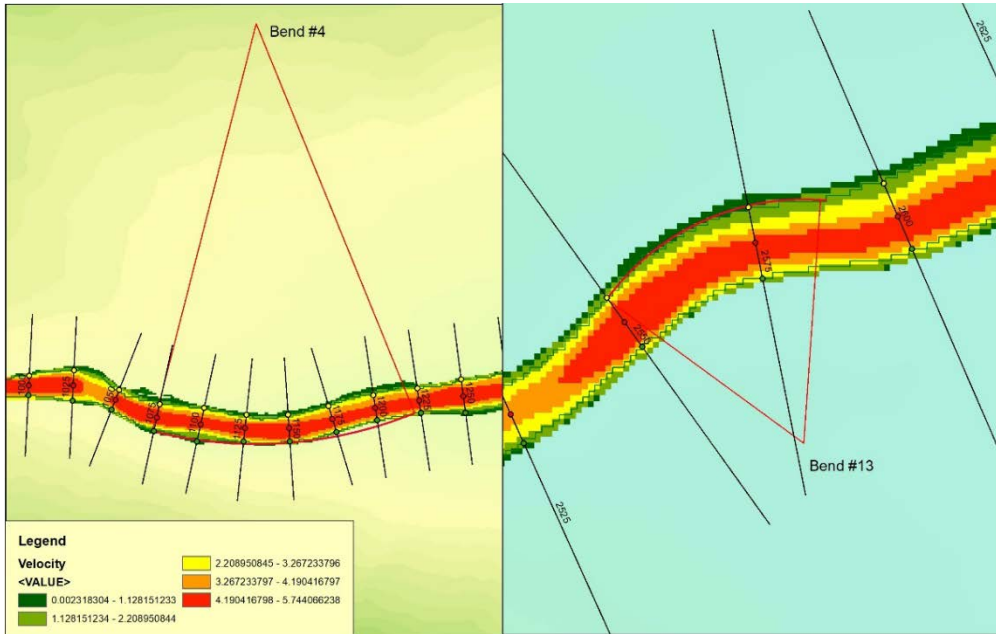


*Figure 5-61 Influence of Bends on Velocity*

### **5.5.3 Influence of Bends on Shear Stress**

In river sections with bends, shear stress follows a pattern similar to that of velocity in bends *i.e.* high shear stress at the convex banks progressively increasing towards the center of the section and finally reducing to low shear stress at the concave bank. It was also observed that shear stress is intensified in post bend sections which experience a contraction ( $W_{xs} < 1$ ). Bend angle does not seem to influence shear stress significantly, however, the relative section width ( $W_{xs}$ ) in pre- and post-bend sections appears to be more relevant. Figure 5-62 represents the variation of shear stress along the river at different bend sections.





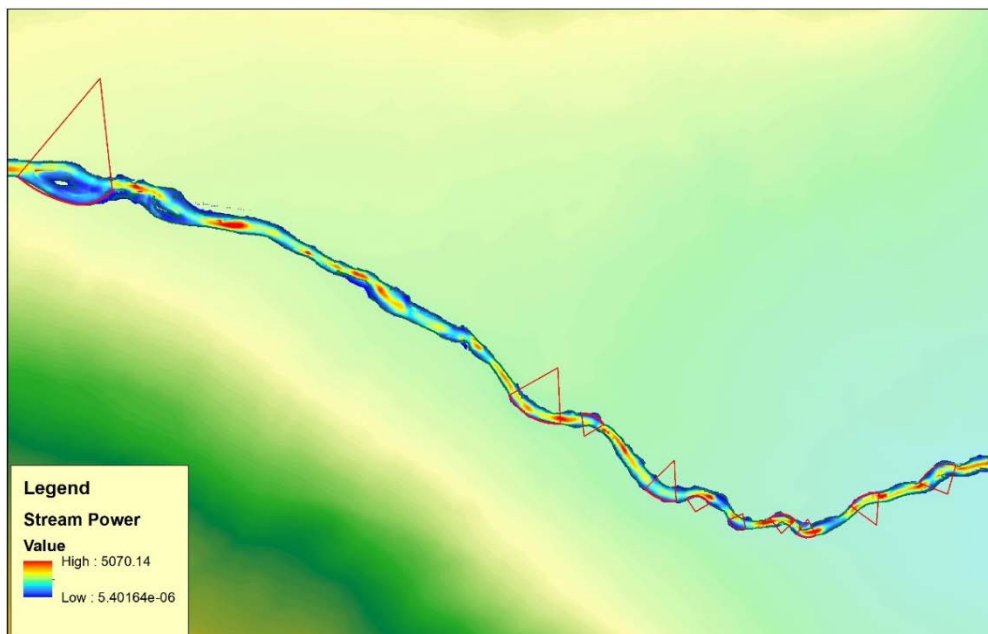


*Figure 5-63 Influence of Bends on Stream Power*

## 5.6 Class Summary

The results of the simulations were categorized into classes based on stream power since it is a good measure of a stream’s geomorphic stability. Table 5-11 presents the classes for the stream power based on data from the center of the river reach modelled.

*Table 5-11 Classes for Stream Power based on Data from Stream Center*

Stream Power (W/m)		Freque- ncy	W <sub>xs</sub>		W <sub>r</sub>		Q (m <sup>3</sup> )		S (%)	
L.B	U. B		L.B	U.B	L.B	U.B	L.B	U.B	L.B	U.B
22.26	998.56	481	0.39	2.05	1.12	5.48	30	105	0.040	0.055
1000.8	1999.5	1053	0.32	3.07	1.12	6.20	30	105	0.040	0.055
2000.9	2998.4	629	0.35	2.97	1.32	6.20	30	105	0.040	0.055

Stream Power (W/m)		Frequency	W <sub>xs</sub>		W <sub>r</sub>		Q (m <sup>3</sup> )		S (%)	
L.B	U. B		L.B	U.B	L.B	U.B	L.B	U.B	L.B	U.B
3000.8	3969.6	192	0.65	1.57	1.36	5.00	60	105	0.040	0.055
4010.4	4959.5	42	0.76	1.50	1.45	5.09	75	105	0.045	0.055
5009.5	5441.4	3	0.99	1.38	1.83	2.67	105	105	0.050	0.055

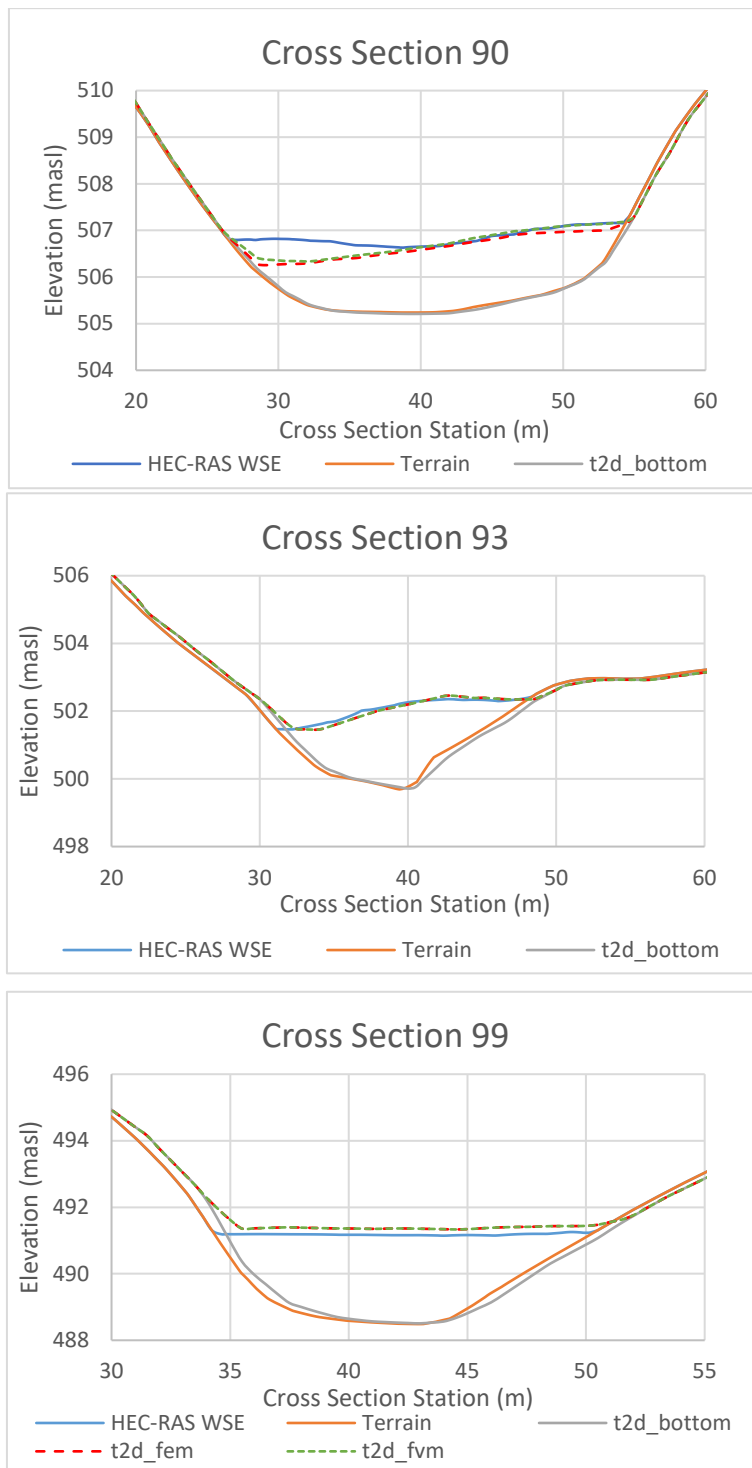
L.B: Lower Bound  
U.B: Upper Bound

Table 5-11 also confirms the poor correlation of stream power with topographic features such as relative section width  $W_{xs}$  and confinement ratio  $W_r$ . It shows the dependency of stream power over slope and discharge, that a stream will experience extreme stream power at high discharge and high slope. The influence of bends, however, cannot be ignored.

### 5.7 Comparison Results from TELEMAC 2-D

In order to ensure the health of output data obtained from HEC-RAS (v. 5.0.7), parallel simulations of a scenario were carried out in TELEMAC 2-D (**section 4.4**). The results from the simulations in terms of Water Surface Elevation comparison are presented in Figure 5-64. The results show good agreement between the water surface elevations computed by the two packages with minor differences. The terms used in Figure 5-64 are explained below:

- HEC-RAS WSE = Water Surface Elevation from HEC-RAS
- Terrain = Topography as interpreted by HEC-RAS
- t2d\_bottom = Topography as interpreted by TELEMAC
- t2d\_fem = Finite Element Method results from TELEMAC 2-D
- t2d\_fvm = Finite Volume Method results from TELEMAC 2-D



**Figure 5-64** Computed Water Surface Elevation Comparison between *HEC-RAS* and *TELEMAC 2-D*



## **6 Discussion**

The aim of this work was to find critical locations in steep rivers and determine correlations between hydraulic and topographical parameters so that a methodology could be developed in a GIS-based environment that can be used as a preliminary test to identify these areas without the carrying out hydrodynamic modeling of the entire river. The reason behind this approach is to save computational expense and time on hydrodynamic modeling of an entire river reach by focusing only on shorts sub-reaches of critical nature.

The simulation program designed for this work involved idealized rivers with constant slope throughout the modeled reach and idealized flood discharges. The reason behind this approach was to avoid effects of slope changes within the modeled reach and study the influence of slope as a discrete parameter. Similarly, discharge idealization was a logical approach since the river, it served input to, itself was an idealized one. Flood discharges during the simulation period were also kept constant under the same approach as to study discharge as a discrete parameter and avoid variations so that the different scenarios modeled, and the defined data extraction points remained comparable.

The output hydraulic parameters selected for this study included water depth, velocity, shear stress and stream power. Confinement ratio and relative section width were identified as topographical parameters derived from the river's flow width.

The following sections discuss the influence of discharge and slope changes on hydraulic parameters.

## 6.1 Slope

The slope range idealized for this work was kept from 4% to 5.5% increasing at an interval of 0.5, which equals to an incremental gradient of 12.5% of the base slope value *i.e.* 4%.

In nature, river slope is a continuous parameter and slope changes can be abrupt such as a step-pool situation which is encountered often in steep rivers. The reason behind the choice of small incremental gradient for slope in this study was not only for simplification purpose but also to study the effect of slope logically; aimed to find out the nature of relationship between slope and other hydraulic parameters and whether it is explained by a linear or a non-linear behavior.

The results presented in **section 5.2**, show that the average percent change in all the hydraulic parameters *i.e.* water depth, velocity, shear stress and stream power is satisfactorily explained by a linear relationship, however, the direct or inverse proportionality of slope varies from parameter to parameter. For instance, the relationship between percent slope change and average percentage change in depth is an inverse linear fit. For velocity, shear stress and stream power the average percentage change relationships with slope change is a direct linear fit. However, this trend is based on averaged percentage change values, moreover, the number of slope scenarios are insufficient to draw this conclusion in entirety.

The effects of slope change on stream banks is similar to the center of the stream. This behavior is common for all hydraulic parameters. However, one bank experiences greater change as compared to the other bank. This behavior indicates that apart from slope change at a constant discharge stream morphology (bends, relative section width, bed morphology etc.) also controls the response of hydraulic parameters.

## **6.2 Discharge**

The discharge range selected for this work was kept from 30 m<sup>3</sup>/s to 105 m<sup>3</sup>/s with an increment of 15 m<sup>3</sup>/s for each flood return scenario (return periods ranging from mean flood to a 200-year flood). This fixed increment amounted to an incremental gradient of 50% of the base discharge value *i.e.* 30 m<sup>3</sup>/s. This idealization was based on the same concept as discussed for slope *i.e.* simplification and logical approach to determine the nature of relationship that exists between different parameters.

The results presented in **section 5.3**, show that discharge has a directly proportional relationship with all the hydraulic parameters. This means that increasing discharge will see increased response in the river reach for water depth, velocity, shear stress and stream power.

Discharge variation has drastic impacts on river banks owing to the fact that increasing discharge leads to an increase in the river width hence, increasing the submergence of banks and probable overtopping. In steep river, width of flow is a function of discharge. These rivers often have in V-shaped cross sections, especially in case of deep-seated rivers (or deeply entrenched rivers). In such cases, river width and river banks are not fixed but variate as a function of discharge and slope. This is the main reason that bank points show large variation in percentage change for each parameter with changing discharge as compared to the percentage change in parameters at the river center.

The results show that out of the two input parameters *i.e.* slope and discharge, the influence of discharge variation is larger than slope variation. This result is also supported by the correlation matrix which shows better correlation hydraulic parameters with discharge than slope (**section 5.4.3, Table 5-9**).

### 6.3 Correlation Between Hydraulic and Topographical Parameters

The correlation between the topographic parameters (*i.e.* slope, relative section width and lateral confinement) and hydraulic parameters (discharge, water depth, velocity, shear stress and stream power) were presented in **section 5.4.3**. The correlations between topographic and hydraulic parameters are weak. Response parameters, such as water depth, velocity, shear stress and stream power correlate better with discharge than slope or other topographic parameters, in fact with topographic parameters the correlation ranges from weak to very weak.

The correlation test applied was the Pearson correlation test which is a linear correlation test. An idiosyncrasy of correlation tests is that they are sensitive to outliers (*i.e.* values beyond Interquartile Range), a single outlier can disturb the correlation test results significantly. The dataset used for the correlation test contained outliers since they cannot be discarded as their incidence location is logically correct *i.e.* near bends in the stream. This is one explanation for weak correlation between different parameters. Moreover, slope and discharge were defined as discrete parameters instead of continuous, in this work, the correlation test is also sensitive to the nature of parameters involved and usually works well with continuous parameters.

Non-linear correlation tests were not tried in this study however, different curve fitting methods were tried. Figure 6-1 shows the curve fitting method applied to evaluate a nonlinear correlation between relative section width and stream power. The curve fit statistics for this model are presented in Table 6-1. The non-linear curve fitting also returned weak correlation between the hydraulic and topographical parameters. This suggests that the hydraulic parameters are not dependent on just one parameter or their sensitivity is not related to one parameter but on multiple parameters simultaneously and this



relationship could be identified by carrying out a multi-variable regression technique.

**Table 6-1 Non-Linear Curve fitting Model Statistics for Stream Power**

Equation	Model Summary	Parameter Estimates			
	R <sup>2</sup>	Constant	b1	b2	b3
Quadratic	0.001	863.833	39.423	-46.035	
Cubic	0.003	289.027	1481.014	-1115.498	225.16
Power	0.013	351.232	-0.741		
S	0.009	5.305	0.535		
Exponential	0.013	727.001	-0.701		

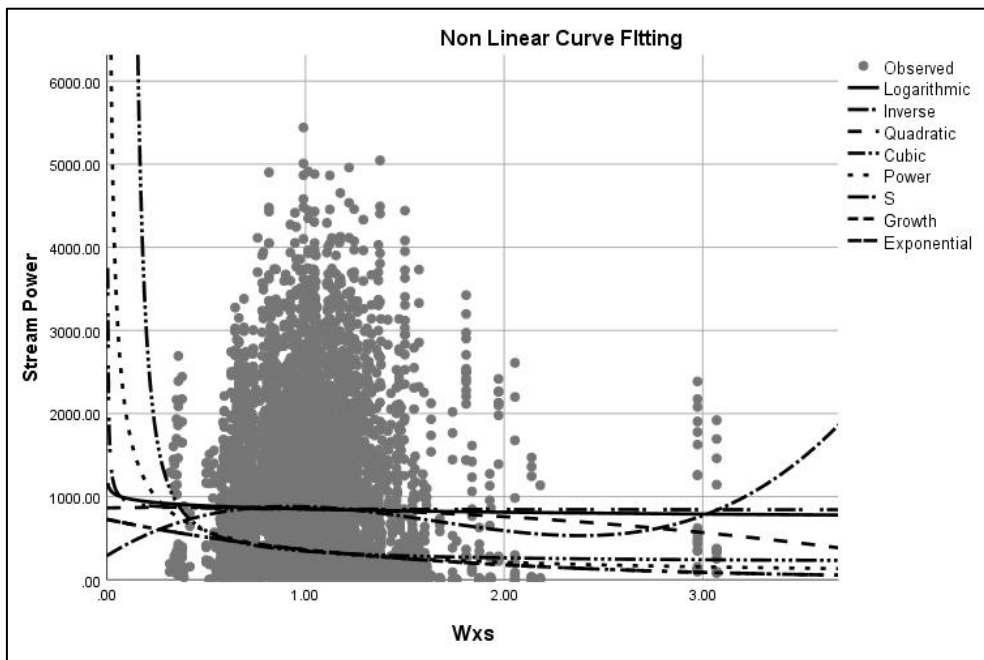


**Figure 6-1 Non-Linear Curve fitting to Stream Power Data**

#### **6.4 Bends in Rivers**

The simulations of different scenarios carried out under this study highlighted the significance of bends in river hydraulics. Bends significantly alter the flow pattern and hydraulic parameters through recirculation of flow, especially in steep rivers where flow velocities are already high. Bends tend to accelerate flow towards the convex bank and retard flow at the concave bank, thereby, increasing the flow depth. At high floods (or high river discharges) this can lead to excessive erosion of the convex bank and possible over topping of the concave bank since the difference in water surface profile can in some cases be as high as 1 m (**section 5.5.1**). Bend angle becomes critical in this regard, as sharp bends (Bend angle  $\geq 60^\circ$ ) show are more pronounced affect as compared to moderate bends ( $30^\circ < \text{Bend angle} < 50^\circ$ ) or mild bend (Bend angle  $< 30^\circ$ )

Quantification of influence of bends and bend angles on hydraulic parameters is complex because of flow recirculation (or secondary flows) which causes a complex three-dimensional fluid flow in the bends. This behavior is not simulated in a two-dimensional hydraulic analysis therefore, it is not considered advisable to recognize bend angle as a parameter in statistical analysis in this study. Moreover, quantification of bend angle should be done very carefully. An important parameter to consider when quantifying a bend is its radius of curvature and the width of flow in the bend.

#### **6.5 Critical Areas in Steep Rivers**

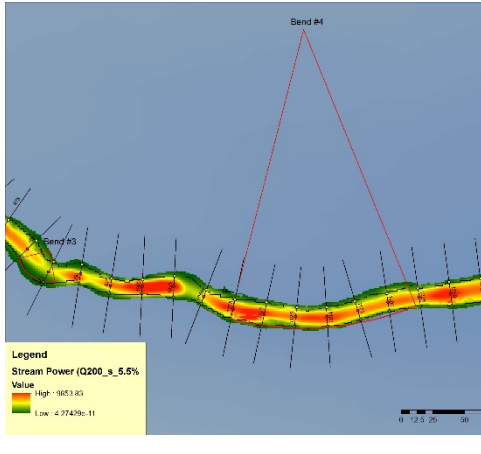
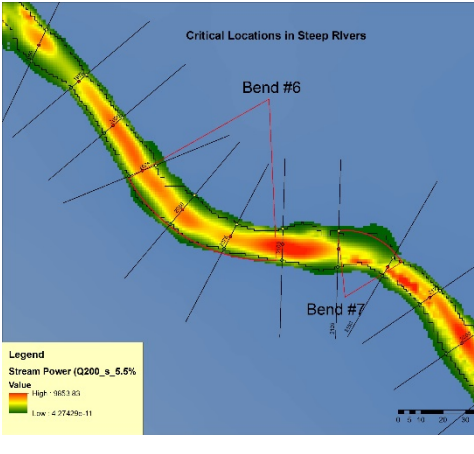
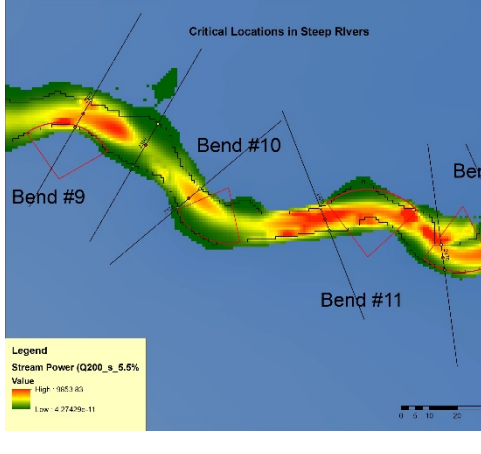
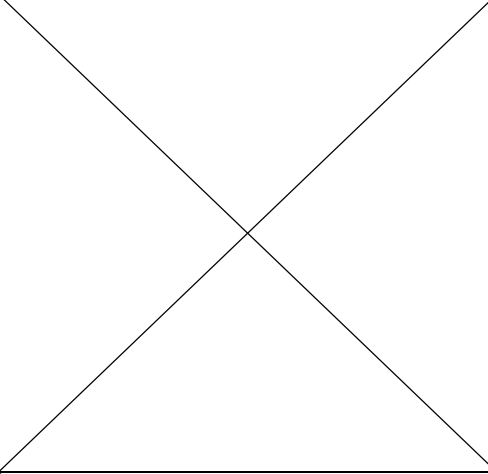
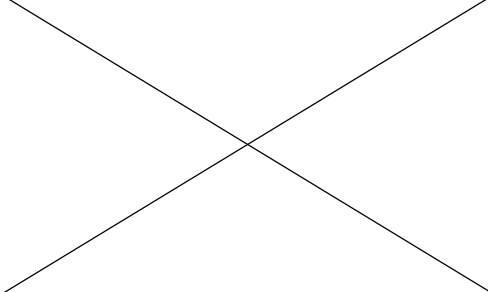
Based on the simulations of different scenarios and the discussion above critical locations in steep rivers depend on a cluster of parameters which force extreme response from the river. These parameters include flood discharge, river bed slope, the relative section width (contraction or expansion of cross-section), lateral confinement and river bends. These parameters may not have provided meaningful correlations with hydraulic parameters individually, due

to limited range of these parameters in this study but based on scenario comparison their relevance can be ascertained.

Critical locations in steep rivers arise in bends and in cross-sections downstream of the bends. This situation is dire in cases where the sections downstream of the bends experience contraction ( $W_{xs} < 1$ ) and high to medium lateral confinement due to river catchment topography (section 5.6, Table 5-11 also support this behavior) or the downstream section marks the initiation of another bend turning in opposite direction. In these river sections, the combined effect of secondary flows generated in bend, lateral confinement and cross-section contraction leads acceleration of flow and high stream power which indicates erosion of the stream bed and banks. Table 6-2 presents a summary of critical locations identified in the modeled rivers.

**Table 6-2 Critical Locations in the Modeled Steep Rivers**

<p>Critical locations in the modeled river (Reference Map) corresponding to scenario <math>Q = Q_{200}</math>, <math>S = 5.5\%</math>.</p>	<p>Sharp bend followed by successive cross-section contractions (<math>W_{xs} = 0.87</math>) and laterally confined (<math>W_r = 2.6</math>) area.</p>

	
<p>Mild laterally confined bend (<math>W_r = 1.9</math>).</p>	<p>Two bends interacting in “S” shape in a laterally confined area (<math>W_r = 1.6</math>) followed by sudden contraction at the end of the bend.</p>
	
<p>Series of sharp bends interacting in “W” shape in a laterally confined area (<math>W_r = 2.05</math>) and consistent contractions throughout the reach (<math>W_{xs} = 0.89</math>)</p>	

## 7 Recommendation and Future Work

The hydraulics of steep rivers is very complex and is still developing. More efforts are needed to understand the physical processes involved that influence the flow in these rivers, in order to develop a sound understanding and make these rivers safe. Most of the hydraulics knowledge applied in this work is developed from low gradient streams. In this work, some key elements of steep rivers were ignored such as steps and pools; slope and discharge were treated as discrete parameters rather than continuous and exclusion of sediment transport due to technical limitations of the modeling packages. These simplifications were although logical for the scope of this work but may not have provided the best results. Therefore, the author of this work makes the following recommendations for future work in this area:

- i. Any future investigations should consider slope and discharge as continuous parameters rather than discrete.
- ii. Geomorphology of the river bed and sediment transport shall be considered in any future work in extension to this work.
- iii. In order to understand flow dynamics at bends and quantification of bend angles, 3-D hydrodynamic simulations should be carried out. Moreover, considerations with reference to radius of curvature of the bends should also be made. Bends should be studied in terms of central angle of the arc fitting the bend as well as the ratio of radius of curvature and stream width.
- iv. Actual steep rivers should be studied so that data for model calibration is available and model results could be validated.
- v. Channel bed roughness is an important characteristic. It should be estimated reasonably as it will vary from case to case, although in steep rivers estimation of bed roughness is a great challenge due to debris and continuous erosion of the bed.

- vi. Data analysis should be done using nonlinear multivariable techniques such as multivariable non-linear regression analysis.

## 8 References

- Abdeyazdan, M., & Jodaki, A. Z. (2015). *Geographic Information System (GIS) Application in Flood Crisis Management*. Paper presented at the 2nd International conference on Innovative Engineering Technologies (ICIET'2015), Bangkok, Thailand.
- Akoglu, H. (2018). User's guide to correlation coefficients. *Turkish Journal of Emergency Medicine*, 18(3), 91-93. doi:<https://doi.org/10.1016/j.tjem.2018.08.001>
- ALCRUDO, F. (2004). A state of the art review on mathematical modelling of flood propagation.
- Amadio, M., Mysiak, J., Carrera, L., & Koks, E. (2016). Improving flood damage assessment models in Italy. *Natural Hazards*, 82(3), 2075-2088. doi:10.1007/s11069-016-2286-0
- Amadio, M., Scorzini, A. R., Carisi, F., Essenfelder, A. H., Domeneghetti, A., Mysiak, J., & Castellarin, A. (2019). Testing empirical and synthetic flood damage models: the case of Italy. *Nat. Hazards Earth Syst. Sci.*, 19(3), 661-678. doi:10.5194/nhess-19-661-2019
- Bathurst, J. C. (1993). Flow resistance through the channel network. *Channel Network Hydrology*, 69-98.
- Bizzi, S., & Lerner, D. (2015). The use of stream power as an indicator of channel sensitivity to erosion and deposition processes. *River Research and Applications*, 31(1), 16-27.
- Brunner, G. W. (2016a). *HEC-RAS River Analysis System. Hydraulic Reference Manual. Version 5.0*. Retrieved from
- Brunner, G. W. (2016b). *HEC-RAS River Analysis System. 2D Modeling User's Manual. Version 5.0*. Retrieved from
- Caleffi, V., Valiani, A., & Zanni, A. (2003). Finite volume method for simulating extreme flood events in natural channels. *Journal of Hydraulic Research*, 41(2), 167-177. doi:10.1080/00221680309499959
- Caletka, M., Šulc Michalková, M., Koli, M., & Trizna, M. (2019). Quality of flood extents delineated by a non-hydrodynamic GIS tool. *CATENA*, 175, 367-387. doi:<https://doi.org/10.1016/j.catena.2018.12.032>
- Caminha, G. (2019). The CFL Condition and How to Choose Your Timestep Size. Retrieved from <https://www.simscale.com/blog/2017/08/cfl-condition/>

- Carisi, F., Schröter, K., Domeneghetti, A., Kreibich, H., & Castellarin, A. (2018). Development and assessment of uni- and multivariable flood loss models for Emilia-Romagna (Italy). *Nat. Hazards Earth Syst. Sci.*, *18*(7), 2057-2079. doi:10.5194/nhess-18-2057-2018
- Chow, V. T. (1959). *Open-channel hydraulics*. New York: McGraw-Hill.
- Clement, M. A., Kilsby, C. G., & Moore, P. (2018). Multi-temporal synthetic aperture radar flood mapping using change detection. *Journal of Flood Risk Management*, *11*(2), 152-168. doi:10.1111/jfr3.12303
- Comiti, F., Cadol, D., & Wohl, E. (2009). Flow regimes, bed morphology, and flow resistance in self-formed step-pool channels. *Water Resources Research*, *45*(4). doi:10.1029/2008wr007259
- Comiti, F., & Mao, L. (2012). Recent Advances in the Dynamics of Steep Channels. In *Gravel-Bed Rivers*.
- Coon, W. F. (1998). *Estimation of roughness coefficients for natural stream channels with vegetated banks* (Vol. 2441): US Geological Survey.
- Cox, D., Hunt, J., Mason, P., Wheeler, H., Wolf, P., & Young, P. C. (2002). Advances in real-time flood forecasting. *Philosophical Transactions of the Royal Society of London. Series A: Mathematical, Physical and Engineering Sciences*, *360*(1796), 1433-1450. doi:doi:10.1098/rsta.2002.1008
- Dano, U. L., Balogun, A.-L., Abubakar, I. R., & Aina, Y. A. Transformative urban governance: confronting urbanization challenges with geospatial technologies in Lagos, Nigeria. *GeoJournal*, 1-18.
- Demissie, M., Soong, T.-W., Bhowmik, N. G., Fitzpatrick, W. P., & Maxwell, W. (1986). Secondary circulation in natural streams.
- Finnegan, N. J., Roe, G., Montgomery, D. R., & Hallet, B. (2005). Controls on the channel width of rivers: Implications for modeling fluvial incision of bedrock. *Geology*, *33*(3), 229-232.
- Galia, T., & Skarpich, V. (2015). *Bankfull widths in steep headwaters of the flysch Carpathians* (Vol. 14).
- Gartner, J. (2016). Stream power: Origins, geomorphic applications, and GIS procedures.
- Gharbi, M., Soualmia, A., Dartus, D., & Masbernat, L. (2016). Comparison of 1D and 2D hydraulic models for floods simulation on the medjerda riverin tunisia. *J. Mater. Environ. Sci.*, *7*(8), 3017-3026.



- Gigović, L., Pamučar, D., Bajić, Z., & Drobnjak, S. (2017). Application of GIS-Interval Rough AHP Methodology for Flood Hazard Mapping in Urban Areas. *Water*, 9(6), 360.
- Gouldby, B., Sayers, P., Mulet-Marti, J., Hassan, M. A. A. M., & Benwell, D. (2008). A methodology for regional-scale flood risk assessment. *Proceedings of the Institution of Civil Engineers - Water Management*, 161(3), 169-182. doi:10.1680/wama.2008.161.3.169
- Harada, E., Ikari, H., Shimizu, Y., Khayyer, A., & Gotoh, H. (2018). Numerical Investigation of the Morphological Dynamics of a Step-and-Pool Riverbed Using DEM-MPS. *Journal of Hydraulic Engineering*, 144(1), 04017058. doi:doi:10.1061/(ASCE)HY.1943-7900.0001392
- Hodges, B. R. (2014). Hydrodynamical Modeling☆. In *Reference Module in Earth Systems and Environmental Sciences*: Elsevier.
- Jongman, B., Kreibich, H., Apel, H., Barredo, J. I., Bates, P. D., Feyen, L., . . . Ward, P. J. (2012). Comparative flood damage model assessment: towards a European approach. *Nat. Hazards Earth Syst. Sci.*, 12(12), 3733-3752. doi:10.5194/nhess-12-3733-2012
- Kvočka, D., Ahmadian, R., & Falconer, R. A. (2017). Flood Inundation Modelling of Flash Floods in Steep River Basins and Catchments. *Water*, 9(9), 705.
- Lee, A. (2000). *The hydraulics of steep streams*. University of Sheffield,
- Lhomme, J., Bouvier, C., Mignot, E., & Paquier, A. (2006). One-dimensional GIS-based model compared with a two-dimensional model in urban floods simulation. *Water Science and Technology*, 54(6-7), 83-91. doi:10.2166/wst.2006.594
- Lhomme, J., Sayers, P., Gouldby, B., Samuels, P., Wills, M., & Mulet-Marti, J. (2008). Inundation modelling Recent development and application of a rapid flood spreading method. In *Flood risk management: research and practice* (pp. 30-39): CRC Press.
- Liu, Q., Qin, Y., Zhang, Y., & Li, Z. (2015). A coupled 1D–2D hydrodynamic model for flood simulation in flood detention basin. *Natural Hazards*, 75(2), 1303-1325. doi:10.1007/s11069-014-1373-3
- Ma, H., & Fu, X. (2012). Real time prediction approach for floods caused by failure of natural dams due to overtopping. *Advances in water resources*, 35, 10-19.
- Marcus, W., Roberts, K., Harvey, L., & Tackman, G. (1992). *An Evaluation of Methods for Estimating Manning's n in Small Mountain Streams* (Vol. 12).

- Moraru, A. (2017). *Streambank erosion and channel widening: implications for flood hazard*.
- Néelz, S., & Pender, G. (2013). *Benchmarking the latest generation of 2D hydraulic modelling packages* Retrieved from [http://evidence.environment-agency.gov.uk/FCERM/Libraries/FCERM\\_Project\\_Documents/SC12\\_0002\\_Benchmarking\\_2D\\_hydraulic\\_models\\_Report.sflb.ashx](http://evidence.environment-agency.gov.uk/FCERM/Libraries/FCERM_Project_Documents/SC12_0002_Benchmarking_2D_hydraulic_models_Report.sflb.ashx)
- Nobre, A. D., Cuartas, L. A., Hodnett, M., Rennó, C. D., Rodrigues, G., Silveira, A., . . . Saleska, S. (2011). Height Above the Nearest Drainage – a hydrologically relevant new terrain model. *Journal of Hydrology*, 404(1), 13-29. doi:<https://doi.org/10.1016/j.jhydrol.2011.03.051>
- Nobre, A. D., Cuartas, L. A., Momo, M. R., Severo, D. L., Pinheiro, A., & Nobre, C. A. (2016). HAND contour: A new proxy predictor of inundation extent. *Hydrological Processes*, 30(2), 320-333. doi:10.1002/hyp.10581
- Norwegian Mapping Authority. Retrieved from <https://hoydedata.no/LaserInnsyn/>
- NVE. Retrieved from <http://nevina.nve.no/>
- NVE Hydra II. Retrieved from <https://www.nve.no/hydrologi/hydrologiske-data/historiske-data/data-i-hydra-ii-databasen/>
- Pender, G. (2006). Briefing: Introducing the Flood Risk Management Research Consortium. *Proceedings of the Institution of Civil Engineers - Water Management*, 159(1), 3-8. doi:10.1680/wama.2006.159.1.3
- Peterson, D. F., & Mohanty, P. K. (1960). Flume studies of flow in steep, rough channels. *Journal of the Hydraulic Division*, 86(9).
- Petrucci, O., M, P., & Pasqua, A. (2010). *Flash floods risk variation of steep drainage basins in Calabria (Italy) and the role of rainfall and anthropogenic modifications since 1800*. Paper presented at the 6th World FRIEND Conference, Fez (Morocco).
- Prakash, M., Rothauge, K., & Cleary, P. W. (2014). Modelling the impact of dam failure scenarios on flood inundation using SPH. *Applied Mathematical Modelling*, 38(23), 5515-5534. doi:<https://doi.org/10.1016/j.apm.2014.03.011>
- Priestnall, G., Jaafar, J., & Duncan, A. (2000). Extracting urban features from LiDAR digital surface models. *Computers, Environment and Urban Systems*, 24(2), 65-78. doi:[https://doi.org/10.1016/S0198-9715\(99\)00047-2](https://doi.org/10.1016/S0198-9715(99)00047-2)

- Richards, K., Dove, M., Cleary, P. W., & Prakash, M. (2004). Discrete element modelling and smoothed particle hydrodynamics: potential in the environmental sciences. *Philosophical Transactions of the Royal Society of London. Series A: Mathematical, Physical and Engineering Sciences*, 362(1822), 2003-2030. doi:doi:10.1098/rsta.2004.1428
- Rinaldi, M., Surian, N., Comiti, F., Bussetini, M., Belletti, B., Nardi, L., . . . Golfieri, B. (2015). *Guidebook for the evaluation of stream morphological conditions by the Morphological Quality Index (MQI), Deliverable 6.2, Part 3, of REFORM (REstoring rivers FOR effective catchment Management), a Collaborative project (large-scale integrating project) funded by the European Commission within the 7th Framework Programme under Grant Agreement 282656.*
- Rosgen, D. L. (1994). A classification of natural rivers. *CATENA*, 22(3), 169-199. doi:[https://doi.org/10.1016/0341-8162\(94\)90001-9](https://doi.org/10.1016/0341-8162(94)90001-9)
- Rossi, G. (1994). Historical development of flood analysis methods. In G. Rossi, N. Harmancıoğlu, & V. Yevjevich (Eds.), *Coping with Floods* (pp. 11-34). Dordrecht: Springer Netherlands.
- S. Neelz, G. P. (2009). *Desktop Review of 2D Hydraulic Modelling Packages* Retrieved from [http://evidence.environment-agency.gov.uk/FCERM/Libraries/FCERM\\_Project\\_Documents/SC08\\_0035\\_Desktop\\_review\\_of\\_2D\\_hydraulic\\_packages\\_Phase\\_1\\_Report\\_sflb.ashx](http://evidence.environment-agency.gov.uk/FCERM/Libraries/FCERM_Project_Documents/SC08_0035_Desktop_review_of_2D_hydraulic_packages_Phase_1_Report_sflb.ashx)
- Schumann, G. J. P., Bates, P. D., Apel, H., & Aronica, G. T. (2018). *Global Flood Hazard: Applications in Modeling, Mapping, and Forecasting*: Wiley.
- Scorzini, A. R., & Frank, E. (2017). Flood damage curves: new insights from the 2010 flood in Veneto, Italy. *Journal of Flood Risk Management*, 10(3), 381-392. doi:10.1111/jfr3.12163
- Stelling, G. S., & Verwey, A. (2006). Numerical Flood Simulation. In *Encyclopedia of Hydrological Sciences*.
- Syme, B. (2006). *2D or not 2D?—an australian perspective*. Paper presented at the Defra Flood and Coastal Risk Management Conference.
- Teng, J., Jakeman, A. J., Vaze, J., Croke, B. F. W., Dutta, D., & Kim, S. (2017). Flood inundation modelling: A review of methods, recent advances and uncertainty analysis. *Environmental Modelling & Software*, 90, 201-216. doi:<https://doi.org/10.1016/j.envsoft.2017.01.006>
- Teng, J., Vaze, J., & Dutta, D. (2013). Simplified methodology for floodplain inundation modelling using LiDAR DEM. *Climate and land surface*

- changes in hydrology, IAHS Red Book, by Boegh E, Blyth E, Hannah DM, Hisdal H, Kunstmann H, Su B, Yilmaz KK (eds) pp, 198-204.*
- Teng, J., Vaze, J., Dutta, D., & Marvanek, S. (2015). Rapid Inundation Modelling in Large Floodplains Using LiDAR DEM. *Water Resources Management, 29*(8), 2619-2636. doi:10.1007/s11269-015-0960-8
- Ticehurst, C., Dutta, D., Karim, F., Petheram, C., & Guerschman, J. P. (2015). Improving the accuracy of daily MODIS OWL flood inundation mapping using hydrodynamic modelling. *Natural Hazards, 78*(2), 803-820. doi:10.1007/s11069-015-1743-5
- Toro, E. F. (2001). *Shock-capturing methods for free-surface shallow flows*: John Wiley.
- Toro, E. F., & Garcia-Navarro, P. (2007). Godunov-type methods for free-surface shallow flows: A review. *Journal of Hydraulic Research, 45*(6), 736-751. doi:10.1080/00221686.2007.9521812
- Wallemacq, P., & House, R. (2018). *Economic Losses, Poverty & Disasters: 1998-2017*: Centre for Research on the Epidemiology of Disasters, CRED.
- Ward, P. J., Jongman, B., Salamon, P., Simpson, A., Bates, P., De Groeve, T., . . . Winsemius, H. C. (2015). Usefulness and limitations of global flood risk models. *Nature Climate Change, 5*, 712. doi:10.1038/nclimate2742
- Weisstein, E. W. Box-and-Whisker Plot. Retrieved from <http://mathworld.wolfram.com/Box-and-WhiskerPlot.html>
- White, F. M. (1991). *Viscous fluid flow* (Vol. 3): McGraw-Hill New York.
- Wilcox, A. C., Nelson, J. M., & Wohl, E. E. (2006). Flow resistance dynamics in step-pool channels: 2. Partitioning between grain, spill, and woody debris resistance. *Water Resources Research, 42*(5). doi:10.1029/2005wr004278
- Wilcox, A. C., Wohl, E. E., Comiti, F., & Mao, L. (2011). Hydraulics, morphology, and energy dissipation in an alpine step-pool channel. *Water Resources Research, 47*(7).
- Willingford, H. (2006). *Rapid Flood Spreading Methodology (RFSM)-Thames Estuary 2100 DT4*. Retrieved from [http://www.sayersandpartners.co.uk/uploads/6/2/0/9/6209349/2006\\_sayers\\_and\\_marti\\_-\\_rsfm\\_-\\_rapid\\_flood\\_spreading\\_method\\_-\\_te2100\\_dt4\\_rsfm\\_thames\\_estuary\\_2100\\_5b.pdf](http://www.sayersandpartners.co.uk/uploads/6/2/0/9/6209349/2006_sayers_and_marti_-_rsfm_-_rapid_flood_spreading_method_-_te2100_dt4_rsfm_thames_estuary_2100_5b.pdf)
- Yang, C. R., & Tsai, C. T. (2000). DEVELOPMENT OF A GIS-BASED FLOOD INFORMATION SYSTEM FOR FLOODPLAIN

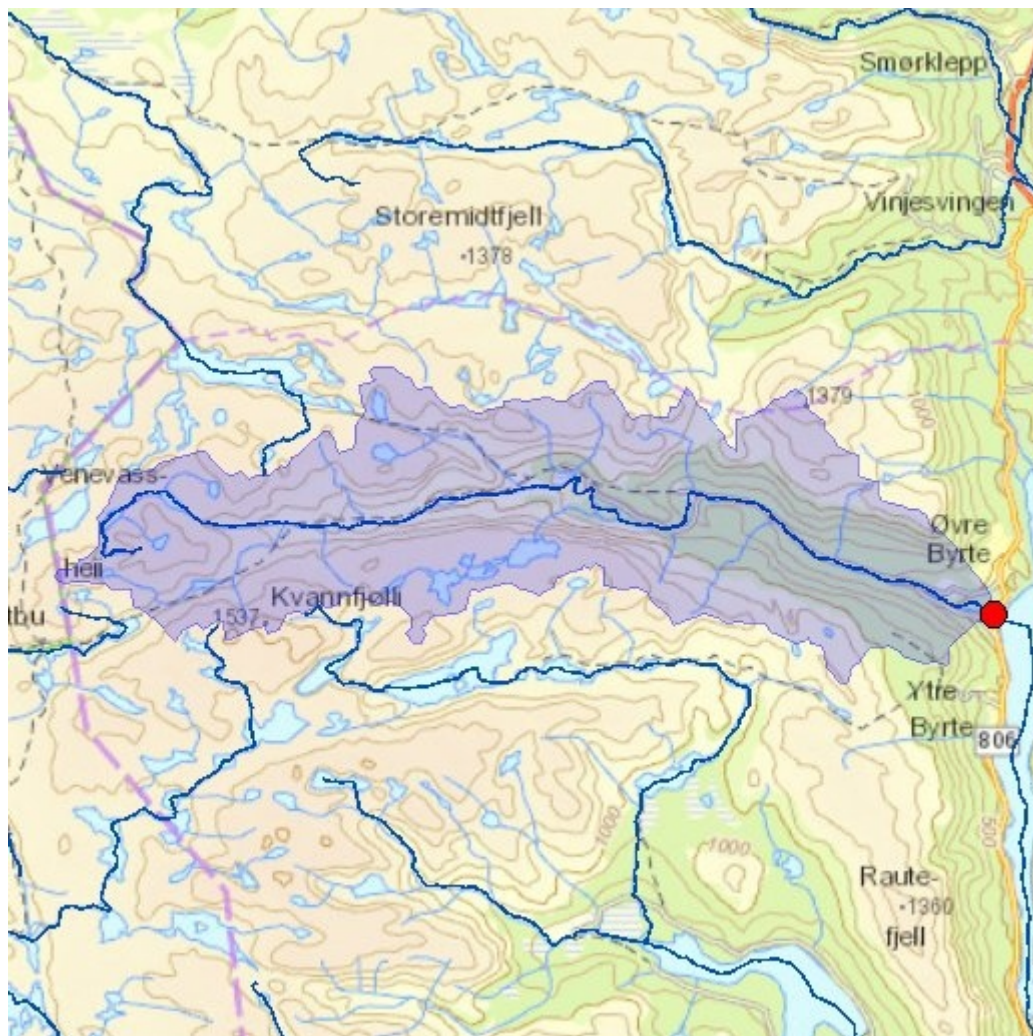
MODELING AND DAMAGE CALCULATION1. *JAWRA Journal of the American Water Resources Association*, 36(3), 567-577.  
doi:doi:10.1111/j.1752-1688.2000.tb04287.x

Zhang, J., Huang, Y.-F., Munasinghe, D., Fang, Z., Tsang, Y.-P., & Cohen, S. (2018). Comparative Analysis of Inundation Mapping Approaches for the 2016 Flood in the Brazos River, Texas. *JAWRA Journal of the American Water Resources Association*, 54(4), 820-833.  
doi:doi:10.1111/1752-1688.12623



## **A. APPENDIX A – Byrteåi Lavvannskart**





## Lavvannskart

Vassdragsnr.: 016.BE2C  
 Kommune: Tokke  
 Fylke: Telemark  
 Vassdrag: Rukkeåi

### Feltparametere

Areal (A)	49,3 km <sup>2</sup>
Effektiv sjø (S <sub>eff</sub> )	0,1 %
Elvelengde (E <sub>L</sub> )	20,5 km
Elvegradient (E <sub>G</sub> )	45,9 m/km
Elvegradient <sub>1085</sub> (G <sub>1085</sub> )	46,0 m/km
Feltlengde(F <sub>L</sub> )	16,5 km
H <sub>min</sub>	452 moh.
H <sub>10</sub>	781 moh.
H <sub>20</sub>	914 moh.
H <sub>30</sub>	1023 moh.
H <sub>40</sub>	1103 moh.
H <sub>50</sub>	1182 moh.
H <sub>60</sub>	1259 moh.
H <sub>70</sub>	1315 moh.
H <sub>80</sub>	1349 moh.
H <sub>90</sub>	1383 moh.
H <sub>max</sub>	1534 moh.
Bre	0,0 %
Dyrket mark	0,6 %
Myr	0,2 %
Sjø	3,5 %
Skog	25,4 %
Snau fjell	67,9 %
Urban	0,0 %

### Vannføringsindeks, se merknader

Middelvannføring (61-90)	47,2 l/(s*km <sup>2</sup> )
Alminnelig lavvannføring	1,8 l/(s*km <sup>2</sup> )
5-persentil (hele året)	1,8 l/(s*km <sup>2</sup> )
5-persentil (1/5-30/9)	6,6 l/(s*km <sup>2</sup> )
5-persentil (1/10-30/4)	1,5 l/(s*km <sup>2</sup> )
Base flow	18,4 l/(s*km <sup>2</sup> )
BFI	0,4

### Klima

Klimaregion	Sor
Årsnedbør	1122 mm
Sommernedbør	486 mm
Vinternedbør	636 mm
Årstemperatur	0,3 °C
Sommertemperatur	5,4 °C
Vintertemperatur	-3,4 °C
Temperatur Juli	7,3 °C
Temperatur August	8,4 °C

1) Verdien er editert



Kartbakgrunn: Statens Kartverk  
 Kartdatum: EUREF89 WGS84  
 Projeksjon: UTM 33N

Nedbørfeltgrenser, feltparametere og vannføringsindekser er automatisk generert og kan inneholde feil. Resultatene må kvalitetssikres.

Det er generelt stor usikkerhet i beregninger av lavvannsindekser. Resultatene bør verifiseres mot egne observasjoner eller sammenlignbare målestasjoner.

I nedbørfelt med høy breprosent eller stor innsjøprosent vil tørrværsavrenning (baseflow) ha store bidrag fra disse lagringsmagasinene.



# Flomberegning

Vassdragsnr.: 016.BE2C

Kommune: Tokke

Fylke: Telemark

Vassdrag: Rukkeåi

*Flomverdiene viser størrelsen på kulminasjonsflommer for ulike gjentaksintervall. De er beregnet ved bruk av et formelverk som er utarbeidet for nedbørfelt under ca 50 km<sup>2</sup>. Feltparametere som inngår i formelverket er areal, effektiv sjøprosent og normalavrenning (l/s\*km<sup>2</sup>). For mer utdypende beskrivelse av formelverket henvises det til NVE –Rapport 7/2015 «Veileder for flomberegninger i små uregulerte felt». Det pågår fortsatt forskning for å  
Det pågår fortsatt forskning for å bestemme klimapåslag for momentanflommer i små nedbørfelt. Frem til resultatene fra disse prosjektene foreligger anbefales et klimapåslag på 1.2 for døgnmiddelflom og 1.4 for kulminasjonsflom i små nedbørfelt.*

Rukkeåi	
Areal (km <sup>2</sup> )	49,3
Klimafaktor	1,4

	Q <sup>M</sup>		Q <sub>5</sub>	Q <sub>10</sub>	Q <sub>20</sub>	Q <sub>50</sub>	Q <sub>100</sub>	Q <sub>200</sub>
	m <sup>3</sup> /s	l/(s*km <sup>2</sup> )						
Flomfrekvensfaktorer	-	-	1,23	1,44	1,66	2,00	2,29	2,62
95% intervall øvre grense (m <sup>3</sup> /s)	63,6	1291,1	80,0	95,7	113,0	140,0	164,6	188,4
Flomverdier (m <sup>3</sup> /s)	36,0	729	44,2	51,7	59,8	71,8	82,3	94,2
95% intervall nedre grense (m <sup>3</sup> /s)	20,3	412	24,4	28,0	31,6	36,8	41,1	47,1
Flommer med klimapåslag (m <sup>3</sup> /s)	50,3	1021,2	44,2	72,4	83,7	100,5	115,2	131,9

Beregningene er automatisk generert og kan inneholde feil. Det er generelt stor usikkerhet i denne typen beregninger. Resultatene må verifiseres mot egne observasjoner eller sammenlignbare målestasjoner. Resultatene er ikke gyldig som grunnlag til flomberegninger for klassifiserte dammer.

